A Review of Anthropomorphic Robotic Hand Technology and Data Glove Based Control

Stephen Arthur Powell

Thesis submitted to the faculty of the Virginia Polytechnic Institute and State University in partial fulfillment of the requirements for the degree of

Master of Science
In
Mechanical Engineering

Shashank Priya, Chair
Andrew Kurdila
Reza Mirzaeifar

July 19, 2016
Blacksburg, VA

Keywords: humanoid, anthropomorphic, hand, mechatronics, rapid prototyped, manipulation, data glove, human-machine interfaces, piezoluminescence

Copyright © 2016 Stephen Arthur Powell

A Review of Anthropomorphic Robotic Hand Technology and Data Glove Based Control

Stephen Arthur Powell

ABSTACT (Academic)

For over 30 years, the development and control of anthropomorphic robotic hands has been a highly popular sub-discipline in robotics research. Because the human hand is an extremely sophisticated system, both in its mechanical and sensory abilities, engineers have been fascinated with replicating these abilities in artificial systems. The applications of robotic hands typically fall under the categories of standalone testbed platforms, mostly to conduct research on manipulation, prosthetics, and robotic end effectors for larger systems. The teleoperation of robotic hands is another application with significant potential, where users can control a manipulator in real time to accomplish diverse tasks. In controlling a device that seeks to emulate the function of the human hand, it is intuitive to choose a human-machine interface (HMI) that will allow for the most intuitive control. Data gloves are the ideal HMI for this need, allowing a robotic hand to accurately mimic the human operator's natural movements. In this paper we present a combined review on the critical design aspects of data gloves and robotic hands. In literature, many of the proposed designs covering both these topical areas, robotic hand and data gloves, are cost prohibitive which limits their implementation for intended tasks. After reviewing the literature, new designs of robotic hand and data glove technology are also presented, introducing low cost solutions that can serve as accessible platforms for researchers, students, and engineers to further the development of teleoperative applications.

A Review of Anthropomorphic Robotic Hand Technology and Data Glove Based Control

Stephen Arthur Powell

General Audience Abstract

For over 30 years, the development and control of anthropomorphic robotic hands has been a highly popular sub-discipline in robotics research. Because the human hand is an extremely sophisticated system, both in its mechanical and sensory abilities, engineers have been fascinated with replicating these abilities in artificial systems. The applications of robotic hands typically fall under the categories of standalone testbed platforms, mostly to conduct research on manipulation, prosthetics, and robotic end effectors for larger systems. The teleoperation of robotic hands is another application with significant potential, where users can control a manipulator in real time to accomplish diverse tasks. In controlling a device that seeks to emulate the function of the human hand, it is intuitive to choose a human-machine interface (HMI) that will allow for the most intuitive control. Data gloves are the ideal HMI for this need, allowing a robotic hand to accurately mimic the human operator's natural movements. In this paper we present a combined review on the critical design aspects of data gloves and robotic hands. In literature, many of the proposed designs covering both these topical areas, robotic hand and data gloves, are cost prohibitive which limits their implementation for intended tasks. After reviewing the literature, new designs of robotic hand and data glove technology are also presented, introducing low cost solutions that can serve as accessible platforms for researchers, students, and engineers to further the development of teleoperative applications.

Acknowledgements

I would like to thank everyone who has helped me achieve my goals during my educational journey here at Virginia Tech. I could not have done it without all of you.

A big thank you to my advisor, Dr. Shashank Priya, for giving me the opportunity to pursue my dream of working in the field of robotics and his support over my graduate school career.

I would also like to thank all of my lab mates for their assistance, advice, and friendship.

Finally, I cannot forget to thank my family and friends who I have always been able to count on for encouragement and love during this journey.

Table of Contents

List of Figures

List of Tables

Attributions

This thesis provides a comprehensive review of anthropomorphic robotic hand designs and data glove technology for their control. The two subjects are very closely related in their applications, in fact depend on each other, and thus needs to be discussed together. There is currently no published literature that discusses both the subjects of anthropomorphic robotic hands and data gloves together, despite the two being designed to operate each other. In this thesis an initial design of an anthropomorphic robotic hand platform is presented. The initial design of the robotic hand was a joint effort between myself and Mike Stevens, where I designed the forearm unit and he designed the hand portion. The hand portion is the design that is featured in his thesis entitled, "Design and Teleoperative Control of Humanoid Robot Upper Body for Task-driven Assistance." Upon his graduation, it became my responsibility to test the complete system. In conducting extensive tests, I uncovered the need for improvement in several aspects of the design in order to make progress in the goals that our group set out to accomplish in the project. With Mike's permission, some pertinent sections of his thesis appear in the manuscript. The low-cost data glove design presented in this paper was developed by my colleague, Matthew Paluszek, for his thesis entitled, "Methods and Applications for Controlling Biomimetic Robotic Hands." In our research group's project scope, the data glove was created to be the input device for the anthropomorphic robotic hand platform. Integrating the concept of remote control of the robotic hand with the data glove technology was key overall goal of the program. In order to complete this goal, I was involved in extensive testing of the glove to control the robotic hand and provide understanding of the limitations of the current system. With Matt's permission, some pertinent sections of his thesis appear in the manuscript. For this thesis, a comprehensive review is presented for both technologies, covering the progress made in design, fabrication and implementation of low-cost robotic hand and data glove based remote control. I would like to acknowledge the contributions of my co-authors in providing input to this review. Gregory Krummel and Min Gyu Kang assisted in the compilation of data glove literature, and Michael Okyen assisted in making suggestions for the design of the impedance control of the hand. In order to overcome the limitations of the present design, a new type of data glove that utilizes a piezoluminescent (PZL) rubber material was developed. In collaboration with Min Gyu Kang, I was able to propose an implementation scheme for the non-contact PZL glove. Combined together, this review provides an important compilation of design approaches for robotic hand with various degree of freedom, range of motion and control schemes. I believe this extensive review will serve two purpose: (i) facilitate the transition of the low-cost robotic hand designs into research labs and practical applications, and (ii) provide opportunity for implementing data gloves in various control scenarios. The low cost robotic hand design that I have developed will provide easy entry point for other graduate students and early stage researchers around the world to experiment with various controls schemes in implementing the intended robotic tasks.

1. Introduction

The human hand is an extremely sophisticated system allowing one to interact and manipulate objects in their environment, and also to gather information to arrive at intelligent decisions. In the field of robotics, anthropomorphism has been a large thrust in robotic end effectors to achieve high dexterity in imitating the human hand's kinesthetic and sensory abilities. Additionally, in applications where a robot is functioning in a human environment, it is intuitive to design an end effector to have a human-inspired form factor. For applications where a human will be operating or programming a robotic end effector system, designing an anthropomorphic system will allow for intuitive control. The use of data gloves allows for the most intuitive control of any human-machine interface, as the operator can function as naturally as they would if they were completing a task with their very own hands.

Over the past two decades, review papers have been published on both subjects of data gloves (Sturman & Zeltzer, 1994; Dipietro, Sabatini, & Dario, 2008) and robotic hands (Pons, Ceres, & Pfeiffer, 1999; Saliba & Ellul, 2013; Sousa, Couceiro, Barbosa, Figueiredo, & Ferreira, 2013); however, both these topics have been presented independent of each other. The goal of this paper is to provide an integrated overview of progress in the design of robotic hands and their control using data gloves. The design of these systems is highly dependent upon each other. In this paper we also explore the current strengths and limitations of the designs for both these systems, and propose our own new designs that reduces the operational complexity and cost significantly. The designs presented include a 16 degree of freedom (DoF) robotic hand, a 10 DoF data glove, and a novel concept for future data glove that utilizes piezoluminescent (PZL) materials. All of these designs were developed to lower the barriers of entry in the data glove controlled robotics hand research.

In many instances there are tasks in which human lives are put at risk. Replacing humans with robots in these situations can allow these tasks to be carried out safely. In the line of duty of law enforcement and military personnel, explosives are encountered and must be handled and disarmed with very careful dexterity. Scenarios in which dangerous chemicals or radioactive materials must be handled can also benefit from telerobotics. Teleoperated robotics can allow people to work in extreme environments, without the need of enduring them in person. Extreme environments can include locations that are alkaline, acidic, extremely hot/cold, hypersaline, under high pressure, radioactive, without water, without oxygen, and polluted. The exploration of space as well as the deep sea has attracted the attention of roboticists. NASA has created two generations of their teleoperated humanoid robot, Robonaut, which are designed to work onboard of the International Space Station (ISS), utilizing the same areas that human astronauts occupy. Operators equipped with data gloves and virtual reality headsets can operate the system to perform tasks both inside and outside of the ISS (Berka & Goza, 2012).

A teleoperated robotic hand can be applied to allow users to access equipment, navigate facilities, and provide specialized expertise without the need to physically travel to a location. Often times, a research lab will have specialized tools or equipment that are not commonly available in other labs due to cost or space restrictions. Typically in these situations, the individual who desires to use them must travel to the other location in order to carry out their work, which requires a great deal of time and expense. This

inconvenience can be alleviated through the use of a teleoperated robotic system. A platform with humanoid hand end effectors can help to create a telepresence that can be intuitively controlled. Additionally, unique professional skills can be shared as well, such as those of a medical doctor. Doctors possess extremely specialized skills which can save people's lives if applied in a timely manner. If a robotic hand can possess the necessary dexterity and the doctors have a data glove that is precise enough, medical treatment can be conducted remotely. In situations and locations where medical personnel may not be readily present or able to be dispatched quickly, availability of remote controlled robotic manipulator could be critical. Locations such as this could include airplane flights, oil rigs, and secluded research stations in remote locations. Another specific example of a potential application would be emergency medical response in a hostile warzone, where a medic might not be immediately be able to access the injured in fear of causing further casualties. Likewise, first responders such as emergency medical technicians (EMT) are sometimes delayed in performing their duties upon arriving on the scene due to potential threats to their own safety, sometimes resulting in the injured individual's death. In these cases, a robot can be teleoperated by the EMT to attempt to provide medical treatment, until the scene has been assessed as safe for intervention from human personnel.

Social robotics is another sub-discipline in robotics, where the focus is to develop robots that can interact with humans meaningfully, often times providing a companion-like presence. In many cases, these robots are designed for a therapeutic use, such as helping autistic child with learning and practicing social skills (Dautenhahn et al., 2009). The hands are very expressive in human body language, so it is a desirable feature in robots that are designed to emulate human behavior, such as in the Robovie R3 platform developed to teach sign language through its use of facial expressions and articulated hands and arms (Uluer, Akalın, & Köse, 2015). Other purposes for social robots include helpers which can assist people particularly the elderly and disabled with tasks of daily living, such as cleaning or retrieving items for them. An example of similar available technology is the JACO 3 Fingers system, a non-anthropomorphic gripper and arm system mounted to a wheelchair, designed to help handicapped individuals in performing activities of daily living which allows them to retain independence in spite of their afflictions (Maheu, Archambault, Frappier, & Routhier, 2011). Robotic end effectors that can function in a human occupied environment is very important, so a system will certainly benefit from human-like end effectors.

It has long been a dream of the general public that there will come a day when personal robots will perform domestic duties in the home, such as cleaning, doing laundry, washing dishes, etc. Such assistance could allow people to have more time to themselves, improve their quality of life, and help them be more productive. In 1998, the Humanoid Robots Project was created by the Ministry of Economy, Trade and Industry (METI) of Japan, as a thrust project to develop humanoid robots that can assist humans in industry and domestically, producing the HRP-2 platform (Cheng, 2014). More recently, robotic platforms such as PR2 (Willow Garage), Baxter (Rethink Robotics, 2015), and Care-O-Bot (Graf et al., 2009) have been developed and sold as a platforms for the development and implementation of applications of performing tasks in human environments. The PR2 has been shown folding towels (Miller et al., 2012), retrieving and serving beverages (Bohren et al., 2011), and playing the game of pool (Willow Garage, 2010). In tasks involving manipulation, data gloves could allow a user to "teach"

a robot new chore or manipulate a new item with learning through demonstration (Dillmann, 2004). In research labs and industry this has been a practiced method of robot programming, and for the average untrained user this would be quite intuitive and won't require a background in engineering, programming, or robotics (Aleotti & Caselli, 2006). Additionally, another possibility would be to put a data glove onto a robotic hand, and allow a robot to heuristically learn how to handle objects and perform tasks.

In a research environment, an anthropomorphic hand can serve as an output device to provide useful physical feedback for a variety of applications. There have been many robotic hands developed to serve as standalone testbeds for implementing new sensors, control systems, and grasping strategies. Data gloves have been used by human operators in teaching robotic hands new grasp synergies, which are analogous to how humans can activate multiple muscles simultaneously in a specified pattern to perform complex actions (Geng, Lee, & Hülse, 2011). This biomimetic approach can teach robots new skills and simplify the control of motors. Additionally, often times the robotic hand systems serve as end effectors, attached to humanoid robotic platforms, where tasks and experiments are carried out with full upper body articulation (Kim et al., 2014; Roccella et al., 2004; Schmitz et al., 2010).

The advancement of prosthetic technology is a practical motivation for the development of anthropomorphic robotic systems. The loss of a limb either through an accident or from amputation is a debilitating event in that it affects a person's ability to function in performing necessary tasks in their daily life. Prosthetic hands in particular can benefit greatly from the development of robotic solutions. In recent years, there has been a push for the development of more sophisticated robotic prostheses, such as the creation of DARPA's Revolutionizing Prosthetics program (Sanchez) where actuator and sensing technology as well as controls engineering are pushed to their limits. However, advances in prosthetic hardware is outpacing the progress of controlling the devices. In the field of prosthetic hands, most conventional products are mechanically simple, with few degrees of freedom, and limited in their functionality. Most typical prosthetic hands fall under the categories of body-operated, where the user controls the device with the movement of their remaining upper extremity, and myoelectric control which senses electrical signals from the muscle of the remaining extremity. Controllability with EMG signals, however, is also limited in its ability, resulting in many devices that utilize at least two EMG inputs. Data gloves have proven to be useful in contributing to the advancement of prosthetic technology, and in the creation of the NINAPRO database where the EMG and kinematic data was collected from users (Atzori et al., 2012). With this data, researchers hope to further the understanding of the relationship between the two in order to improve EMG prostheses controllability.

2. **Overview of anthropomorphic hand designs in literature**

A survey of anthropomorphic robotic hands reported in literature is provided here. In this survey, only anthropomorphic designs have been covered, cataloging systems with at least 3 fingers and a thumb-like finger. Though many robotic gripper systems have been developed, their function is often limited to a specific task and they lack dexterity. Beginning with the classic designs of the early 1980's and proceeding up to 2015, key mechanical design details are covered in Table 1, and then in Table 2 the sensing, design purpose, integration, and other parameters are covered.

Table 1. Anthropomorphic Robotic Hands - Mechanical Design.

	Extrinsic / Intrinsic	# of Fingers	Total Hand Joints	Active Hand DoF	Wrist DoF	Total Actuators	Actuation and Transmission
Stanford/JPL Hand [1] [2] (1982)	E	3	9	9	-	12	DC, Tendon, Pulleys, Sheath
UTAH/MIT [3] (1986)	E	4	16	16	-	32	Pneumatic, Tendon, Pulleys
Belgrade/USC Hand [4] (1988)	E	5	18	4	-	4	DC, Linkages
NTU [5] Hand (1996)	I	5	17	17	-	17	micro DC, Gear train
DIST Hand [6] (1998)	E	4	16	16	-	20	DC, Tendons, Pulleys, Sheaths
DLR Hand 1 [7] (1998)	I	4	16	12	-	12	BLDC, Tendon, Pulleys
LMS Hand [8] (1998)	E	4	17	16	-	16	DC servo, Tendons
Gifu Hand [9] (1999)	I	5	16	16	-	16	DC servo, Differential bevel gears, Linkages
Manus Hand [10] (1999)	I	5	9	2	1	2	DC, Tendons, gears
Robonaut Hand [11] (1999)	E	5	20	12	2	12	BLDC, Tendons, linkages
TUAT/Karlsruhe Hand [12] (2000)	E	5	20	1	-	1	Ultrasonic motors, Linkages

[1] (Pellerin, 1991)
[2] (Salisbury & Craig, 1982)
[3] (Jacobsen, Iversen, Knutti, Johnson, & Biggers, 1986)
[4] (Bekey, Tomovic, & Zeljkovic, 1990)
[5] (Lin & Huang, 1998)
[6] Caffaz, Casalino, Cannata, Panin, & Massucco, 2000)
[7] (Butterfass, Hirzinger, Knoch, & Liu, 1998)
[8] (Gazeau, Zehloul, Arsicault, & Lallemand, 2001)
[9] (Mouri, Endo, & Kawasaki, 2011)
[10] (Pons et al., 2004)
[11] (Lovchik & Diftler, 1999)
[12] (Fukaya, Toyama, Asfour, & Dillmann, 2000)

DLR Hand II [13] (2001)	I	4	17	13	-	13	BLDC, Timing belts, Bevel gears
Harada Hand [14] (2001)	I	5	14	5	-	5	DC, Tendon, Pulleys, Springs
Gifu hand II [15] (2002)	I	5	20	16	-	16	DC servo, Bevel gears, Linkages (PIP-DIP)
Gifu Hand III [16] (2002)	I	5	20	16	-	16	DC servo, Bevel gears, Linkages (PIP-DIP)
Shadow Hand [17] (2002)	E	5	23	23	-	36	Pneumatic, Tendons, sheath
RCH-1 [18] [19] (2003)	I & E	5	16	6	-	6	DC, Tendons, Pulley, Torsion springs
RTR II Hand [20] (2004)	I	3	11	2	-	2	DC, Tendons, pulleys
Shadow Dextrous Hand [21] [22] (2005)	E	5	23	23	-	36	Pneumatic, Tendons
MAC Hand [23] (2005)	I	4	22	12	-	16	DC, Tendons
NAIST Hand [24] (2005)	I	4	16	12	-	12	DC w/ harmonic drive, Bevel gears, Linkages
UB Hand 3 [25] (2005)	E	5	20	20	-	20	DC servo, Tendons, sheaths
Cyber Hand [26] (2006)	I	5	16	6	-	6	DC, Tendons
DLR-HIT Hand [27] (2006)	I	4	13	13	-	13	BLDC, DC, Belts, Gears, Linkages

[13] (Butterfass, Grebenstein, Liu, & Hirzinger, 2001)
[14] (Keymeulen & Assad, 2001)
[15] (Kawasaki, Komatsu, & Uchiyama, 2002)
[16] (Mouri, Kawasaki, Yoshikawa, Takai, & Ito, 2002)
[17] (Tuffield & Elias, 2003)
[18] (Roccella et al., 2004)
[19] (Zecca et al., 2013)
[20] (Zecca et al., 2004)
[21] (Kochan, 2005)
[22] (Shadow Robot Company, 2013)
[23] (Cannata & Maggiali, 2005)
[24] (Ueda, Ishida, Kondo, & Ogasawara, 2005)
[25] (Lotti et al., 2005)
[26] (Carrozza et al., 2006)
[27] (Liu et al., 2007)

HRP-3P Hand [28] (2007)	I	4	17	13	-	13	DC servo, harmonic drive, Linkages
SKKU II Hand [29] (2006)	I	4	16	10	-	10	DC, Bevel gears, Timing belt & Pulley, Linkages
University of Tokyo Hand [30] (2006)	I	5	12	12	3	12	DC servo, Tendons, Sheaths, Springs
DLR/HIT II Hand [31] [32] (2008)	I	5	20	15	-	15	flat BLDC, harmonic drives, Belts
Dong-Eui Hand [33] (2008)	I	5	15	6	-	6	DC, Tendons, Pulleys, Linkages
FRH-4 Hand [34] (2008)	E	5	11	11	-	12	Flexible fluidic actuators, Direct drive, Elastic elements
iCub Hand (low cost) [35] (2008)	E	5	22	18	2	18	DC, Tendons, Springs
SmartHand [36] (2008)	I	5	16	4	-	4	DC, Tendons, Pulleys, Springs
iLimb [37] (2009)	I	5	11	6	-	6	DC, Tendons
Meka H2 [38] (2009)	I	4	12	5	-	5	SEA, Elastic elements
NAIST Hand 2 [39] (2009)	E	5	21	16	1	16	DC servo, Tendon, Linkage (PIP-DIP)
TWENDY-ONE Hand [40] (2009)	I	4	16	13	-	13	DC, Linkages

[28] (Kaneko, Harada, & Kanehiro, 2007)
[29] (Choi, Lee, Choi, & Kang, 2006)
[30] (Arieta, Katoh, Yokoi, & Wenwei, 2006)
[31] (Liu et al., 2008)
[32] (Zhang, Liu, Jin, & Liu, 2010)
[33] (Jung & Moon, 2008)
[34] (Gaiser et al., 2008)
[35] (Davis, Tsagarakis, & Caldwell, 2008)
[36] (Cipriani, Controzzi, & Carrozza, 2011)
[37] (Belter & Segil, 2013)
[38] (MekaBot, 2009)
[39] (Kurita, Ono, Ikeda, & Ogasawara, 2009)
[40] (Iwata & Sugano, 2009)

ARTS Hand [41] (2010)	E & I	5	20	12	2	12	DC, Tendons, Pulleys
GCUA Hand II [42] (2010)	I	5	14	10	-	10	DC, Tendon, Pulleys, Springs
Dexterous iCub Hand [43] (2010)	E & I	5	19	9	2	9	DC, Tendons, Pulleys
iLimb Pulse [44] (2010)	I	5	11	6	-	5	DC, Tendons
OCU Hand [45] (2010)	I	5	19	12	3	15	DC, DC Servo, Bevel gears, Linkages (PIP-DIP)
BeBionic [46] (2011)	I	5	11	6	-	5	DC, Linkage
DLR DEXHAND [47] (2011)	I	4	16	12	-	12	DC, Harmonic drive, Tendons, Pulleys
Modular Prosthetic Limb [48] (2011)	I	5	26	17	3	17	BLDC, Direct drive
DART Hand [49] (2011)	E	5	19	16	2	19	DC Servo, Tendons, Springs
DLR Hand Arm System [50] (2011)	E	5	19	19	2	42	DC Servo, Tendons, Pulleys
KIST Hand [51] (2011)	I	4	15	9	-	9	DC, Linkages, Ball Joints
ZJUT Hand [52] (2011)	I	5	20	20	-	20	Pneumatic
Adroit MK2 Manipulator [53] [54] (2012)	I	3	10	4	-	4	Linkages

[41] (Controzzi, Cipriani, Jehenne, Donati, & Carrozza, 2010)
[42] (Che & Zhang, 2010)
[43] (Schmitz et al., 2010)
[44] (Belter & Segil, 2013)
[45] (Mahmoud, Ueno, & Tatsumi, 2010)
[46] (Belter & Segil, 2013)
[47] (Chalon et al., 2011)
[48] (Johannes et al., 2011)
[49] (Thayer, & Priya, 2011)
[50] (Grebenstein et al., 2011)
[51] (Kim, Lee, & Lee, 2011)
[52] (Wang, Zhang, Bao, Qian, & Yang, 2011)
[53] (HDT, 2015)
[54] (RoboticsTomorrow, 2012)

KITECH Hand [55] (2012)	I	4	16	16	-	16	DC Servo, Spur geartrain
Michelangelo Hand [44] (2012)	I	5	6	2	-	2	DC, Cam mechanism, Gears
Robonaut 2 Hand [56] (2012)	E	5	20	12	2	16	BLDC, Tendons, Linkages, Ball Screw
Vanderbilt Hand [57] [58] (2012)	I	5	9	4	-	4	Brushless DC, Clutches, Tendons, Pulleys
Low-cost and Modular Hand [59] (2013)	E	5	20	20	-	40	Pneumatic, Tendons
TUAT/Karlsruhe Hand (updated) [60] (2013)	I	5	24	6	-	6	DC Servo, Linkages
UB Hand IV [61] [62] (2013)	E	5	20	16	2	24	DC, Tendons
CEA Dexterous Hand [63] (2014)	I	5	24	20	2	20	DC, Leadscrew, Tendons, Pulley
DEKA Arm [64] [65] (2014)	I	5	12	6	2	6	DC, Gears, Linkages, Belts
DEXMART Hand [66] (2014)	E	5	24	24	2	24	DC, Tendons, Pulleys
Dextrus Hand (Open Hand Project) [67] (2014)	I	5	15	6	-	6	DC, Tendons, Pulleys
IRIS Hand [68] (2014)	E & I	5	16	6	-	6	DC, Tendons, Linkages
Low-Friction Tendon-Driven Robot Hand [69] (2014)	E	5	19	11	-	12	Pneumatic, Tendons, Pulleys, Elastic elements

[55] (Bae et al., 2012)
[56] (Bridgwater et al., 2012)
[57] (Bennett, Dalley, Truex, & Goldfarb, 2015)
[58] (Dalley, Bennett, & Goldfarb, 2012)
[59] (Xu, Kumar, & Todorov, 2013)
[60] (Fukaya, Asfour, Dillmann, & Toyama, 2013)
[61] (Ficuciello, Palli, Melchiorri, & Siciliano, 2011)
[62] (Melchiorri, Palli, Berselli, & Vassura, 2013)
[63] (Martin & Grossard, 2014)
[64] (Perry et al., 2012)
[65] (Resnik, Klinger, & Etter, 2014)
[66] (Palli et al., 2014)
[67] (Open Hand Project, 2014)
[68] (Casley et al., 2014)
[69] (Treratanakulwong, Kaminaga, & Nakamura, 2014)

RoboRay Hand [70] (2014)	E & I	5	20	12	2	14	DC, BLDC, Tendons, Pulleys
Sandia Hand [71] (2014)	I	4	12	12	-	12	BLDC, Tendons, Pulleys
UT Hand 1 [72] (2014)	I	5	12	3	-	3	BLDC, DC, solenoids, Tendon, Pulleys, Linkages, Torsion springs
Schunk SVH [73] (2014)	I	5	20	9	-	9	DC servo, Direct drive, Linkages
Ambi-Hand [74] (2015)	E	5	15	14	-	17	Pneumatic, Tendon, Pulley
Tact [75] (2015)	I	5	11	6	-	6	DC, Tendons, Linkage

Table 2. Anthropomorphic Robotic Hands – Sensing, Purpose, and Other Details.

Name	Sensing	Purpose	Forearm / Integration	3D Printed
Stanford/JPL Hand [1] [2] (1982)	Tendon tension, Position/Velocity	Research	N / Y	N
UTAH/MIT [3] (1986)	Tendon tension, Tactile, Joint position	Research	Y / Y	N
Belgrade/USC Hand [4] (1988)	Position, Tactile	Platform End Effector	N / Y	N
NTU Hand [5] (1996)	Position, Tactile	Platform End Effector, Prosthesis	N / Y	N
DIST Hand [6] (1998)	Position, Tactile, Fingertip force	Platform End Effector	N / Y	N
DLR Hand 1 [7] (1998)	Joint position, Joint torque, Tactile, Motor position, Temperature, Vision, Force-torque	Research	N / Y	N
LMS Hand [8] (1998)	Motor encoders, Joint position	Research	Y / N	N
Gifu Hand [9] (1999)	Motor position	Research	N / N	N

[70] (Kim et al., 2014)
[71] (Quigley, Salisbury, Ng, & Salisbury, 2014)
[72] (Peerdeman et al., 2014)
[73] (Schunk)
[74] (Kalganova et al., 2014)
[75] (Slade, Akhtar, Nguyen, & Bretl, 2015)

Manus Hand [10] (1999)	Joint position	Prosthesis	N / Y	N
Robonaut Hand [11] (1999)	Joint position, Motor position, Tactile	Platform End Effector	Y / Y	N
TUAT/Karlsruhe Hand [12] (2000)	-	Platform End Effector	Y / Y	N
DLR Hand II [13] (2001)	Joint torque, Joint position, Force-torque, Motor position	Platform End Effector	N / Y	N
Harada Hand [14] (2001)	-	Prosthesis	N / Y	N
Gifu hand II [15] (2002)	Fingertip force-torque, Tactile, Motor position	Platform End Effector, Research	N / Y	N
Gifu Hand III [16] (2002)	Fingertip force, Tactile, Motor position	Platform End Effector, Research	N / Y	N
Shadow Hand [17] (2002)	Joint position	Research, Platform End Effector	Y / Y	N
RCH-1 [18 19] (2003)	Tactile, Force	Platform End Effector	Y / Y	N
RTR II Hand [20] (2004)	Joint position, Tendon tension, Fingertip force	Prosthesis	N / Y	N
Shadow Dextrous Hand [21 22] (2005)	Joint position	Research	Y / Y	N
MAC Hand [23] (2005)	Joint Position, Force, Tactile	Platform End Effector	N / N	N
NAIST Hand [24] (2005)	Motor Position, Tactile	Platform End Effector	N / Y	N
UB Hand 3 [25] (2005)	Tendon tension, Joint position	Research	Y / -	Y
Cyber Hand [26] (2006)	Joint position, Tendon tension, Tactile, Motor position	Prosthesis	N / Y	N
DLR-HIT Hand [27] (2006)	Joint position, Joint torque, Motor position, Force, Temperature	Platform End Effector, Research	N / Y	N
HRP-3P Hand [28] (2007)	Joint position, Force	Platform End Effector, Research	N / Y	N
SKKU II Hand [29] (2006)	Force	Research	N / -	N
University of Tokyo Hand [30] (2006)	Motor Position	Prosthetic	Y / Y	N

DLR/HIT II Hand [31] [32] (2008)	Joint position, Joint torque, Force, Motor Position, Temperature	Platform End Effector, Research	N / Y	N
Dong-Eui Hand [33] (2008)	-	Prosthesis	N / Y	Y
FRH-4 Hand [34] (2008)	Joint position, Tactile	Platform End Effector	N / Y	N
iCub Hand (low cost) [35] (2008)	Joint Position, Tendon tension, Motor torque	Platform End Effector	Y / Y	Y
SmartHand [36] (2008)	Motor current, Tendon tension, Tactile	Prosthesis	N / Y	N
iLimb [37] (2009)	-	Prosthesis	N / Y	N
Meka H2 [38] (2009)	Tendon position, SEA displacement, Motor current, Motor temperature, Electronics temperature	Platform End Effector	N / Y	N
NAIST Hand 2 [39] (2009)	Joint Position	Research, Platform End Effector	N / N	N
TWENDY-ONE Hand [40] (2009)	Joint position, Tactile, Force-torque	Platform End Effector	N / Y	N
ARTS Hand [41] (2010)	-	Prosthesis	Y / Y	N
GCUA Hand II [42] (2010)	-	Platform End Effector	N / Y	Y
Dexterous iCub Hand [43] (2010)	Joint Position, Tactile	Platform End Effector	Y / Y	N
iLimb Pulse [44] (2010)	-	Prosthesis	N / Y	N
OCU Hand [45] (2010)	Joint position	Prosthesis, Research	N / -	Y
BeBionic [46] (2011)	-	Prosthesis	N / Y	N
DLR DEXHAND [47] (2011)	Joint position, Joint torque, Temperature	Platform End Effector, Research	N / Y	N
Modular Prosthetic Limb [48] (2011)	Joint temperature, Joint torque, Joint position, Motor current, Motor position, Tactile, Force-torque	Prosthesis	N / Y	N
DART Hand [49] (2011)	Joint position	Research	Y / Y	Y
DLR Hand Arm System [50] (2011)	Joint Position	Research, Platform End Effector	Y / Y	N

KIST Hand [51] (2011)	Motor/Joint position, Tactile	Research	N / N	N
Adroit MK2 Manipulator [53 54] (2012)	Joint position, Joint torque, Joint temperature, Motor current	Platform End Effector	N / Y	N
KITECH Hand [55] (2012)	Motor position	Research	N / Y	-
Michelangelo Hand [44] (2012)	-	Prosthesis	N / Y	N
Robonaut 2 Hand (2012)	Joint position, Force-torque, Tactile, Tendon tension, Motor position, Motor current	Platform End Effector	Y / Y	N
Vanderbilt Hand [57 58] (2012)	Tendon position, Tendon force	Prosthesis	N / Y	Y
Low-cost and Modular Hand (2013)	Tactile	Research	N / N	Y
TUAT/Karlsruhe Hand (updated) (2013)	Motor position	Research	N / N	N
UB Hand IV [61 62] (2013)	Joint position, Tendon tension, Tactile	Research	Y / Y	Y
CEA Dexterous Hand [63] (2014)	Tendon tension, Position sensor	Research	Y / N	N
DEKA Arm [64 65] (2014)	Joint position, Tactile	Prosthesis	Y / Y	N
DEXMART Hand (2014) [66]	Motor force, Motor position, Tendon tension, Tactile, Joint position	Research	Y / Y	Y
Dextrus Hand (Open Hand Project) [67] (2014)	-	Prosthesis	N / Y	Y
IRIS Hand [68] (2014)	Motor position, Vision	Prosthesis	Y / -	Y
Low-Friction Tendon-Driven Robot Hand [69] (2014)	Joint position	Research	Y / N	Y
RoboRay Hand [70] (2014)	Force, Current	Platform End Effector	Y / Y	N
Sandia Hand [71] (2014)	Motor position, Tactile, Inertial, Joint force-Torque, Vision	Platform End Effector	N / Y	N
UT Hand 1 [72] (2014)	Tactile	Prosthesis	N / Y	N
Schunk SVH [73] (2014)	Fingertip force	Platform End Effector	N / Y	N

Ambi-Hand [74] (2015)	Position	Research	N / N	Y
Tact [75] (2015)	-	Prosthesis	N / N	Y

2.1 Actuator Location

In the designing of robotic hands, the actuation locations are classified as either extrinsic or intrinsic. Intrinsic robotic hands have their actuators located typically inside of the volume of the palm and fingers of the system. Conversely, in an extrinsic robotic hand, the actuators are located outside of the volume of the palm and fingers, in many cases they are placed in the volume of the forearm. Both configurations have their own advantages and disadvantages, and their selection depends upon the intended application.

Intrinsic robotic hands make for a more modular compact system compared to an extrinsic robotic hand. Because of this advantage, in most cases prosthetic hands fall under the intrinsic category, allowing them to be adapted to differing levels of upper limb amputation which can range from wrist disarticulation (amputation of hand at the wrist) to a forequarter amputation (the removal of the shoulder, clavicle, and scapula). Disadvantages of intrinsic designs include the limited amount of space for actuators, motion transmission components, and sensors as everything must be packaged into a small volume, often times a human-like form factor in the case of anthropomorphic robotic hands. Frequently there exists a trade-off between human-like size and human-like grasping strength, due to the aforementioned reasons (Melchiorri & Kaneko, 2008). Additionally, because of the limited volume, intrinsic robotic hands typically have less active DoF than their extrinsic counterparts due to the limit of the number of actuators that can be integrated. It is worth mentioning that in designing a robotic hand, the weight of the hand must be considered as increasing weight will affect the dynamics and performance of the total system (Melchiorri & Kaneko, 2008).

Extrinsic robotic hands, typically are not used in prosthetic applications, due to the issues mentioned in the previous paragraphs, though there have prostheses where the motors are located outside of the hand (Johannes, Bigelow, Burck, Harshbarger, Kozlowski, & Van Doren, 2011; Scott, 2013). Extrinsic robotic hands allow for more flexibility in actuator selection due to availability of extra space to package components. Along with the common choice of DC motors, there have been robotic hands that are actuated with hydraulic actuators and pneumatic air muscles (Akyüreket al., 2014; Shadow, 2013). Extrinsic systems must transmit force over the distance between the actuators and the actuated links in the system, adding some more complexity to the design. Typically this is accomplished through the use of flexible tendons which are routed through sheaths, pulley networks, or a combination of both.

2.2 Actuator Configuration

In robotic hand design there are many configurations of the number of actuators relative to the number of joints they must control. Depending upon the design goals regarding system size, power, complexity, application, control, etc. one particular configuration might be more desirable over the other.

2.2.1. M < N

The *M < N* configuration, corresponds to when there are fewer actuators than there are joints, is typically referred to as under-actuated. This type of system usually has the advantage of being simple in that there are a reduced amount of actuators that reduces complexity in both the physical design and the control system. Under-actuated systems can be designed with the ability to perform self-adaptive gripping, where the links of the system will move until they make contact with an object. The remaining links in the chain can continue to move until contact is made, eventually allowing all links to conform around an object. Four bar linkage mechanisms are commonly used in the design of under-actuated manipulators (Robotiq, 2014). Many robotic grippers have been designed in this configuration, featuring an impressive amount of compliance (Dollar & Howe, 2010). Prosthetic hands are also commonly designed in the *M < N* configuration for the aforementioned advantages (Belter, 2013).

2.2.2. M = N

A fully actuated *N* actuation scheme is classified by having a single actuator to drive each joint. In the case of a double-acting actuator, the joint can be driven in either direction. In the case of tendon-based force transmission, special care must be taken to keep the length and tension of the tendons constant. If these conditions are not maintained, backlash can affect the performance of the system. Often to maintain tension, additional hardware such as cams, springs, etc. are required, introducing additional complexity to the design. Another case of an *N* actuation scheme is having an actuator that applies force in one direction, and relies on an elastic element, such as a spring, to passively provide the return force in the opposite direction. This arrangement requires an actuator that can be back-driven and the elastic elements must provide adequate return force for a quick response.

2.2.3. M > N

Systems that possess more actuators than joints are classified as *M > N* systems, or also referred to as redundantly actuated.

2.2.3.1. M = 2N

A fully actuated *2N* actuation scheme is designed with two actuators per joint, allowing for the joint to be controlled in either direction. Analogously, this is very similar to biological muscles which only provide force in tension, so antagonistic-agonistic pairs of muscles are necessary to provide movement in opposite directions of each other. In robotic systems, one motor acts as the antagonistic actuator and the other as the agonistic actuator. Controllability of the system is very good in this arrangement. The clear disadvantage of this actuation scheme, in comparison to the others, is the increased size and weight due to the additional actuation, as well as the increased complexity of the control system.

2.2.3.2. M = N + 1

The *N + 1* actuation is considered to be the most biomimetic schemes as it most closely emulates the tendon system of the human hand (Melchiorri, 2008). In the simple

case of two consecutive links and joints, there is an actuator for each that pulls in one direction, and then on the distal most link, there is an actuator applying force in the opposite direction. In this configuration, the motions of the actuators are all coupled. Due to the coupled movements, the control system must compensate for this. This arrangement has the disadvantage of some added complexity, in both mechanical design and control, over some of the other schemes. Due to the coupled nature of the system, in the event of one of the actuators failing, the system will not be able to function.

2.3 Overview of Actuation Technology

Actuator type is a very crucial design parameter in robot hand design, as performance, cost, size, and controllability are all dependent on this choice. For the majority of robotic hand designs, the actuators typically are either DC motors, hydraulic, or pneumatics. In our survey of 58 designs, brushed DC motors were the most prevalent of the four.

2.3.1. DC Motors

Electric DC motors are an extremely popular choice for robotic actuation. DC motors operate with approximately 90% efficiency, provide a decent power density, and are considered reliable. Position and velocity control of DC motors is very good making them the logical choice for applications demanding precise control. Additional hardware, such as gearheads or harmonic drives, as well as force transmission components are often necessary.

2.3.1.1. Brushed DC motors

Brushed DC motors are one of the most common actuator choices in robotic hand actuation. Some of the key advantages of this motor type is that they are considered to be reliable, inexpensive, and easy to implement and control. The disadvantages of this type of actuator stems from moving contact of the brushes requiring maintenance for the mechanical wear from extended use. From a performance standpoint, as speeds increases, torque suffers due to the friction between the commutator and brushes. Other disadvantages also include heat dissipation which occurs because the armature produces heat which is insulated by the air gap between the stator and itself. Arcing in the brushes can occur causing electromagnetic interference (EMI).

2.3.1.2. Brushless DC (BLDC) motors

Brushless DC motors differ from brushed motors in that they have contactless commutation, which is controlled electronically. This motor type offers superior torque-speed characteristics over brushed DC, where a loaded motor can run continuously, up to its rated speed and torques. Additionally, the issues stemming from mechanical wear are eliminated with the brushless design. The operation of a BLDC is quieter than a brushed DC motor. Because of superior heat dissipation from the windings being on the stator, the size of a BLDC motor is reduced compared to a similar brushed motor. BLDC motors are at a disadvantage over brushed DC motors when cost is an issue, as they are more expensive to manufacture and the controllers can also be equally expensive. Control of BLDC motors is more complex than it is for brushed DC motors.

2.3.2. Pneumatic Air Muscles

Pneumatic air muscles (PAMs), sometimes called McKibben muscles, are a common actuator type that mimic the function of human muscles. The actuators are typically comprised of a bladder surrounded by a woven mesh shell. The PAMs are connected to a system complete with control valves and an air supply. When inflated, the PAM expands radially and contracts axially. With two PAMs, antagonistic and agonistic movement can be created to move a joint in two directions. PAMs themselves are lightweight and can provide substantial force. Because of the compressible nature of air, these actuators have compliancy which makes them safe for use around humans (Tuffield, P., & Elias, H., 2003). However, PAMs have shortcomings such as difficulty in accurate position control and friction and stiction due to the non-linearity due to the compressibility of the air (Ahn & Yokota, 2005). Portability is a shortcoming of systems containing PAMs because of the necessity of being connected to an air supply and valves.

2.3.3. Hydraulics

Hydraulic actuators are similar in principle to pneumatic actuators, except they utilize a pressurized incompressible liquid as the working fluid. Hydraulic actuators can apply much more force than pneumatic actuators, possessing the highest power to weight ratio of the mentioned actuation methods. Because they are mechanically stiff systems, the system response is good, but they have very little compliancy. Like pneumatics, additional hardware such as pumps, reservoirs, hoses, cylinders, control valves, etc. are necessary for actuation, making portability difficult. Maintenance is important as the hydraulic fluid can leak as well as become contaminated, resulting a loss in performance.

2.4 Overview of Sensing Technology

2.4.1. Position Sensing

Position sensors are necessary for providing position and velocity feedback in a control system, allowing the position of the robot's joints as well as the motor shaft position to be known.

2.4.1.1. Hall Effect

Hall Effect sensors output a change in voltage proportional to changes in the magnetic field as a permanent magnet is displaced, either in an angular or linear fashion. In most cases, this sensor type is used for the absolute angular position of a joint, where a magnet is mounted to the joint rotational center of one link and a Hall Effect IC is positioned onto another link. Hall Effect based ICs can be digital or analog. This sensing is contactless as the magnet and the sensor do not touch which eliminates the concern for physical wear and tear. The friction is only limited to that of the bearing friction in the joint. Because of its precision and low profile size, it is one of the most popular choices for position sensing in robotic hands.

2.4.1.2. Optical

A popular choice for position measurements is the optical encoder. Optical encoders are sold in linear and rotary configurations, with rotary optical encoders being

the most popular, especially for measuring motor shaft position. A rotary optical encoder consists of a code disc that spins with the shaft of the motor, an LED, and a photosensor. The code disc has radial markings or patterns which create an interruption of the LED light to the photosensor, as the disc rotates. These interruptions are counted in order to resolve shaft position. Typically, optical encoders are incremental, which only measures relative position. The position is indexed from a starting position. Absolute encoders are available, where the code disc has several unique patterns and several photosensors to measure the absolute positon. Unlike incremental encoders, homing the sensor to a starting reference position is unnecessary. Encoders for the most part are used for motor position measurements. Because of the nonlinearities due to force transmission component such as friction, tendon slack, etc., a direct joint position alone may not be completely reliable. More recently, researchers have created simple, low cost optoelectronic position sensors, from a conventional LED and phototransistor pair, which provides direct absolute joint position of a finger (Melchiorri et al, 2013). These sensors possess good linearity and are impervious to electromagnetic interference. Optical based sensors require very little conditioning as well, making them easy to implement.

2.4.1.3. Potentiometers

Potentiometers, which measure a change in resistance, are commonly used for low-cost position feedback. The implementation of potentiometers is quite simple and they offer a high amplitude output signal. The integration into a system can be complicated, as they must be rigidly connected to the joint that will be measured. For this reason, potentiometers can incorporate additional friction into the system. Though considered reliable, potentiometers can physically wear out, requiring replacements. Additionally, the size of the potentiometer can be an issue when integrating them onto a joint, because even low profile potentiometers are typically larger than the setup of a Hall Effect based sensing system.

2.4.2. Force and Torque Sensing

2.4.2.1. Strain Gauge Based

In robotic hand design, many strain gauge based sensors have been devised and implemented for detecting force and torque. They are inexpensive, compact, and precise, measuring up to 0.1 degrees of deflection (Konux). Disadvantages of strain gauges include needing to be manually applied and frequently recalibrated. The basis for many designs is the application strain gauges to an elastic element that is subjected to force and/or torque. The deformation of the element is then correlated to a change in resistance, and a Wheatstone bridge circuit can be devised to output a voltage. In the design of tendon driven robotic hands, monitoring tendon tension is commonly practiced. Often times, tension sensors are fabricated by bonding strain gauges onto an elastic element, and placing the element in series with the tendons (Bridgwater et al., 2012). In other designs, the strain gauges are placed onto the support structures of an idler pulley (Jacobsen et al., 1986), and the support structure will deflect in response to the change in tendon tension. In combined force-torque sensors, typically used as fingertip sensors, special elements structures are designed containing several strain gauges, allowing for 6 DoF of force and torque sensing (Butterfass, Hirzinger, Knoch, & Liu, 1998).

2.4.2.2. Force Sensing Resistors

Force sensing resistors (FSR) are sensors made from a polymer thick film or an ink, which changes its resistance when an external pressure is applied. Because of their thin profile, ability to be fabricated in various shapes, and low cost, FSRs are an attractive option for sensing force in robotic systems. FSRs are known to have low accuracy.

2.4.3. Tactile Sensing

Similar to how the skin on the human hand provides sensory feedback, tactile sensing allows a robotic system to better perceive objects during manipulation as well as environmental conditions. Sensing vibration, pressure, temperature, texture, object presence, object shape and size, slip, and grasp stability and force are components of the sense of touch. Traditional synthetic tactile sensor designs are based on a wide variety of transduction principles: piezoresistive, piezoelectric, capacitive, resistive, optoelectric, magnetic, inductive, and the quantum tunneling effect. The sense of touch is so complex, that there is not just one type of transduction that can accomplish all of the components of touch (RobotCub, 2005). More comprehensive reviews on tactile sensing in robotic hands can be found in (Yousef, Boukallel, & Althoefer, 2011) and (Saudabayev & Varol, 2015).

2.5 Number of Fingers

In robotic hand design, there are several key mechanical, kinematic, and sensory system features that contribute to a design's dexterity and degree of anthropomorphism. Kinematic properties such as the total number of fingers, joints, active DoF, active wrist DoF are documented in Table 1. The number of fingers in a design are a key metric in anthropomorphism and dexterity, where obviously the hands that possess 5 fingers best mimic the human hand. However, it is not an end-all and be-all criterion, as many anthropomorphic designs feature fewer fingers. Two of the most classic and well-studied anthropomorphic hand designs, the Stanford/JPL hand (Pellerin, C., 1991) and the UTAH/MIT Hand (Jacobsen et al., 1986), possess 4 and 3 fingers, respectively. Even years after their development, studies were being carried out using them as platforms in manipulation research (Challoo, Johnson, McLauchlan, & Omar, 1994; Wright & Stanisic, 1990). Hand designs such as the DLR Hand 1, DLR Hand II, and DLR-HIT Hand were developed with 4 fingers in order to meet a goal of miniaturizing all of the sensory and actuation components to fit in a system that closely approaches the performance and overall size of a human hand (Butterfass, Grebenstein, Liu, & Hirzinger, 2001; Butterfass, Hirzinger, Knoch, & Liu, 1998; Liu et al., 2007). Additionally, by omitting a finger or two, an entire system can be simplified, not only physically but also in terms of the control system. The inventor of the Stanford/JPL Hand, John Salisbury, points out that "giving a robot more fingers and motion freedoms does not solve problems of planning and perception in the face of uncertainty," meaning that emphasis on sensory systems and controls are imperative in hand development (Pellerin, 1991).

2.6 Total number of joints, actuated DoF, and actuators

Among the surveyed hands, the total number of joints, number of actuated DoF, and actuators are key mechanical parameters that differentiate the designs from each other in their dexterous capacity. In general, increasing the number of each of these will lead to more capable and dexterous hand, however, there are often alternate objectives in robotic hand design. Some robotic hands designs aim to replicate the human hand functionality as closely as possible such as the 5 fingered Shadow Dexterous Hand by the Shadow Robotics Company, which features 36 pneumatic air muscles and has 20 active DoF in the hand almost matching the 22 DoF of the human hand (Kochan, 2005). The Robotics Institute at Carnegie Mellon developed a highly anatomically correct robotic hand called the Anatomically Correct Testbed (ACT) Hand (Weghe, Rogers, Weissert, & Matsuoka, 2004) that recreates the complex web structure of the human tendon network, requiring 6 actuators each for the middle and index fingers and 8 for the thumb. Often times, these numbers are indicative of the type of application of the hand. For example, prosthetic hands (Belter & Segil, 2013; Pons et al., 2004; Zecca et al., 2004) can only accept a small number of signals from EMG, so they tend to have a fewer joints in total and fewer actuators. The TUAT/Karlsruhe Hand (Fukaya, Toyama, Asfour, & Dillmann, 2000) contains a total of 20 joints that are actuated by a single motor, seeking to create a highly self-adapting grasping hand. Finally, as mentioned previously regarding the number of fingers, the goal of the some systems is to do more with less, placing an emphasis on the development of other aspects of design.

2.7 Force Transmission Hardware

2.7.1. Tendon Driven

2.7.1.1. Tendon-Sheath

Extrinsically actuated robotics hands are commonly tendon-sheath driven in order to transmit motion over a distance (Caffaz, Casalino, Cannata, Panin, & Massucco, 2000; Lotti et al., 2005; Salisbury & Craig, 1982). The attractiveness of the system lies in the ability to locate the actuators outside of the boundary of the hand, allowing for more flexibility in the finger and palm design. A tendon cable is affixed to an actuator and routed through a tubular, flexible conduit called a sheath, which terminates near the actuated link. Special care must be taken when implementing tendon-sheath transmission as to minimize sharp bends in the routing. Nonlinear behavior, such as hysteresis and backlash, due to tendon compliance as well as friction between the tendon and sheath are inherent (Kaneko, Yamashita, & Tanie, 1991). These issues, however can be overcome through compensation in the control system (Palli & Melchiorri, 2006).

2.7.1.2. Tendon-pulley

Similar in principle to tendon-sheath transmission, the tendon can be routed over network of pulleys which serve to reduce friction. This transmission method is most commonly found in extrinsic designs (Jacobsen, Iversen, Knutti, Johnson, & Biggers, 1986), but is featured in several intrinsic designs (Che & Zhang, 2010; Martin & Grossard, 2014; Quigley, Salisbury, Ng, & Salisbury, 2014; Zecca et al., 2004). Networks of idler pulleys can be designed and optimized to reduce friction and improve performance. While often times, pulleys are constrained to a particular cartesian plane,

Treratanakulwong, Kaminaga, and Nakamura created an optimized orientation of idler pulleys inside the 3D space palm of their underactuated design to minimize friction in their underactuated design (Treratanakulwong, Kaminaga, & Nakamura, 2014). While pulleys offer the benefits as shown, design complexity often increases proportionally with their integration, as seen in the UTAH-MIT Hand (Jacobsenet al., 1986) which contains a total of 184 pulleys in its hand and wrist. Coupling between serial joints is occasionally an issue associated with tendon-pulleys that must be overcome in control, but through careful design, pulleys can be arranged to overcome the issue, as done in the RoboRay Hand wrist design (Kim et al., 2014).

2.7.2. Gears

The use of gears is simple approach to force transmission. It is common practice, especially in intrinsic hand designs, to use a differential bevel gear arrangement (Butterfass, Grebenstein, Liu, & Hirzinger, 2001; Choi, Lee, Choi, & Kang, 2006; Mahmoud, Ueno, & Tatsumi, 2010; Mouri, Endo, & Kawasaki, 2011; Ueda, Ishida, Kondo, & Ogasawara, 2005). In the effort to allocation space most efficiently, motors are typically placed longitudinally with their driven finger segments or in the palm and bevel gears redirect the motion by 90°. The NTU Hand (Lin & Huang, 1998) is a gear driven intrinsic design that utilizes a gear train rather than a differential bevel gear setup, which allows decoupled actuation of its finger segments. In a case such as this, the complexity of the system is quite high as each segment contains at least 10 gears inside. Geared systems have a very high stiffness, which depending on the application may or may not be advantageous. An advantage of gears is their potential for bidirectional operation. However, backlash is an inherent issue with gear driven systems, where bevel gears have a large amount (Namiki, Imai, Ishikawa, & Kaneko, 2003). With high quality gears and a capable control system, the effects can be minimized. Other potential issues to consider with gear transmission, is their weight and in some cases the noise during operation. In an application such as prostheses, noise could be an unpleasant to a user.

2.7.3. Linkages

Linkage systems are a simple and robust method of force transmission. Linkages commonly are synthesized into four bar linkage mechanisms, which are typically used for coupling the motion between links. Typically four bar linkage mechanisms are used to couple PIP and DIP finger DoF to emulate the behavior seen in the human finger (Kurita, Ono, Ikeda, & Ogasawara, 2009; Mouri, Endo, & Kawasaki, 2011; Thayer & Priya, 2011; Ueda, Ishida, Kondo, & Ogasawara, 2005). Linkages can be synthesized to fit into a specified form factor, as well as be synthesized to follow a specified trajectory. Razo and Sanchez developed a 3 DoF mechanical finger comprised of a slider-crank mechanism and two serial four bar linkage mechanisms, synthesized from the ranges of motion and dimensions of a human finger (Prudencio, Morales, García, & Lozano, 2014). The design is able to closely match the trajectory of a flexing finger. Self-adaptive grasping is another design objective that can be accomplished through the use of linkages. Complex branching linkages are also featured in the palms of self-adaptive, underactuated grasping hands, such as the Belgrade/USC Hand (Bekey, Tomovic, & Zeljkovic, 1990) and the TUAT/Karlsruhe Hands (Fukaya, Toyama, Asfour, & Dillmann, 2000; Fukaya, Asfour, Dillmann, & Toyama, 2013). Self-adaptive systems allow finger

segments to stop upon making contact with an object, while allowing the others to continue moving until contact is made. The resulting pose will envelop the object in a secure grasp. Hands such as these have among the lowest number of active DoF.

2.7.4. Belts

Belt driven transmission is accomplished through the use of toothed pulleys with their motion coupled by timing belts with matching teeth. One pulley is driven by the actuator and the other is driven. In our survey of the literature, belt driven designs are far less common than the other methods. Similar to gear transmission and tendon-pulley transmission, the speed reduction can be modified based on the size of the pulleys. Belts are lightweight and occupy less space than gears and linkages. In the SKKU Hand II (Choi, Lee, Choi, & Kang, 2006), the PIP and DIP joints motion are coupled using a timing belt, and because of the low volume of the belt, plenty of space is available for sensorization. In the designs of the DLR/HIT Hand I (Liu et al., 2007), DLR/HIT Hand II (Liu et al., 2008), and the DLR Hand II (Butterfass, Grebenstein, Liu, & Hirzinger, 2001) the actuator and the harmonic drives could only be packaged in the finger in a parallel arrangement, necessitating the use of timing belts. In a case such as this, belts are advantageous in their quiet operation, compliance, and weight reduction over linkage and gear alternatives.

2.7.5. Elastic elements

Elastic elements such as extension springs, torsion springs, strips of rubber, etc. are typically found in robotic hand design to passively provide return force in finger flexion, as well as compliance. By utilizing an elastic element in this manner, both physical designs and control can be simplified. Torsion springs are a common elastic element which are compact and can be placed directly at the joint center of rotation. The RCH-1 (Roccella et al., 2004), GCUA Hand II (Che & Zhang, 2010), Low Friction Tendon Driven Robot Hand (Treratanakulwong, Kaminaga, & Nakamura, 2014), iCub Hand (low cost) (Davis, Tsagarakis, & Caldwell, 2008), and the DART Hand (Thayer & Priya, 2011) are designs that utilize torsion springs in this manner. The Meka H2 compliant hand used a strip of rubber along the top of each finger (Meka, 2009). In the UB Hand III, coiled spring sheaths routed along the length of fingers, also cleverly served as elastic hinges at each joints (Lotti et al., 2005). Because the joints were not constrained transversely, the fingers would unintentionally move in this plane, under transverse loads. In the development of the UB Hand IV, living hinges were considered at each joint in spiral and helical geometries, reducing the need for individual components as well as assembly (Melchiorri, Palli, Berselli, & Vassura, 2013).

In traditional robotic design, stiff systems have been desirable for precise, stable, and high bandwidth control, however, these systems do little to absorb energy in the event of unexpected collisions, have high inertia, and can pose a danger to people and objects (Pratt & Williamson, 1995). Elastic elements are frequently implemented to create Series Elastic Actuators (SEAs) which introduce compliance into a robotic system through the integration of an elastic element, often a spring, between the motor and the driven link. The Meka H2 Compliant Hand (Meka), the IRIS Prosthetic Hand (Casley et al., 2014), and the hand of the DLR Hand Arm System (Grebenstein et al., 2011) utilize elastic elements to provide series elastic actuation.

2.8 Design Purpose

In this survey, the designs are classified in one or more of the main design purposes: research platform, prosthesis, or platform end effector. Many designs serve as research platforms in order to test control and grasping schemes. Often times, the system does not need to be compact in size, have a human-like appearance, or have a method or interface to be integrated with a larger system. A research platform frequently is a device that stands alone, so human-like appearances and size are not prioritized. Conversely, a prosthetic hand design will typically aim to embody all of those characteristics. Robotic end effectors will function as a subsystem of a larger platform, requiring the ability to integrate with another system, both structurally and electronically. They will need to have a compact enough design to some degree as the hardware must fit onto the larger platform, but does not necessarily need have a humanlike appearance.

2.9 Wrist, Forearms, and Integration

The presence of wrists and forearms in a design, and mechanical integration with other systems, are often interrelated. The presence of articulated wrists in designs was examined, as they increase the level of functionality and anthropomorphism. The majority of designs in the survey did not feature a wrist. Some robotic hand designs, such as the Schunk SVH (Schunk), are commercially available end effectors that are not designed with articulated wrists, because they intended to be integrated with industrial robots that typically will have the wrist DoF built-in. In many cases, a robotic hand designs does not necessitate an articulated wrist nor integration such as standalone research platforms investigating grasping techniques because it is an unnecessary addition of complexity. In the field of prosthetics, there is a paucity of designs that incorporate articulated wrists, most likely because the control of prosthetics is not sophisticated enough to process the wrist movement (Resnik, Klinger, & Etter, 2014). In literature only two prosthetic devices featured articulated wrists, with the Modular Prosthetic Limb (Johannes et al., 2011) possessing flexion/extension, radial/ulnar deviation, and forearm pronation/supination and the DEKA Arm Hand (Resnik, Klinger, & Etter, 2014) with flexion/extension and radial/ulnar deviation. Many robotic hands were designed to be integrated with other systems, such as humanoid and industrial arm platforms. The Dexterous iCub Hand (Schmitz et al., 2010) as well as its low cost counterpart (Davis, Tsagarakis, & Caldwell, 2008), were designed as end effectors for the iCub humanoid platform, which was modeled after a 2 year old child, for researching cognitive processes. In 1999 (Lovchik & Diftler, 1999) and then again in 2012 (Bridgwater et al., 2012), NASA developed robotic hands, complete with articulated 2 DoF wrists, capable of human-like strength for their Robonaut platform which was designed to work alongside humans as well as perform tasks deemed too dangerous for humans.

2.10 Cost

Data regarding the cost of robotic hand systems is not presented in this survey due to how few authors and designers report it. However the magnitude of cost can be inferred by examining a design. The use of BLDC motors, harmonic drives, machined metal fabrication, and number and type of sensors, for example, can all imply a high cost.

With the advances of rapid prototyping in the past several years, there have been several low cost designs found in literature (Davis, Tsagarakis, & Caldwell, 2008) (Open Hand Project, 2014) (Slade, Akhtar, Nguyen, & Bretl, 2015). Many of these designs possess a low number of active DoF, typically less than 10 and rely on under actuated grasping. Low cost systems also typically employ COTS actuators and sensor components. Some designs attempt to reach a high level of performance, with high DoF designs (Palli et al., 2014; Thayer & Priya, 2011).

2.11 Discussion of Select Designs

Out of the 68 designs that are covered in Table 1 and Table 2 there are several key designs which embody the state of the art and are discussed in more detail this section. These selected designs each embody the state of the art in anthropomorphic robotic hand technology.

2.11.1. Shadow Dexterous Hand (2005)

The Shadow Dexterous Hand (Figure 1) by the Shadow Robot Company is a well-known robotic hand platform that is commercially available. According to the official documentation for the Shadow Dexterous Hand, it has been utilized in the research of grasping and manipulation research, brain-computer interfaces, neural control, the handling of dangerous materials, as well as quality control (Shadow, 2013).

Initially designed to closely replicate the size and kinematics of an average human male's hand, it features 20 actuated DoF and 4 underactuated DoF. Finger flexion/extension motions are provided with an $N + 1$ tendon-sheath actuation system. The index, middle, ring, and pinky possess 2 flexion DoF and 1 extension DoF for the MP and PIP joints, as well as an abduction/adduction DoF. The motion of the DIP joint is kinematically coupled to the actuated PIP joint. To simplify the design, the fingers are identical modules but offset along the palm to locate the fingertips at the proper anthropomorphic locations. With 5 active DoF, the thumb very closely mimics the movements of the human thumb. A unique feature of the Shadow Dexterous Hand is an actuated DoF of the palm that mimics the function of the opponens digiti minimi muscle, which allows the metacarpal of the pinky to oppose the thumb. The forearm unit is equipped with a 2 DoF wrist, to increase potential dexterity in manipulation.

The Shadow Dexterous hand and forearm unit contains a total of 129 sensors (Shadow, 2013). Hall Effect sensors located in each finger joint precisely measures the absolute joint position. The fingertip of each digit is standardly equipped with pressure sensors, though the integration of the SynTouch BioTac fingertip (Fishel, Lin, & Loeb, 2013), which senses force, vibration, and temperature, is offered as a premium option. The hand can be controlled using PID position, force, or torque control. Strain gauge based tendon tension sensors provide feedback for force control. In the DC motor actuated version of the system, sensors monitor the operating temperature and current of the motors. For applications demanding compliant operation, the Shadow Dexterous Hand is also sold with the option of pneumatic air muscles for actuation, where 40 air muscles drive the hand movements using pressure or position control. Being an extrinsic design, all actuation hardware as well as electronics such as drivers and controllers are constrained within a non-anthropomorphic forearm. The entire system is capable of being integrated with common industrial robotic arm systems. The Shadow Dexterous Hand

can be purchased in left and right hand configurations. A 4 fingered version called the Hand-Lite is also offered, as a smaller and more inexpensive alternative to the full fingered version. However, at a price of around £100,000 ($133,128.00) (Shadow Robot: Wave Hello, 2010) the Shadow Dexterous Hand is quite expensive.

Figure 1. The Shadow Dexterous Hand (Shadow, 2013). Used under fair use, 2016 (see Appendix A).

2.11.2. DART Hand (2011)

The DART hand (Figure 2), is a low cost, high DoF robotic hand prototype that was developed by the Center of Intelligent Systems and Structures (CIMSS) at Virginia Tech in 2011. As a preliminary objective, the DART hand was designed to type words on a computer keyboard, with future aspirations of expanding its application into assisting elderly or disabled people with activities of daily living. The dexterity of the DART hand has been demonstrated through typing 20 words per minute on a computer keyboard, compared to a human's 33 words per minute (Thayer & Priya, 2011).

As an extrinsically actuated design, there are 19 low cost servomotors packaged into the forearm. The hand possesses 4 actuated DoF for the thumb, 3 actuated DoF for each fingers, a 2 DoF wrist, and 1 DoF for elbow rotation. Each finger is capable of

flexion/extension of the MCP and PIP joints. The function of the metacarpal joint was replicated using a universal joint, to enable a flexion/extension and adduction/abduction. The flexion of the PIP joint is actuated by one tendon, while the extension DoF is completed using a torsion spring. The DIP joint of each finger is kinematically coupled to the PIP joint, allowing for the elimination of a motor and simplifying the control scheme of the hand. This underactuation is accomplished with a four bar linkage mechanism that was synthesized to follow the trajectory of a human fingertip. In order to carry out the task of typing words onto a keyboard, the hand was outfitted with analog Hall Effect sensors for joint position of the DIP joints and pressure sensors at the fingertips. The hand operates with a closed-loop control scheme in which the hand uses the Denavit-Hartenberg parameters to locate the desired keyboard key.

The DART Hand embodies one of the few high DoF, rapid prototyped robotic hands that have been developed. Though the cost is not explicitly reported, the structural components are rapid prototyped, and COTS servomotors are used for actuation, which indicate a lower cost when compared to other robotic hands. The DART Hand has demonstrated very impressive kinematic capabilities in its typing demonstration, but in the inspection of the design, it appears that it would be fragile in applications more physically demanding than typing.

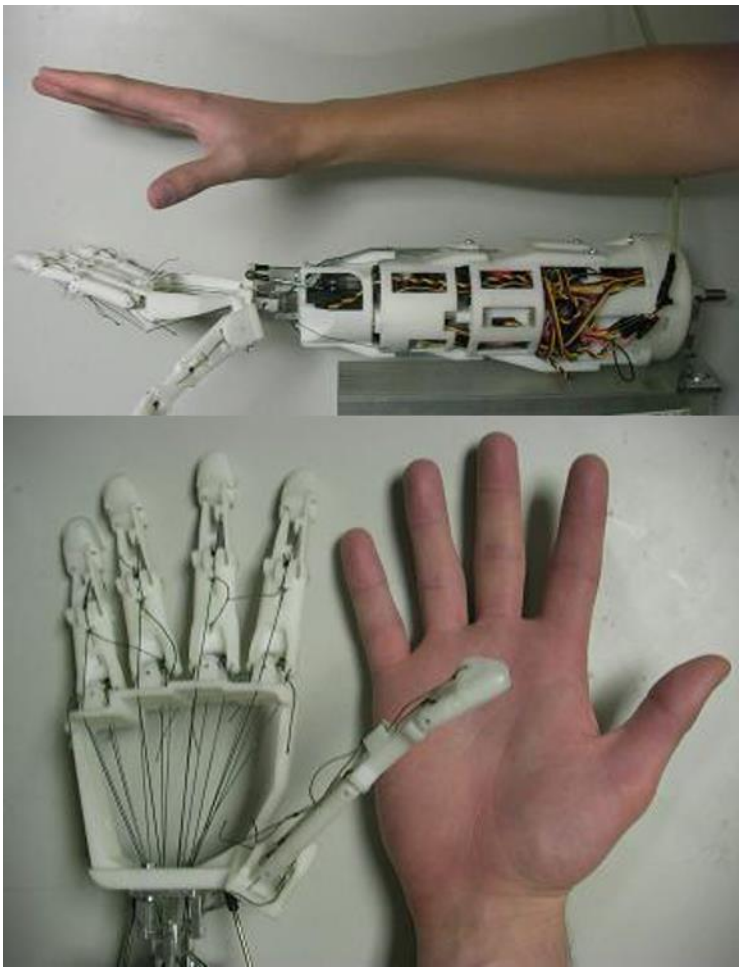

Figure 2. The DART Hand (Thayer & Priya, 2011). Used under fair use, 2016 (see Appendix A).

2.11.3. Modular Prosthetic Limb (2011)

The Modular Prosthetic Limb (MPL), shown in Figure 3, was a complete prosthetic arm and hand system developed under the Revolutionizing Prosthetics program sponsored by DARPA (Johannes et al., 2011). The goal of the program was create a state of the art prosthetic limb for maimed veteran patients with upper limb amputations. The MPL system is perhaps one of the most sophisticated and anthropomorphic hand designs to date. The MPL is not commercially available, and is primarily a research tool.

The total arm system is comprised of 4 upper arm motor drives and 3 wrist drives. The amount of joints in the limb can be altered to accommodate patients with varying levels of amputation. The complete system features 17 active DoF, and 26 DoF in total (Johannes et al., 2011). The thumb contains 4 active DoF and all other fingers have an active flexion/extension DoF with passively coupled, adaptive PIP and DIP movements. In the default hand configuration, the index finger has an abduction/adduction DoF, and there is a combined abduction/adduction DoF for the ring and pinky fingers.

Significant effort was taken to create component level standardization such as common motor drives and mechanical/electrical connections to simplify the fabrication and assembly, as well as maximize modularity of the system. The BLDC motor drives

were cleverly designed as self-contained units with their own embedded controllers, and packaged directly at each joint. The complete system has over 100 integrated sensors, including absolute position, contact, torque, joint temperature, 3 DoF accelerometers, and 3 DoF force sensors (McGee et al., 2014).

The Modular Prosthetic Limb has been the subject of two groundbreaking studies at Johns Hopkins Applied Physics Lab. In one experiment, a bilateral shoulder amputee subject was fitted with two MPL units and was able to control them by thought to complete tasks (Hopkins, 2014). This was made possible with a new surgical procedure called targeted muscle reinnervation that allows the nerves that used to control the missing limbs to be reassigned to existing nerves. In a second high profile experiment, a paralyzed subject, with microelectrode implants connected directly to the motor cortex of the brain, controlled the hand via a brain-machine interface (Bensmaia & Miller, 2014).

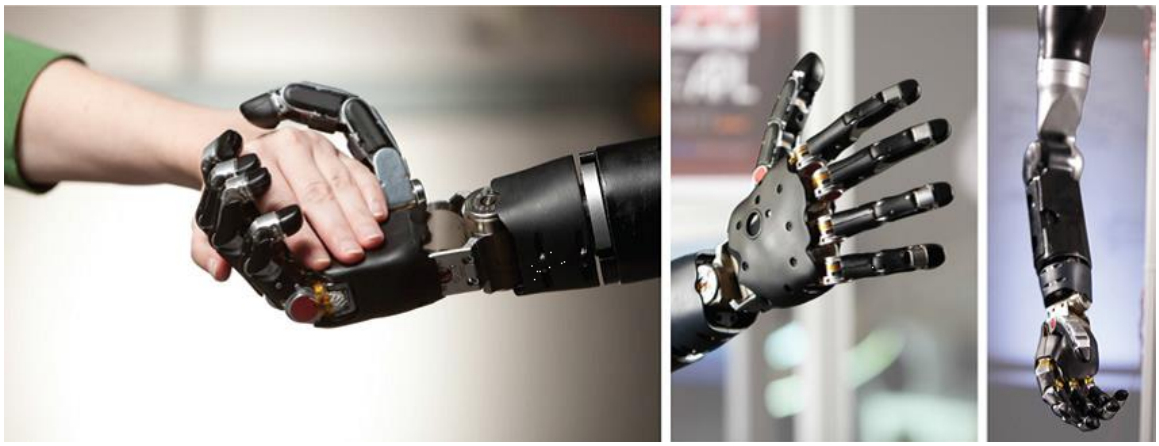

Figure 3. The Modular Prosthetic Limb (Wester et al., 2013). Reprinted with permission, © 2013 IEEE (see Appendix A).

2.11.4. DLR Hand-Arm System (2012)

Developed by the Institute of Robotics and Mechatronics at the German Aerospace Center in 2012, the DLR arm is an extremely sophisticated humanoid limb research platform designed to meet the objectives of human-like size and performance. The system is comprised of a 3 DoF shoulder, a 2 DoF wrist, and 19 DoF hand. A highly bioinspired variable stiffness actuation scheme was developed that mimics the elasticity of human muscle, tendons, and ligaments. Such elasticity will allow the robotic system to store energy which can serve as a protective measure in impacts to the system, by effectively decoupling the actuation from the driven link. In grasping and manipulation tasks, collisions with objects in the environment is unavoidable and often the downfall of many stiff robotic hands. Secondly, the ability to store energy can enhance the dynamic performance of the system, by using the stored energy to create acceleration on top of the motor's efforts, which can exceed the rated dynamic performance that would be achieved by the actuators.

The designers of the DLR Hand Arm sought to recreate the functionality of the human hand's anatomy as closely as possible, but modified with discretion to create a practical engineering solution. For instance, the MCP joints of the hand are classified as

condyloid joints, but due to the difficulty in practically creating and implementing this geometry, the approximate functionality can be derived from a hyperboloid shaped joint (Grebenstein et al., 2012). The hand kinematics are made up of a 4 DoF thumb, index, middle, and little finger and a 3 DoF ring finger. When the finger segments of the hand are overloaded, dislocation occurs in order to prevent further damage. Preliminary testing of the compliance has shown the hand's fingers withstanding blows from a 500g hammer, as well as a demonstration where the hand grasps a hammer and hammers nails into a board (Grebenstein et al., 2012). A unique 2 DoF wrist design provides flexion/extension and radial/ulnar deviation, actuated with 4 actuators. The wrist is a spherical anti-parallelogram linkage mechanism, which allows for the tendons to be routed with minimal friction and elongation.

The hand of the DLR Hand Arm System is an extrinsically actuated design, with an extremely advanced forearm system that houses the actuators, force transmission hardware, and electronics. Similar to human muscles, antagonistic and agonistic (*M=2N* actuation) actuation provides the finger joint movements with two actuators, each with its own nonlinear compliant elastic element, which allow for the stiffness of the joints to be altered. In total, there are 42 ServoModules and 42 compliance mechanisms contained within the forearm. Each ServoModule is a miniaturized package containing the motor, harmonic drive wave generator, position sensors, motor controllers, and communications hardware. Due to the large amount of electronics packaged so tightly together in the forearm, a water cooling system is necessary for heat dissipation.

The design of the DLR Hand Arm system is one of the most advanced and robust extrinsic robotic hand designs to date. As a research tool, the DLR Hand Arm system is not available for purchase and the cost to build one is very high, estimated between 70,000 and 100,000 euros (Guizzo, 2011).

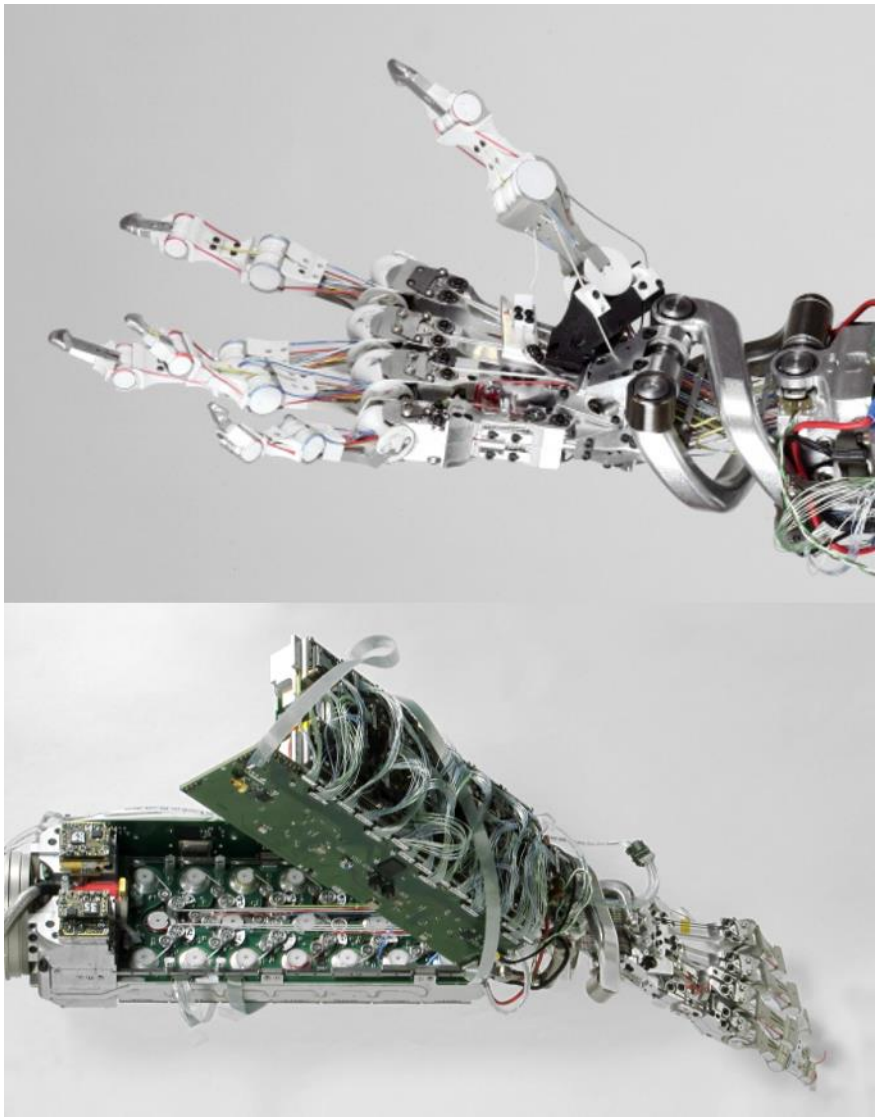

Figure 4. The DLR Hand-Arm System (a) hand and (b) forearm. (Grebenstein et al., 2011). Reprinted with permission, © 2011 IEEE (see Appendix A).

2.11.5. Robonaut 2 Hand (2012)

Robonaut is a teleoperated humanoid robot platform designed by NASA to work on the International Space Station, with its first generation developed in 1998 and then a second generation in 2012. For each generation of Robonaut, an anthropomorphic robotic hand was designed with the capability to perform tasks and manipulate tools that an astronaut would have to operate during a space mission, with human-like strength.

Designed as a joint effort between NASA and GM, the latest generation Robonaut Hand has 12 DoF in the hand and 2 DoF in the wrist. The design is an extrinsically actuated, packaging all of the motors and electronics in the forearm. The fingers of the hand are made up of a dexterous set of fingers for fine manipulation and a grasping set, which provide secure grasping on tools or other objects to be held. The dexterous fingers, comprised of the index and middle finger have 3 actuated DoF, made up of MCP abduction/adduction and flexion/extension and PIP flexion. The grasping

fingers have 2 actuated DoF, and the joints are underactuated using a 7 bar mechanism. The thumb of the Robonaut 2 Hand contains 4 actuated DoF. An *N + 1* actuation configuration is utilized for the fingers. To allow for easy maintenance, each finger is a removable module that can quickly be removed and replaced. Each finger is also non-backdrivable so that in the case of power loss, the hand will retain its grasp on the objects or tools it is holding. The effectiveness of this design's kinematics has been proven through demonstrating 15 of the 16 grasps found in Cutkosky's Taxonomy (Bridgwater et al., 2012).

Within the forearm of the Robonaut 2 Hand, there are 16 actuators for the hand, and 2 for the wrist, and 50 different sensors for joint position, tactile, and tendon tension sensing (Bridgwater et al., 2012). The actuation of the fingers are provided by DC brushless rotary motors with a lead screw to convert the rotary motion to linear. A flexible cable is attached from the actuator to the actuated link, providing a robust and easily maintainable method of force transmission. Each cable is equipped with a strain gauge based tendon tension sensor. The 2 DoF wrist of the system is a universal joint with offset axes that allows the flexible cables to pass through to the hand. The absolute joint position sensing is accomplished using a novel method involving an ellipsoidal shaped magnet that provides a linear signal between position and magnetic field, as opposed to the sinusoidal signal provided by a conventional ring magnet. On each phalange, strain gauge based tactile sensors provide 6 DoF force-torque sensing.

The Robonaut 2 Hand is an exceptionally robust and capable design in order to fulfil its duties as the end effectors of a platform involved in a highly demanding application. Because the Robonaut system was designed for a very specific purpose, it is a one-off system unavailable for purchase. The cost of the hand system alone is not published, but it can be assumed to be expensive as the Robonaut 2 system cost about $2.5 million to fabricate (First Steps: ISS's Robonaut, 2014)

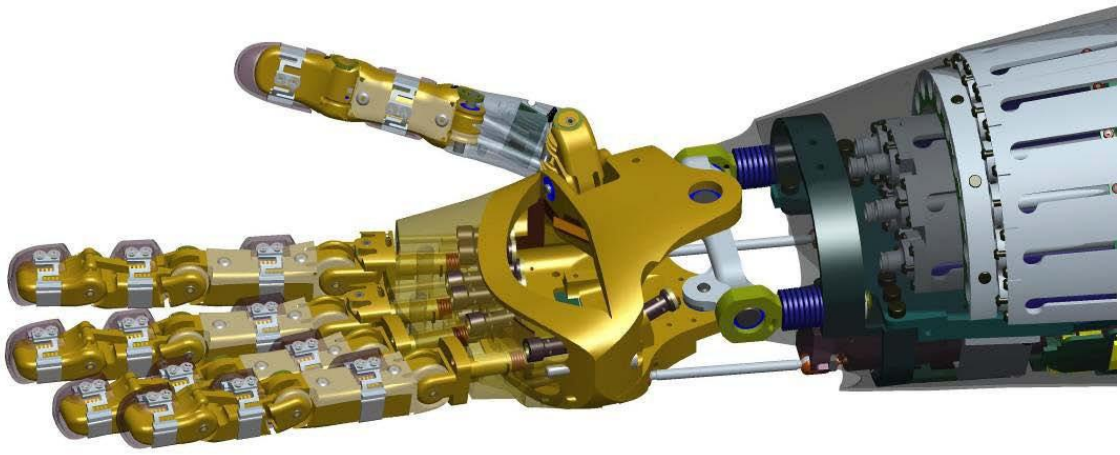

Figure 5. The Robonaut 2 Hand (NASA, 2010). Reprinted from NASA (see Appendix A).

2.11.6. DEXMART Hand (2014)

The DEXMART Project Hand (Figure 6) is one of the more prominent examples of low cost robotic hand platforms that seeks to replicate the function of the human hand. The design philosophy was to utilize FDM 3D printing to create an affordable, reprogrammable system that eliminates the need of traditional mechanical hardware such as bearing, fasteners, etc. This minimizes the time required for fabrication, assembly, and maintenance. It is the DEXMART Hand designers' opinion that a simplified yet capable robotic hand would be able to benefit from a high number of experimental trials (Palli et al., 2014). The designers believes that the users of more complex robotic hands must plan more carefully and ultimately resulting in less experimentation, for fear of damaging their systems which could result in long periods of down time and high expense.

The DEXMART hand is extrinsically actuated, with the motors being contained in the forearm. In total, there are 24 DC motors in located in the forearm to actuate the system: 4 to actuate the wrist, and 4 for each finger. The tendons route from the forearm to their termination points in the hand. In order to minimize motion coupling between the wrist and fingers, an offset was designed between the flexion/extension DoF and the ulnar/radial deviation DoF which allows the tendons to route through the center untouched. An *N+1* approach is used for the finger tendons, where there is a tendon each for the flexion of the proximal and medial phalanges, and then single tendon that performs extension for the whole finger. The medial and distal phalanges are kinematically coupled by a fixed length tendon and there is an antagonistic tendon to provide flexion. In the fingers, the tendons are routed closely to the center of each joint to minimize the coupling of serial joints. The design of the MCP joint allows for the fingers to dislocate when overloaded, in an effort to protect the rest of the hand system. Additionally, all 4 fingers have an abduction/adduction DoF, which is uncommon among most designs. Because of the friction associated with sliding tendons, the designers implement low level controllers for friction compensation (Palli & Melchiorri, 2006).

One of the more unique features of the DEXMART hand is its "twisted string" actuation. In this method of tendon actuation, two or more tendons are affixed to the shaft of a rotary motor, and as the shaft rotates the twisting strings results in linear motion (Palli et al., 2014). This method is advantageous as it functions as a speed reducer for the motors, thus simplifying the design and reducing cost as a motor gearhead is no longer necessary. It is considered virtually non-backdrivable due to the method's inherent high gear ratio. The sensory system of the hand is also particularly innovative, utilizing novel joint position, motor force, and tactile sensors developed from COTS photodetectors and LEDs. Optoelectronic sensors were decided on because of their resistance to EMI and their ease of signal conditioning.

Figure 6. The DEXMART Hand (Palli et al., 2014). Reprinted with permission, © 2014 SAGE Publications (see Appendix A).

2.11.7. Sandia Hand (2014)

The Sandia Hand (Figure 7) is 12 degree of freedom intrinsic robotic hand that was developed as part of the DARPA Autonomous Robotic Manipulation (ARM) program to create low-cost dexterous robot hands for completion of tasks in dangerous environments. Modularity was a key design focus in order to simplify the design, as well as allow the user the ability to configure it based on the desired application. The hand is made up of 4 identical finger modules attached to a base that serves as a palm, with one module serving the role of the thumb. Each finger module attaches to the palm by the use of magnets and springs contacts. In the event of an excessive external load on the fingers, the module can detach itself to prevent damage to the system. The hand can continue operating the hand until a new module is replaced into the palm. The connection interface for the module and the palm contains spring contact connections for power and communications, eliminating the need for wires. Each finger module provides 2 actuated DoF, for flexion/extension as well as abduction/adduction. The finger is under-actuated with the PIP and the DIP flexion/extension DoFs kinematically coupled to the proximal via internal steel cables and pulleys.

Rather than using convention joint sensing hardware that often occupies valuable structural space directly at the joint, the finger modules utilize MEMS 3D accelerometers in the base of the finger module, the proximal phalange and the distal phalange. The

information from these accelerometers is used in tandem with the signal of the motor encoders to control the position fingers.

For tactile sensing on the grasping surfaces of the finger, a novel method of embedding photosensors (LED-phototransistor pair) underneath multi-layer silicone skin was utilized. A clear layer of silicon covers the PCB (Quigley et al., 2014), followed by a white reflective layer. As force is applied, the displacement of the reflective layer varies the photocurrent, allowing for the detection of normal forces on the skin. Additionally, a strain gauge is located at the DIP joint of the finger, which gives a simple indication of external loads being applied at a location such as the back of the finger.

Another unique feature of the Sandia Hand is its visual sensing that allows the hand to sense objects to grasp and then how to do it. To minimize the position estimate errors over a long distance and the possibility of occlusion, the hardware is located directly on the hand as opposed to conventional locations such as the head of a robot (Quigley et al., 2014). Using a laser speckle generator, unstructured light is emitted onto the object allowing for the quick collection of depth data.

In an experimental evaluation, the Sandia hand was found to be very dexterous and capable in teleoperated manipulation. Grasping and in-hand manipulation testing was carried out with ordinary items and tools, such as a key, hammer, drill, screwdriver, wire cutters, a 15 lb. dumbbell, to name a few. For a cost of about $10,000, the Sandia Hand has great potential as a commercial product as well as an accessible research tool.

Figure 7. The Sandia Hand (Sandia National Laboratories, 2015). Used under fair use, 2016 (see Appendix A).

3. The development and design of a low cost dexterous robotic hand

In this section, we present the development and design of the DASH (Dexterous Anthropomorphic Sensor-Driven Hybrid-Actuation) hand and forearm system. The design goals were to create a low cost, dexterous robotic hand platform, while maintaining an anthropomorphic scale. As discussed previously, many robotic hand systems are quite expensive to purchase, and expensive and time consuming to develop and fabricate a custom design. With the increasing availability of rapid prototyping technology in the past several years, there have been a few low cost robotic hand designs to date. Many of these designs, however, fail to possess a high level of dexterity and contain a low number of degrees of freedom. Our design concept utilizes both extrinsic and intrinsic actuation, providing at total of 16 actuated degrees of freedom. The system is capable of being integrated with a humanoid robot platform. The DASH Hand serves as a low cost platform serving as a testbed for research in light duty teleoperation, manipulation, and sensor development, which will make robotic hand technology more accessible to prospective researchers.

3.1 The Human Hand

3.1.1. Anatomy

To achieve an anthropomorphic design, human hand anatomy was investigated. The hand is made up of 27 bones, which are classified by three groups: the carpals, the metacarpals, and the phalanges, shown in Figure 8. The 8 carpal bones are arranged in 2 rows and form the wrist, allowing for radial and ulnar deviation and flexion and extension. Proximal to the carpals, are the 5 metacarpals which make up the palm of the hand. Attached to the metacarpals are the phalangeal bones which make up the digits of the hand. Each finger is made up of a proximal, middle, and distal phalanges. The thumb is made up of a metacarpal bone and 2 phalanges.

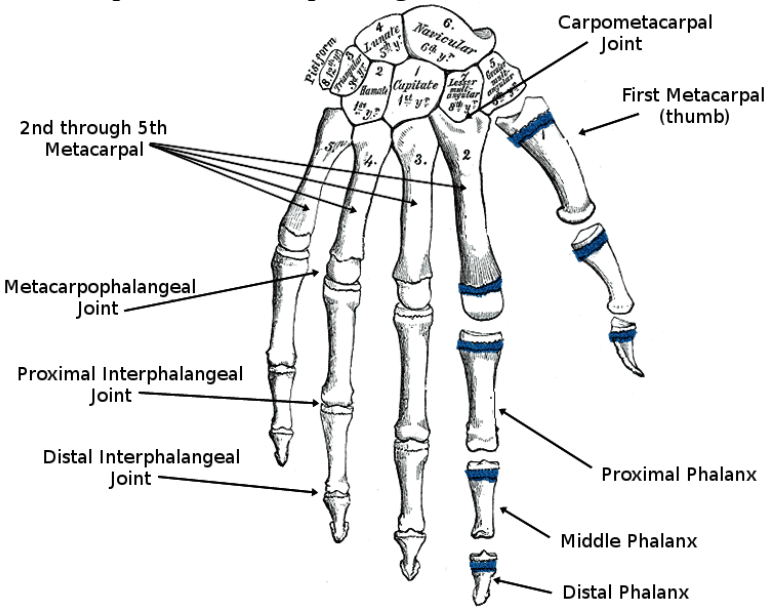

Figure 8. The bones and joints of the human hand (wpclipart). Used under fair use, 2016 (see Appendix A).

The articulations of the hand and wrist provide a total of 21 degrees of freedom. The metacarpophalangeal joints (MP) of the finger is basically a universal joint, having 2 DoF that allow for adduction/abduction as well as flexion/extension movements. The proximal interphalangeal (PIP) and the distal interphalangeal (DIP) joints are simple hinge joints that can only perform flexion/extension. The PIP and DIP joints of the fingers exhibit a linearly coupled motion (Nimbarte et al., 2008). The thumb has unique and complex articulations, in comparison to the fingers, which allows it to move into opposition with the fingers. The metacarpal of the thumb articulates at the carpometacarpal (CM) joint which has 2 degrees of freedom, like the MP, but also performs an axial rotational movement (Jones & Lederman, 2006).

There are a total of 29 muscles that are responsible for the movements of the hand and wrist. These muscles can be categorized as either extrinsic or intrinsic muscles. The majority of the muscles that control the hand are extrinsic muscles which are located within the forearm. These muscles attach to the two bones that form the forearm and are classified as extensor or flexor muscles. Approaching the wrist, the tendons extend from these muscles and attach onto the bony and ligamentous structures located in the hand (Taylor & Schwarz, 1955). The intrinsic muscles are the muscles contained in the hand and they are responsible for the movements of the thumb, little finger, adduction/abduction in the fingers, and extension in the fingers.

3.1.2. Human Hand Kinematics

Human hands are extremely capable in forming a wide variety of different grasps in order to meet the need for manipulating and handling objects of varying geometry and with differing levels of precision and grasp security. Human hand grasping has been extensively investigated in the realm of human hand robotics. An iconic benchmarking method of robotic hand kinematics is Cutkosky's Taxonomy which was developed in the 1980's through the study of machine shop workers' grasps when handling different materials and tools in their daily work (Cutkosky & Howe, 1990). The grasps of Cutkosky's Taxonomy are shown in Figure 9. In designing a robotic hand, simply mimicking the human hand as closely as possible is not the most efficient method, as the human hand is incredibly complex. Often times, hand designs are suggested to create a kinematic model and constraints that will be able to best accomplish the functions of the human hand (Grebenstein, Chalon, Herzinger, & Siegwart, 2010).

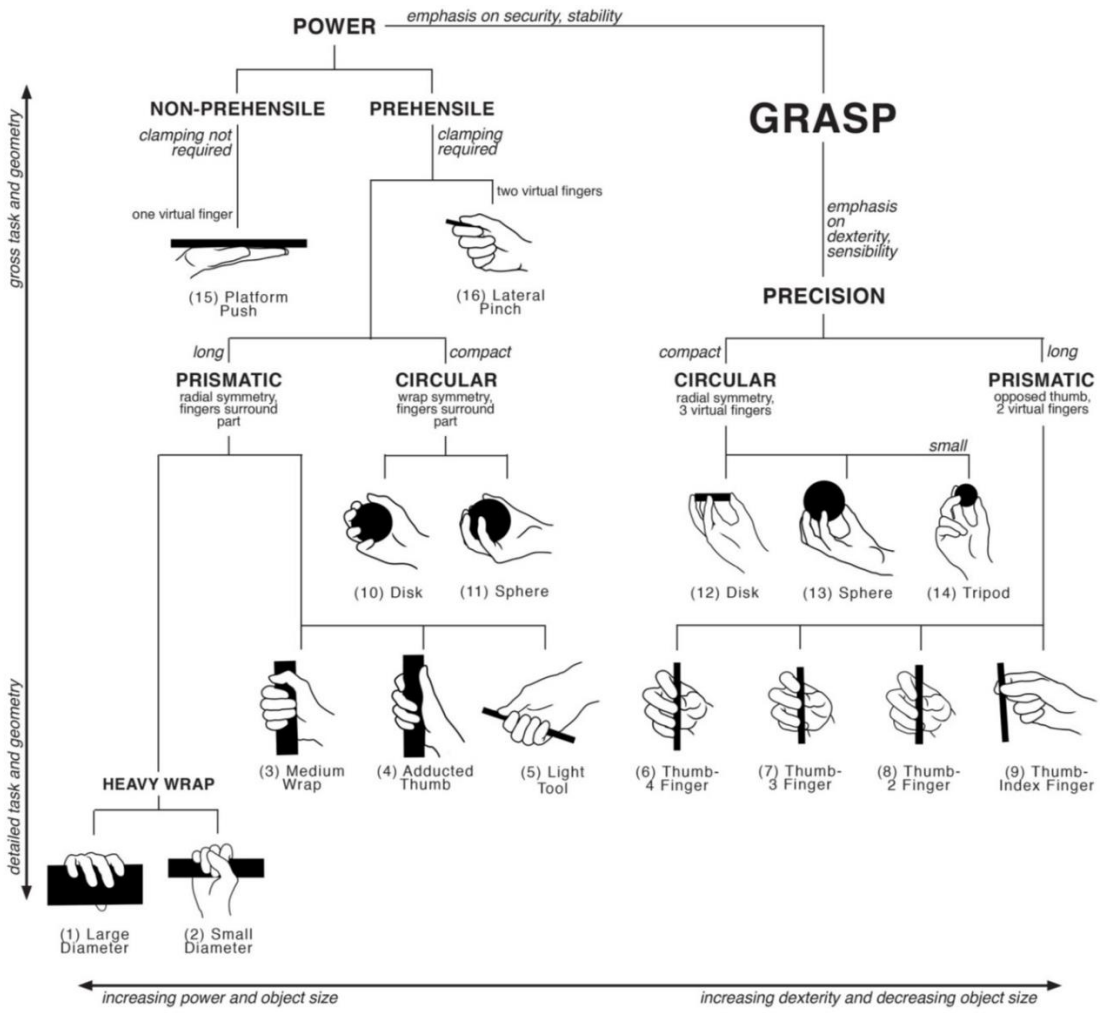

Figure 9. Cutkosky's Taxonomy of human hand grasps (Cutkosky & Howe, 1990). Used under fair use, 2016 (see Appendix A).

3.2 Forearm Design

In human anatomy, the forearm is the location of the muscles that are responsible for the majority of the movement of the hand and similarly, in this system, it was the chosen location for the motors. The forearm was the logical location for the motors due to the large amount of available space, while leaving the space in the fingers available for sensorization. In developing the design of the forearm, modularity was a crucial design attribute so that the system can be maintained and repaired with ease. Placing motors in a logical arrangement is critical to meeting this goal. It is especially challenging task when considering the space constraints are limited to be as close as possible to a human male's forearm. Because of the remote location of the motors relative to the hands, force transmission elements such as tendon sheaths and routing pulleys were required. The addition of this hardware to the forearm presents addition packaging challenges within the confines of the forearm system. When implementing tendon sheaths, special attention must be paid to the manner in which the cable is routed. Cable routing with numerous and/or sharp bends cause frictional losses that can hinder performance and increase difficulty in control. The tendon sheaths must also be routed in a way where the bending

is minimized by routing through the joint center of rotation of the universal joint of the wrist.

The presented design is designed to for versatility and capability, so it serves functions beyond containing the actuation for the hand portion. A fully articulated wrist with the strength to be able to support the weight of the objects being grasped. It was also desired that the forearm be able to attach rigidly to the upper body of a humanoid robot platform, serving as a dexterous end effector.

Consideration was given not only to the physical architecture of the system, but as well as the method of fabrication. Many designs are conventionally fabricated from machined metal, which can be both time consuming and expensive, especially in the event of changing design features. In the past several years with the increasing advances and availability of rapid prototyping machines, robotics designers can iteratively create, build, test, and redesign robots with very little turnaround. Because of this project's intended purpose as a research platform, rapid prototyping is a very advantageous fabrication method. The platform presented in this publication, was created primarily using an Objet Eden 260V 3D Printer. This particular printer is capable of printing in several different materials. In this project, VeroWhite and VeroClear plastics were chosen for the structural pieces, and TangoPlus rubber was also used. The design presented is versatile enough to be adapted for the more traditional fabrication operations of machining and casting, if so desired.

In order to maintain a compact human form factor, the use of tendon sheaths were considered. A tendon-sheath is a method of force transmission where a cable tension element is routed through a flexible outer tube. The ends of the outer tube can be fixed in a desired location. This method of force transmission provides a higher level of flexibility in actuator placement for a designer over other methods such as direct drive, gears, etc.

3.2.1. Actuation Methodology

The robotic hand was designed with almost all of the joints being actively actuated by cables pulling only in the flexion direction while springs force the joint to extend back to the neutral position (here forth referred to as CAFSE for Cable Active Flexion Spring Extension). Several other drive technologies were considered, including single motor bi-directional cables (SMBC), dual motor bi-directional cables (DMBC), and directly driving with motors placed at the joints (DD). Most human hand motions only require flexion of the finger joints, as seen in the Figure 9, and CAFSE allows the achievement of each of these grips. CAFSE was selected because it allowed the design to be simplified while still achieving all the functionality required. However, four joints in the hand require bi-directional motion and therefore do no use CAFSE: thumb rotation, index finger ab/adduction, pinky finger ab/adduction, and wrist movement. The first three are all driven by servos directly connected to the joint. The wrist, discussed in 3.2.6, is unique because the joint has two degrees of freedom and therefore uses a pair of motors connected to the hand using rods to produce motion. A comparative summary of the actuation methods is shown in Table 3.

Table 3. A comparison of the potential robotic hand actuation methods.

	CAFSE	SMBC	DMBC	DD
Required number of actuators	=	=	-	=
Size of motors possible	=	=	=	-
Backlash	=	-	-	-
Software complexity	=	=	-	+

3.2.1.1. CAFSE Advantages Over Bi-directional Cables

Actuating a joint using two cables, one for flexion and one for extension, can most simply be achieved by using one or two motors per joint. In the SMBC method, both cables would be connected to the motion of a single motor. Therefore, when the motor moves, one cable is pulled while the other relaxes. Alternatively, the DMBC method uses a separate motor to actuate the cables individually.

CAFSE overcomes several of the largest difficulties when using bi-directional cables. In both SMBC and DMBC, twice the number of cables is required for each joints which greatly escalates the complexity of routing the cables to the hand, especially through the wrist where it is important to reduce volume to avoid interferences from wrist motion. Both bi-directional methods can also suffer from issues with backlash due to the need to continuously keep tension in each cable for a joint. Without this tension, the finger would be susceptible to uncommanded motion and lag when changing motion direction. Moreover, the cables can be over tensioned, in which case the non-active in a motion (e.g. the extension cable during flexion movement) is constantly fighting the active cable, reducing the max joint torque and increasing the current needed to maintain the position. In SMBC, the two cables must be precisely tensioned through the mechanical structure and changes in that structure, including cable stretch or component wear, can degrade the tension over time. Because the cables are independently actuated, DMBC requires that the motors be tightly calibrated and controlled to avoid lash or over tensioning. CAFSE can be effectively zero backlash since the springs are always pulling in opposition of the motor. Strictly speaking, the servo has internal backlash in its gearing, the cables can stretch, and the Bowden cables can introduce backlash, but all three of these are minimal and are counteracted by the springs. Calibration of joints is also simple using CAFSE, as the most important datum is the first actuator position that will cause joint motion.

Perhaps the greatest advantage of CAFSE over DMBC is the need for half the actuators. The motors account for a large portion of the design weight and cost, both of which are critical parameters to decrease in achieving the project goals. Each motor also requires additional wiring and electronics which add volume and cost. Finally, more actuators requires more sophisticated software, both in calibration and in active control.

3.2.1.2. CAFSE Advantages Over Direct Drive

The major advantages of CAFSE over DD are derived from having additional space. A tendon-based hand allows the motors to be mounted in the forearm. This provides more room to incorporate motors larger and higher-torque (assuming the same types of motors were used) to be used than when employing DD. Furthermore, the space in the forearm allows commercial motor controllers to be incorporated instead of custom, smaller electronics that would drive up cost. Additionally, because of the limited space for actuators at the joint, gearing with high reductions may be necessary to achieve acceptable torque. This gearing adds additional backlash to the joint, which, as previously discussed, is not an issue in CAFSE.

3.2.1.3. CAFSE Limitations

The CAFSE method does have several limitations as compared to other actuation strategies. Because the finger is only actuated in one direction, outside forces can cause uncontrollable extension motion. In order to cause flexion, the motor must also continuously overcome the spring force which increases proportionally to the bend of the joint. CAFSE places motors in the forearm and therefore could not be designed for the hand to be used independently of the forearm, unlike DD which can have this capability. Finally, the hand would be unable to perform any motions requiring extension, such as flicking, unless the springs along are able to generate all the needed force.

3.2.2. Actuator Selection

In order to meet the goal of producing a low-cost platform, only commercial-off-the-shelf (COTS) actuators were considered. Servomotors were selected due to their size, price, form factor, versatility, and power density (Thayer & Priya, 2011). The built in potentiometers for position control was also an attractive feature. Motor manufacturer Hitec offers motors in a variety of torque output and sizes. Each motor is a self-contained, ready to use unit that can be easily integrated into a platform, and replaced and reconfigured easily if necessary. The selected Hitec motors and their specifications are shown in Table 4. Selected extrinsic actuators.

Table 4. Selected extrinsic actuators.

Actuated DoF	Model	Torque at 6.0 V (kg-cm)	Weight (g)	Volume (cm^3)
Proximal/Thumb Flexion	HS-645MG	9.6	55	29.7
Medial-Distal Flexion	HS-225MG	4.8	27.94	16.8
Wrist	HS-7980TH	44	78.2	39.2

3.2.3. Motor Placement

3.2.3.1. Wrist

In designing the actuation of the wrist, a large range of motion and high strength were desired for the wrist joint. To produce flexion/extension and radial/ulnar deviation while minimizing the amount of motors and maintaining a compact form, a differentially actuated spatial mechanism driven by two motors was designed. The motors are placed adjacent to each other and each drives a linkage connected to the hand's palm. The motors can be driven individually or simultaneously, resulting in a degree of freedom similar to that of a ball and socket joint.

3.2.3.2. Proximal finger phalanges and thumb phalanges

The motors responsible for actuating each of the proximal joints of the four fingers, as well as the three thumb flexion degrees of freedom are located behind the wrist motors, in the upper chassis. These motors are Hitec HS-645MG which can output 9.6 kg-cm of torque when operated at 6V. These seven motors are organized such that they line the length of the forearm, with their power cables routing out to the sides and the servo shaft positions alternating from the preceding one, as seen in Figure 10b. This arrangement was chosen because it was the most compact, and it allows the motors to be independently inserted or removed from forearm without interfering with the other motors.

3.2.3.3. Distal finger phalanges

The motors responsible for actuating the distal joints of the four fingers are located on the underside of the forearm assembly, shown in Figure 10c. For this degree of freedom, Hitec HS-225MG motors, rated at 4.8 kg-cm of torque when supplied 6V of power, were selected. This cluster was located more towards the elbow, giving the entire forearm a tapering shape similar to a human forearm. This also aids to move the center of mass of the entire system towards the elbow, in order to decrease the moment arm on the elbow of the robotic platform. The servo shafts face inwards to allow for the tendons to route compactly along the center of the forearm. This lower chassis also contained the HS-7980TH motor that drives the elbow rotation via a gear.

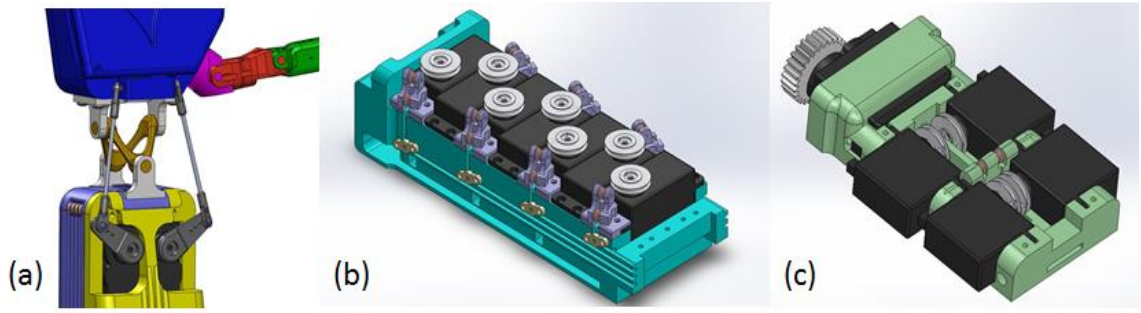

Figure 10. (a) Wrist rotation is accomplished through the use of two parallel motors which can be driven separately or simultaneously, producing two DoF. (b) The upper chassis contains the motors to actuate proximal DoF for each of the fingers and the

flexion DoFs for the thumb. (c) The four motors that actuate the distal DoF for the fingers, along with the elbow rotation motor, are contained in the lower motor chassis.

3.2.4. Tendon-pulley and tendon-sheath network

In designing an extrinsically actuated hand, force transmission hardware must be integrated in a manner which minimizes performance losses such as friction, but also meets the goals of fitting into a compact humanlike form. In the design of the forearm, a combination of tendon-pulley and tendon-sheath actuation was selected. Each of the two transmission techniques has unique advantages over the other, but exclusively utilizing one method over the other would not be optimal for this application. The finalized physical arrangement of the motors allows for the motors to be removed independently from each other, while fitting into a humanlike volume. A flexion tendon is anchored onto a pulley which is rigidly attached to the servomotor shaft. Because the proximal/thumb phalange flexion motors are intended to be removed from the top of the forearm, the tendon routing is redirected to sides of the forearm system, seen in Figure 11c. Sharp bends in tendon-sheath routing must be avoided in design, because performance is severely hindered by the high amount of distributed friction inside the sheath. To redirect the direction of the force, a network of idler pulleys allow the tendons to route along the length of the forearm, with lower friction loss than a tendon-sheath. The tendon path and idler pulleys are inlaid into the side of the forearm to produce a sleek design as well as to protect the tendons from external interference. At the wrist, where the tendons must leave the forearm and enter the articulated wrist, the use of a tendon-pulley system becomes complicated and impractical. Developing a pulley network that decouples the tendon motion from the motion of the wrist would create a great deal of added complexity to the design. To avoid this complication, tendon-sheath transmission is utilized from the forearm to the palm of the hand. The tendon-sheaths can be routed through the center of rotation of the wrist (Figure 11b), eliminating the chance of interference from the wrist movements. The distal phalange flexion motors are located on the underside of the forearm assembly. The orientation in which the distal motors are arranged does not necessitate the use of a tendon-pulley actuation. Because the path to the wrist is fairly straight forward and the distance is short, the tendon-sheath arrangement is used, shown in Figure 11a.

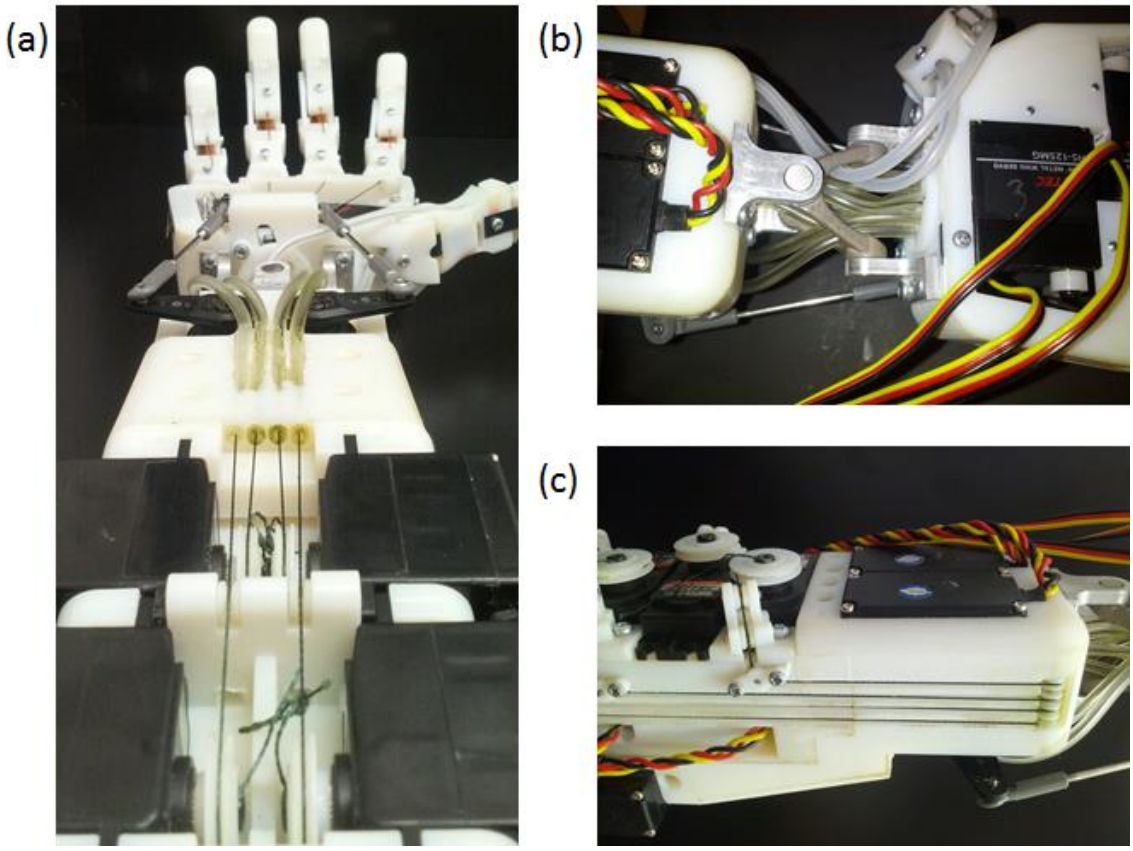

Figure 11. (a) Pulley network which is routed through channels inlaid in forearm surface. (b) Upon reaching the tip of the forearm, the tendons flow through the u-joint into the hand via tendon sheaths which reduce friction and possibility of uncommanded finger actuation. (c) Due to relatively straight path of tendons on the bottom of the forearm, Tendon sheaths are sufficient to transmit the power of the distal motors.

3.2.5. Elbow attachment to humanoid platform

The elbow attachment on the forearm allows the user to integrate the robotic hand as an end effector manipulator on a pre-existing robotic system, shown in Figure 12. The mechanism was devised to provide rotation at the elbow, in order to mimic wrist pronation/supination. It is actuated by a HS-7980TH servo with a 1:1 gear ratio. The driving gear is attached to the motor contained in the lower motor chassis. The driven gear is rigidly attached to a machined hub using four screws. The system can be integrated with any robotic platform using a matching hole pattern. As the motor actuates, the forearm rotates itself about the rigid gear on the elbow.

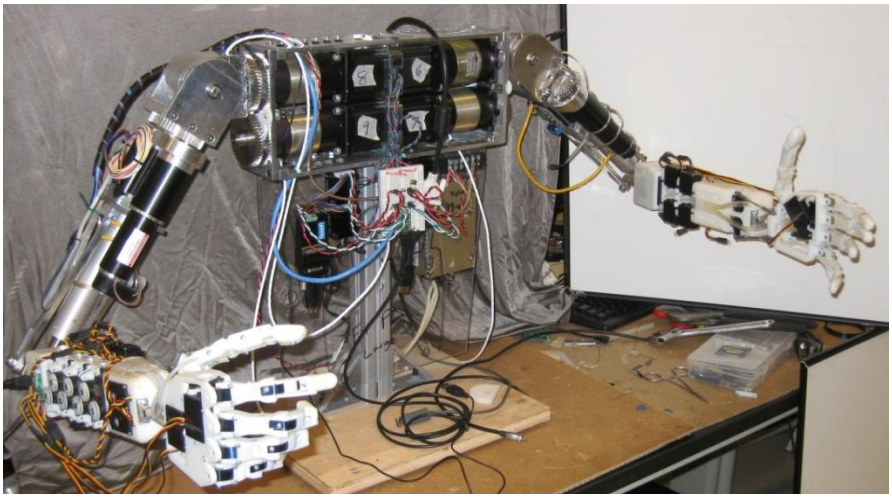

Figure 12. The DASH hands attached to an 8 DoF robotic upper body system.

Much of the mechanism is contained within a structure of the elbow cap. The cap joins with the upper chassis of the forearm with an interlocking geometry, similar to a jigsaw puzzle piece. This allows the interlocking material to bear the cantilevered load, rather than only the screws. When the cap is joined with the lower chassis, the tabs of the elbow rotation motor is locked between the cap and the chassis. Screws from the cap pass through the holes in the tab and thread into the chassis.

The minimize friction of rotation within the elbow cap a radial bearing was selected and implemented. To withstand the axial loads in the elbow, a needle thrust bearing is placed between the hub's base and the elbow cap, and another is located between the outside of the elbow cap and the elbow.

Figure **13** shows the exploded view of the elbow rotation mechanism.

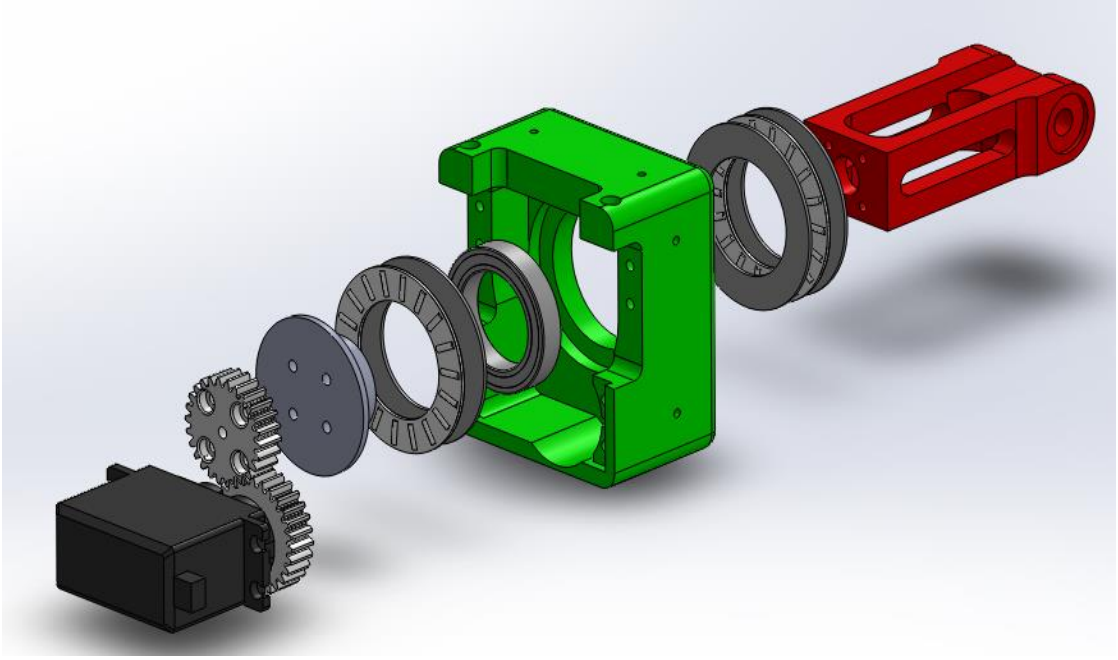

Figure 13. The assembly of the elbow rotation mechanism is comprised of the following components (from left to right): servo with two gear train, elbow hub, needle thrust bearing, radial bearing, elbow cap, needle thrust bearing, elbow mounting bracket.

Additionally, the elbow cap serves as the location of the Pololu Mini-Maestro servomotor controller, shown in Figure 14. The servomotor wires are routed in channels down the length of the arm chassis, and attach to the connectors soldered to the controller. This allows for the quick replacement of a defective motor during maintenance.

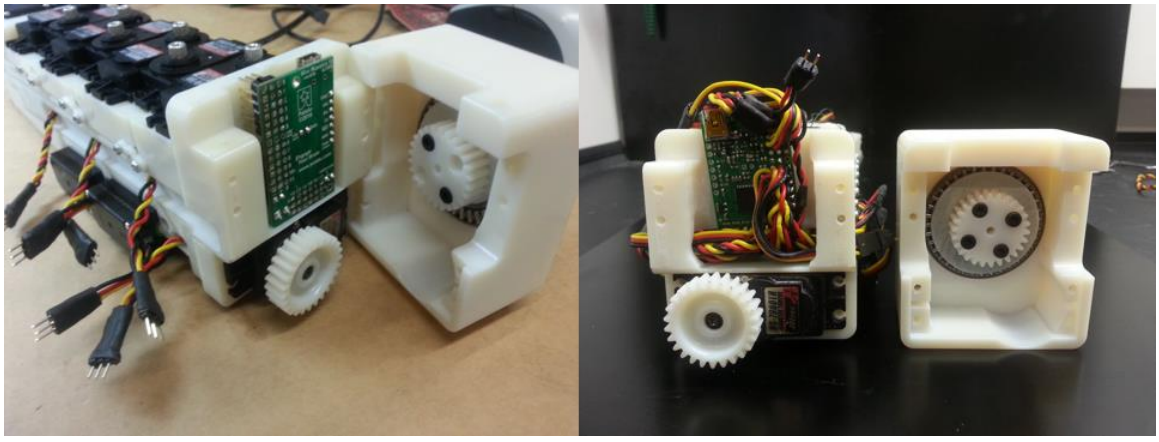

Figure 14. The Pololu Mini-Maestro servo controller located in the elbow of the forearm.

3.2.6. Wrist Design

The wrist design of the hand is based on the universal joint (U-joint), which provides flexion/extension and radial/ulnar deviation, as well as allowing tendon-sheaths to pass through. In the development of the wrist, several designs were prototyped and evaluated. Each design allowed the tendons pass through the center of the U-joint to

ensure the least change in length of tendons as the wrist actuates. The first design featured a central cross with a 20mm diameter hole in the center to allow for multiple tendon sheaths to pass from the forearm to the palm without interference. This design was to be assembled from a milled aluminum central cross, four milled aluminum brackets, and four 3D printed plastic bushings. The major issue with this design was potential interference between the palm of the hand with the supporting brackets if the wrist was fully actuated to one extreme in either direction. In this special case, the supporting bracket would be rotated in line with the hole in which the tendon-sheaths enter the palm thus making unwanted contact with the tendon-sheaths. The next iteration mitigated this issue by offsetting the axes of the U-joint by 12mm and decreasing the bracket height to compensate for the offset. This allows the U-joint to be actuated in any extreme position without making contact with the tendon system on the support brackets. This new design is 3D printed to achieve the desired precision as well as produce its irregular shape. Tensile strength became an issue in this demanding application, as 3D printed plastic is brittle with a yield stress of 58 MPa. The final design uses the thickened offset geometry printed in a stainless steel infused with bronze to produce a more robust wrist joint at 682 MPa. This increased the tensile strength by a factor of 11 and still allows for a large amount of tendons to pass freely through the wrist without interference shown in Figure 15.

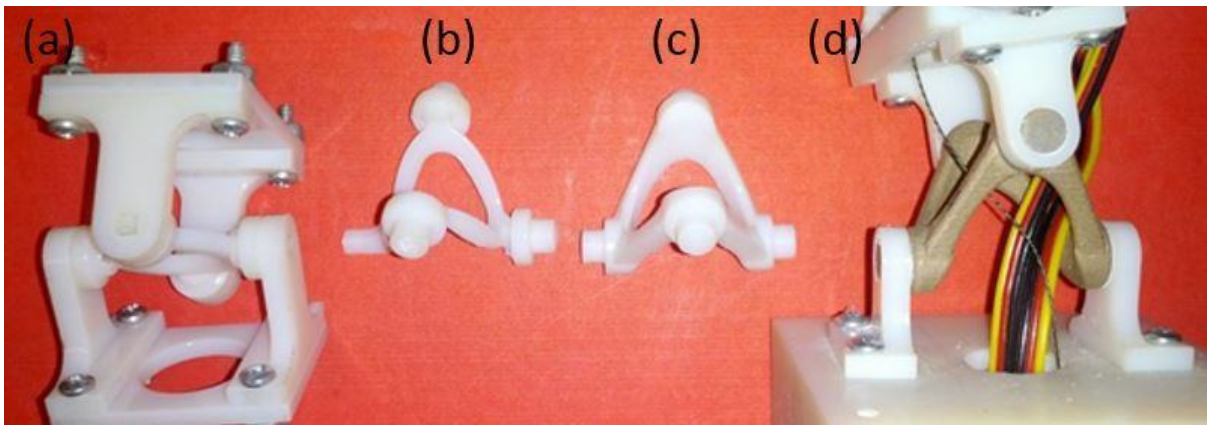

Figure 15. The evolution of the wrist U-Joint (a) in-plane wide u-joint, (b) split-plane thin member u-joint, (c) split-plane thickened member u-joint, and (d) final split-plane u-joint 3D printed in stainless steel and sintered bronze (Stevens, 2013). Reprinted with permission (see Appendix A).

The actuation of the wrist is accomplished using a differential linkage mechanism actuated by two motors. The U-joint serves as the junction of the palm and forearm and is driven by linkage rods that connect at the wrist motors and extend to the palm of the hand, shown in Figure 16. Each connection point of the linkage rods is a ball and socket joint. In this mechanism, motors can be driven individually or together, to create a 2 DoF motion that provides flexion/extension and radial/ulnar deviation. Actuated by two Hitec HS-7980TH servomotors, which provide 44 kg-cm of torque each, the wrist is capable of supporting a 2.56 kg load shown in Figure 17. This load exceeds the maximum requirements established by the initial design specifications.

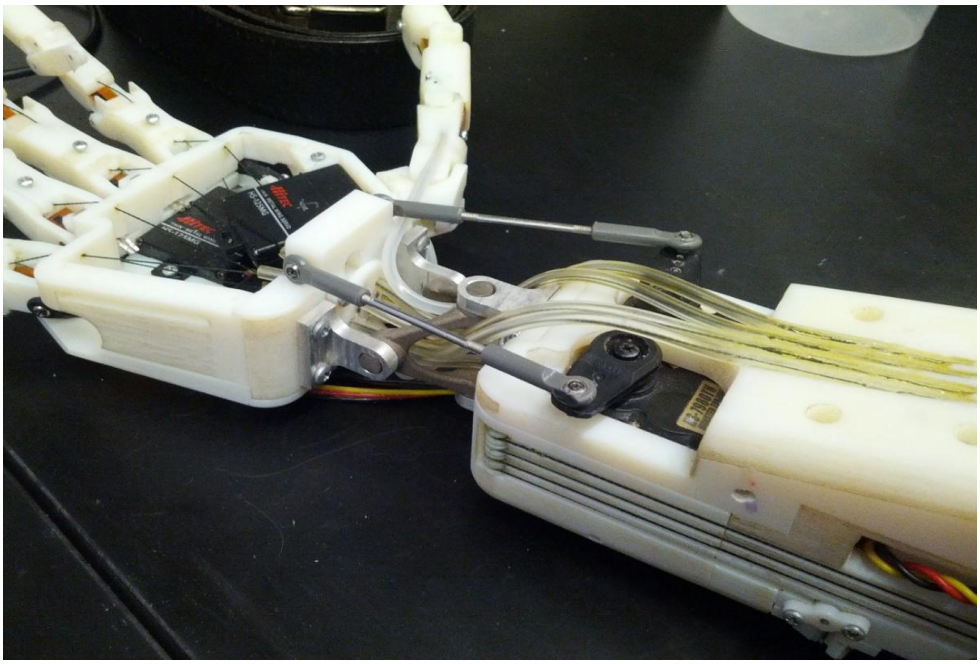

Figure 16. Differential actuation method provides 2 DoF in the wrist. Metal rods connect the servo horns to the base of the palm with ball joints.

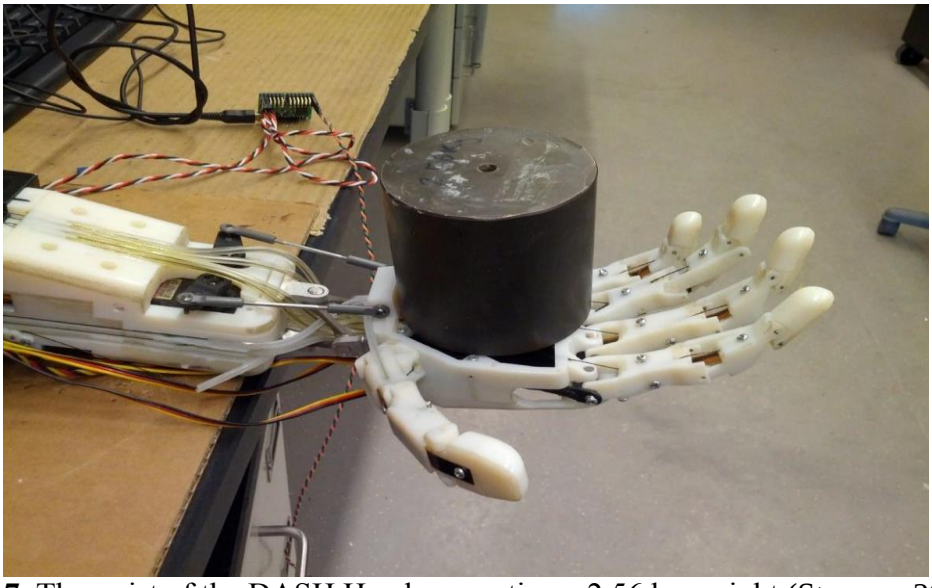

Figure 17. The wrist of the DASH Hand supporting a 2.56 kg weight (Stevens, 2013). Reprinted with permission (see Appendix A).

The kinematics of the wrist were more challenging due to the differential actuation method in the wrist. Typically most robotic systems are serial links in nature with a dedicated actuated for each DoF, but such an arrangement would not be suitable in this application because of the limited space. By having the motors arranged in parallel to

create the differential mechanism, they are able to be packaged in the humanlike form as the design requires. The wrist design also allows for the tendons to pass through the center of the wrist for smooth rotation and reduction in friction. Rotation matrices were used to calculate the required angle of revolution of the two servo joints based on the desired angle inputs of yaw, pitch and roll. The roll angle should be zero if the forearm is not rotation about the elbow joint. The rotation matrices for roll, pitch and yaw are:

$$Rotation\ (x) = \begin{bmatrix} 1 & 0 & 0 \\ 0 & \cos\gamma & -\sin\gamma \\ 0 & \sin\gamma & \cos\gamma \end{bmatrix}$$

$$Rotation\ (y) = \begin{bmatrix} \cos\theta & 0 & \sin\theta \\ 0 & 1 & 0 \\ -\sin\theta & 0 & \cos\theta \end{bmatrix}$$

$$Rotation\ (z) = \begin{bmatrix} \cos\theta & -\sin\theta & 0 \\ \sin\theta & \cos\theta & 0 \\ 0 & 0 & 1 \end{bmatrix}$$

where the concatenation of the three rotations forms:

$R = R_x \times R_y \times R_z$

This final rotation matrix is multiplied by the neutral positions of palm side ball joints to give the ball joint positions of JointR and JointL.

3.3 Initial Hand Design

In this section, the design of the Dexterous Anthropomorphic Sensor-Driven Hybrid-Actuation (DASH) hand is presented. The design focused on a hybrid approach of combining intrinsic and extrinsic actuation in a human-like form factor. The requirement of the hand and forearm maintaining biomimetic dimensions was enforced during the design process. The entire system had to accommodate the required drivers, motors, sensors and other electronics within the confined anatomical geometry. Modularity of the fingers, palm, tendons and forearm were crucial to reduce the maintenance and repair time. Robust positional feedback at the joints was necessary to achieve accurate feedback without relying solely on the servomotor potentiometers. Additionally, high power density ratios, high DoF, humanlike RoM, and low cost were driving goals in the design. The final product seeks to be achieve a system that was dexterous, sufficiently strong, and modular with a cost factor of at least one order of magnitude smaller than any commercially available equally-capable systems. The final design cost less than $1500 per hand system.

3.3.1. Dimensions and Range of Motion

The design specifications for the humanoid hand and forearm required the geometry to fit within the geometry of a 50th percentile adult male shown in Figure 18. This constrained the design to be 193mm x 89.6mm x 42.6mm in length, width and height of the humanoid hand. Humanlike digit lengths for the distal, medial, and proximal phalanges were taken into consideration for each finger. DASH hand, shown in Figure

19, features the ring finger and index finger measuring 96 mm in length from fingertip to proximal joint, while the pinky and middle finger measured 76mm and 101mm respectively.

Body Size of the 40-Year-Old American Male for Year 2000

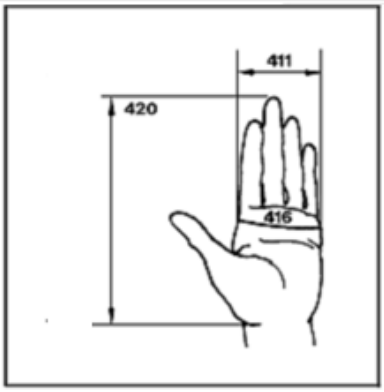

No.	Dimension	5th percentile	50th percentile	95th percentile
420	Hand length	17.9 (7.0)	19.3 (7.6)	20.6 (8.1)
411	Hand breadth	8.2 (3.2)	8.9 (3.5)	9.6 (3.8)
416	Hand circumference	20.3 (8.0)	21.8 (8.6)	23.4 (9.2)

Figure 18. Human hand critical dimensions for the average male of 40 years of age (NASA, 2000). Reprinted from NASA (see Appendix A).

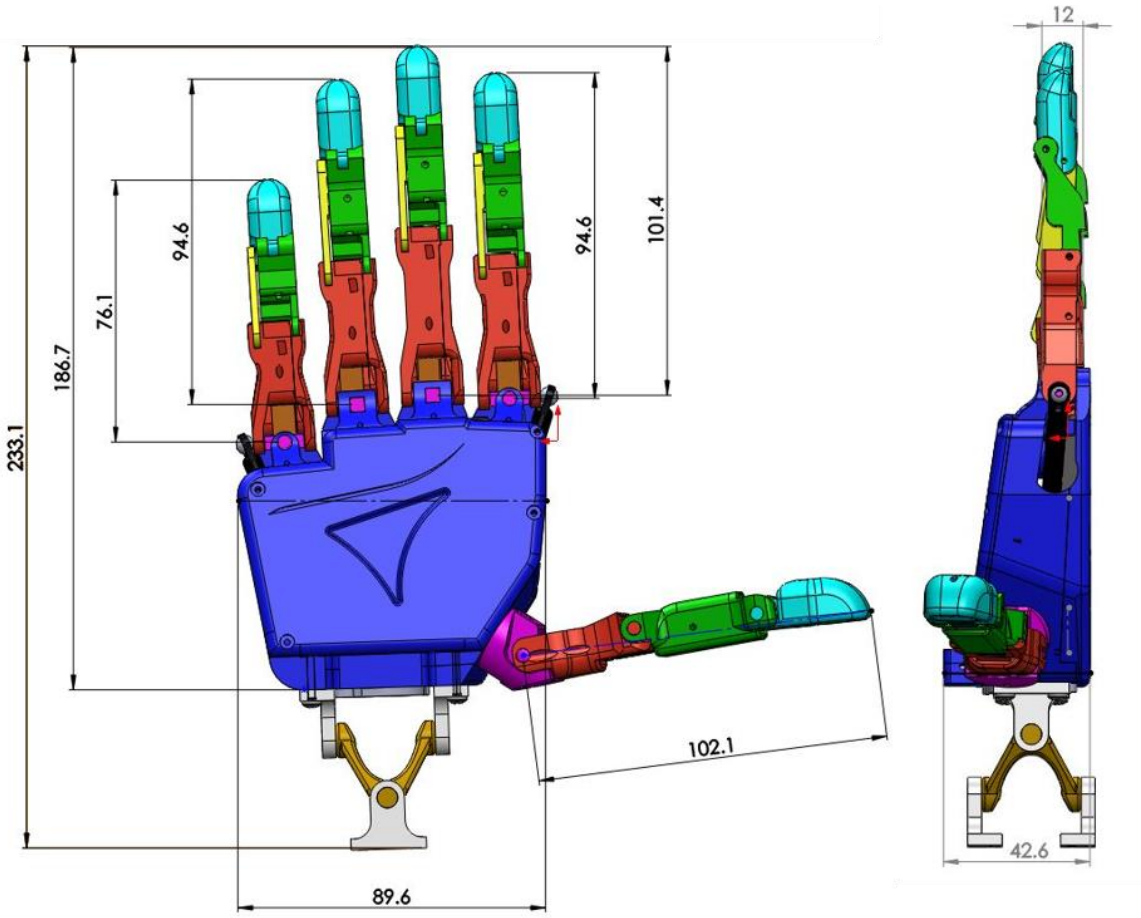

Figure 19. DASH hand design with proximal, medial and distal links of the fingers shown light blue, green and red respectively. The palm is shown in dark blue and each of the fingers attaches to the palm via the pink u-joints (Stevens, 2013). Reprinted with permission (see Appendix A).

Measurements were taken for the ranges of motion of abduction in the index, pinky and thumb joints. Literature suggests that the range of motion is typically between 20-25° for the fingers and 70-80° for the thumb as shown in Figure 20(a). From the measurements that were taken in our laboratory, most hands were capable of a little over 30° at maximum extension for the fingers which became a design constraint as the major abduction range of motion, seen in Figure 20(b).

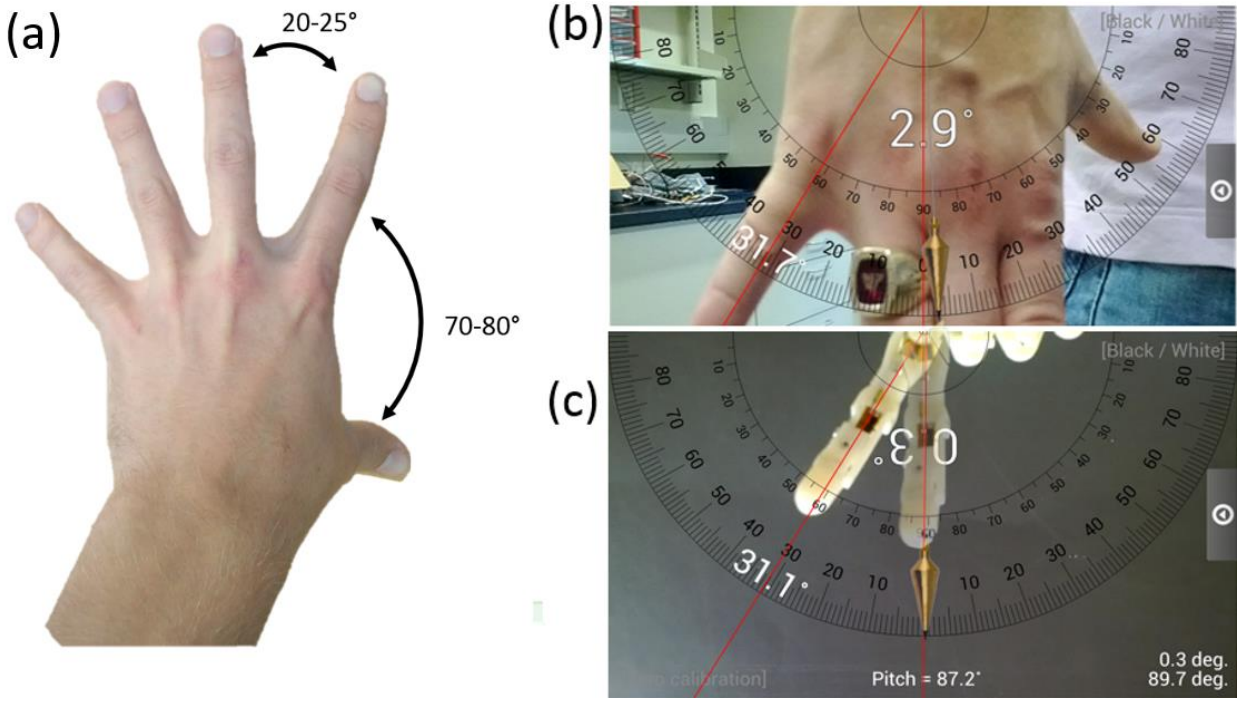

Figure 20. (a) Abduction of index is 25° for the fingers and up to 80° for the thumb. (b) Actual measurements for index and pinky abduction were measured closer to 31°. (c) Final model shows the same range of motion was achieved. Reprinted from "Design and Teleoperative Control of Humanoid Robot Upper Body for Task-driven Assistance" by M. Stevens, 2013. Reprinted with permission (see Appendix A).

3.3.2. Sensor Selection

The addition of sensors in each actuated joint was desired for additional feedback to assist in position control over the flexion motions. Secondly, the inclusion of sensors at each actuated joint monitors the absolute joint position, rather than solely relying on the motors' potentiometers. This is highly desired in cases when the hand was obstructed by a foreign object during extension movements. Additionally, absolute position feedback is desirable over the motor position, because of the nonlinearities that result from tendon actuation, such as friction and tendon elongation. Bend sensors shown in Figure 21 were chosen over typical potentiometers or encoders because of the size, cost-effectiveness, and resistance to mechanical degradation. The Flexpoint bend sensor is a conductive ink based material laminated on a substrate and used to measure the deflection by change of resistance. Essentially, the sensor is a variable resistor that is used to measure the bending. These sensors are offered in a various lengths but are slim enough to fit in the width of a typical human finger. They were attractive for DASH because they do not occupy large area yet they can measure joint angles effectively.

Figure 21. The integrated Flexpoint bend sensors (Stevens, 2013). Reprinted with permission (see Appendix A).

3.3.3. Kinematics

The kinematics of the hand were assumed to have a fixed-base joint located at the center of the palm. Each of the links connecting the thumb were assumed to be in parallel to this initial base joint. The MCP joints of the index and pinky fingers, as well as the thumb's CMC joint, can be approximated as a universal joint with two degrees of freedom. Each of the other revolute MCP joints are 1 DoF. The motion of the proximal interphalangeal (PIP) and the distal interphalangeal (DIP) are coupled via a four bar linkage mechanism, to mimic the actual human finger movement.

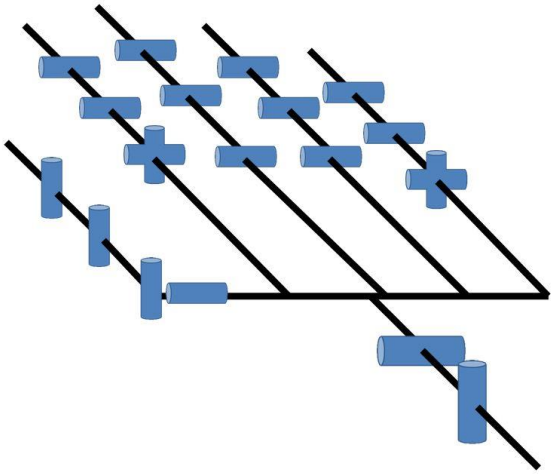

Figure 22. Kinematic model of hand. Each blue cylinder represents a rotational degree of freedom. The distal and medial joints are coupled for each of the fingers. The wrist is driven by a differentially actuated mechanism design (Stevens, 2013). Reprinted with permission (see Appendix A).

The extension movement of the joints relies on a passive actuation to provide a counteracting force to return the joint to its neutral position. Spring steel was implemented to provide this return force instead of torsional springs to allow for more design freedom in sensor and tendon placement. In human anatomy, the motion of the distal and medial is very closely coupled, so a four bar linkage mechanism was used to couple the PIP and DIP flexion motions into one actuated motion, shown in Figure 23. The tendon attaches to the medial phalange and coupled with a rigid rod, the distal phalange actuates simultaneously with the medial phalange. This allows for a passively actuated joint that still produces a natural human motion and eliminates the need for an additional actuator.

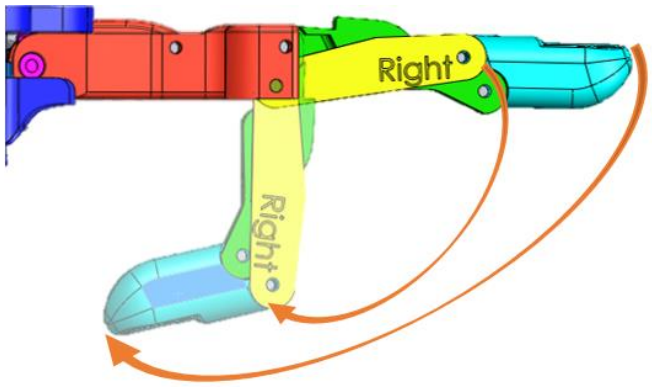

Figure 23. Finger flexion of medial phalange coupled with distal phalange using a four bar linkage mechanism (Stevens, 2013). Reprinted with permission (see Appendix A).

The abduction components of the humanoid hand play an important role in performing different grip articulations. Of all the digits in the hand, the opposable thumb is the most crucial abduction joint. It is the thumb that allows the formation of the c-shaped-grip, power-grip, and the precision-grip. Widening the span of the finger allows for the ability to grasp larger diameter objects in a "C-Shape" fashion. Precision grasps allow for finer dexterity. The capability of these different grasp strategies into the design allowed for versatility over multiple manipulation scenarios. After careful analysis, it was found that the abduction/adduction of the middle and ring finger MP joints are less useful for the different grasp strategies because they do not widen the grasp size but merely make the hand look more realistic by providing equal spacing when abducting each of the fingers in unison. This design choice to exclude these two DoF in the new hand design was also motivated by the availability of space to package the actuators.

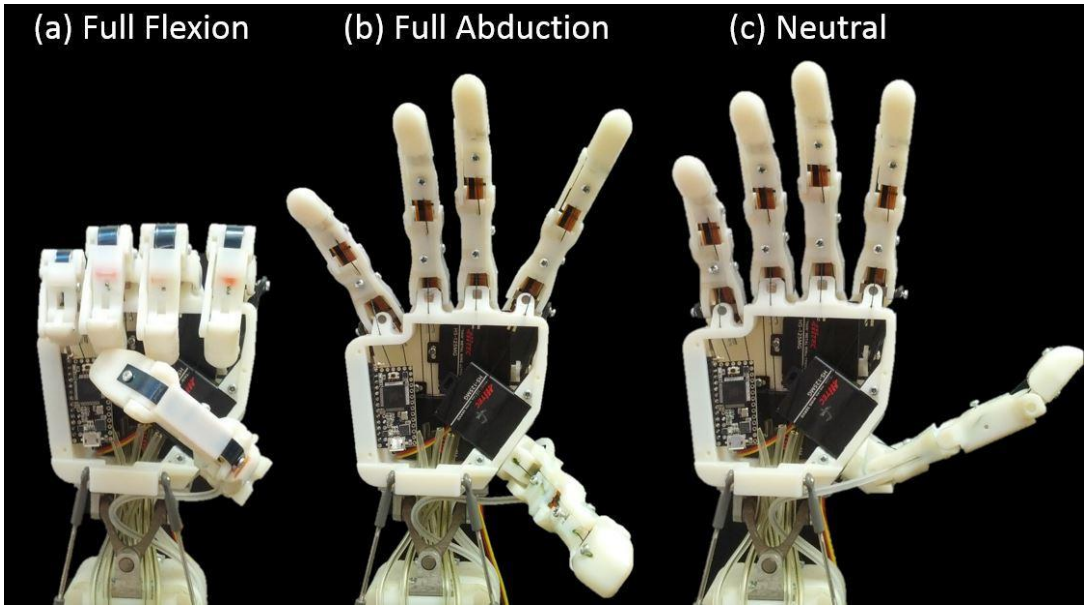

Figure 24. (a) Full finger flexion is possible with the use of 11 actuated degrees of freedom. (b) Widening the grip size is accomplished with the three servos located in the hand responsible for abduction. (c) The neutral position shown is the condition where none of the motors were actuated (Stevens, 2013). Reprinted with permission (see Appendix A).

3.3.4. Finger Design

Each individual finger is an endoskeletal structure consisting of four main pieces: the knuckle, the proximal phalange, the medial phalange, and the distal phalange. The majority of the components were designed to be fabricated using rapid prototyping in order to allow for quick fabrication as well as to provide easily available replacement parts during maintenance of the system.

The metacarpophalangeal (MCP) joints, or the knuckle of the index, middle, ring, and pinky fingers were designed as a universal joint in order to mimic the flexion/ extension as well as abduction/adduction of the proximal phalange. The proximal phalange rotates about X axis of the U-joint. For the index and pinky fingers, the entire finger assembly rotates along the Y axis, which is joined to the palm, for adduction/abduction. The middle and ring fingers do not ab/adduct, so the Y axis is rigidly fixed to the palm. Much of the design of the knuckle component was derived as a result of the decision to utilize bend sensors for joint position sensing. The bend sensor was integrated as closely to center of the joint, in order to measure the angular position of the phalanges. Additionally, the tendon responsible for actuating the medial phalange is routed closely to the center of rotation of the MP. The MP universal joints were rapid prototyped in bronze infused stainless steel to create a compact, yet strong part.

The proximal phalange structure rotates in flexion/extension about the MP joint. This is accomplished using a tendon that is routed from the palm structure into a small tunnel inside of the phalange. This tendon is terminated by pinning it into place using a screw, allowing for quick installation and removal. The bend sensors extend from the MP joint into the center of proximal phalange, seen in Figure 21. Also located in the proximal phalange is another tendon tunnel through which the tendon that is responsible for PIP-

DIP actuation is routed through. A strip of spring steel is rigidly fixed at the MP joint, and the strip extends over the top of the phalange. An attachable piece of plastic serves as a sheath over the spring steel, allowing it to slide along the top of the phalange during flexion and extension.

The medial phalange is attached to the proximal phalange by a 1.6 mm metal pin at the PIP joint. Similarly to the proximal phalange, a single tendon is used for the flexion of the joint and spring steel provides passive extension of the phalange. As previously mentioned, the PIP and DIP joints are kinematically coupled via a four bar linkage mechanism. The ground link of the mechanism is located at the PIP joint on the proximal phalange. The distal phalange serves as the crank link, spanning from the PIP joint to the DIP joint. A thin flat rod makes up the follower linkage and also connects to both the PIP on the proximal phalange and DIP joint on the distal phalange. The distal phalange acts as the coupler link to the mechanism. As the medial phalange's tendon is pulled, the phalange flexes and simultaneously drives the rotation of the distal phalange.

3.3.5. Palm Design

The DASH hand possesses a unique combination of extrinsic and intrinsic actuation. The placement of the majority of the motors in the forearm allows for the tendons to be routed through into the palm but also leaves a large volume available within the hand. Motivated by the anatomy of the human hand, it was logical to place the abduction actuators inside the hand, instead of the forearm (Figure 25). This arrangement also eliminated the need for additional motors in the forearm, helping to maintain anthropomorphic dimensions. The rotation of the thumb and the abduction of the index and pinky proximal joints are driven with a bidirectionally driven, compact servomotor which reduces the need of another motor and maximizes the space shown in Figure 25b. The two motors responsible for driving the index and pinky abduction/adduction DoF were connected to the U-joint via a linkage equipped with a ball joint. This allowed for actuation of the flexion DoF of the joint without drastically interfering with the abduction portion and vice versa. As seen in Figure 25c, the thumb was directly interfaced to the servo without any other force transmission hardware or mechanism. Since each of these motors was integrated into the palm and did not require a set of tendons passing through the actuated wrist, it was confidently assumed that the servomotor position alone was reliable. As a result, these DoF did not necessitate additional position feedback.

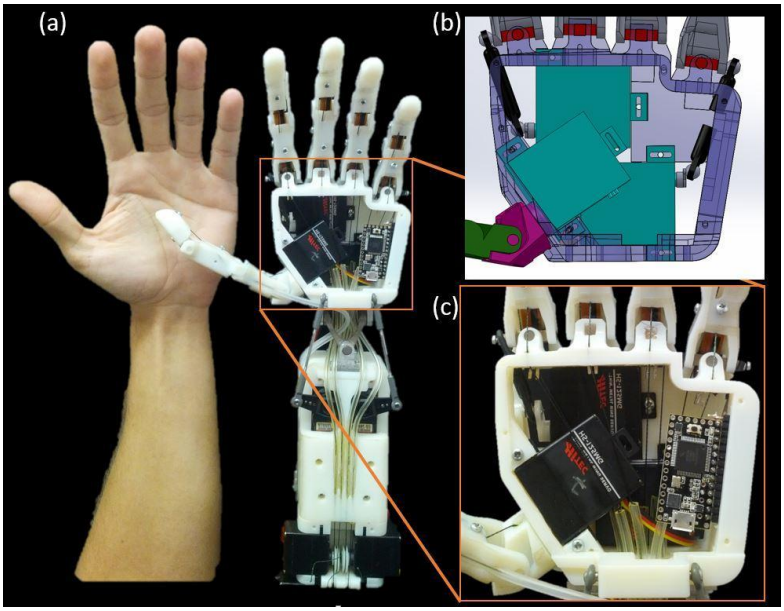

Figure 25. (a) the DASH hand is compared to a human hand to give a sense of dimensional accuracy. (b) Intrinsic motor placement for abduction of the thumb, index and pinky joints. (c) Palm design of intrinsic motors including the microcontroller and tendon routing (Stevens, 2013). Reprinted with permission (see Appendix A).

3.3.6. Electronics and Control

Modularity was an essential design requirement to allow for repair and modification with ease. This design goal led to the creation of an enclosed sensor housing in the palm with a microcontroller that processed the joint positions of each of the actuated fingers. Due to geometric constraints and number of analog pins needed, the *Teensy 3.0* microcontroller was chosen. The *Teensy 3.0* packs 34 I/O, where 10 of which are PWM channels and 14 are analog inputs, shown in Figure 26. An *ARM Cortex* chip runs at 48 MHz and is powered by the micro USB. The entire device measures 35.5mm x 17.8mm and costs around $20. Overall, this device met the requirements of the application in terms of size, speed, ease of use, cost and sufficient input for the 11 analog bend sensors in the hand.

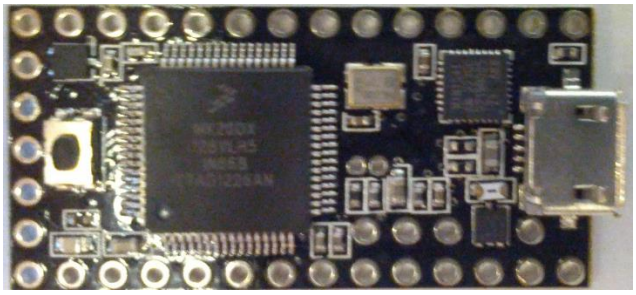

Figure 26. Arduino-based Teensy board measuring 35.5mm in width and 17.8mm in length (Stevens, 2013). Reprinted with permission (see Appendix A).

In order to characterize the analog signal of each joint measurement, a voltage divider was used to find the change in resistance for the angle shown in Figure 27. The bend sensor can be approximated as a variable resistor with an increased resistance proportional to its deflection. The optimal voltage divider, or the one that produces the maximum sensitivity to the change in resistance, can be calculated by finding the minimum and maximum resistance in order to optimize for the correct pull-down resistor. The following voltage divider schematic shows how the sensor input would be implemented.

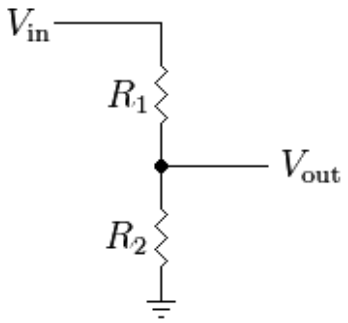

Figure 27. Voltage Divider where V_{in} = 3.3V, R1= Bend Sensor, V_{out} = Analog Reading, and R2 = fixed resistor.

The minimum and maximum resistance of the sensor for 0 to 90° was measured with an ohmmeter to be 10-200 KΩ, respectively. Given the range of R1, the maximum and minimum voltages that the board will read can be calculated as:

$$Vout_{min} = \frac{R2 * Vin}{R2 + R1max}$$

$$Vout_{max} = \frac{R2 * Vin}{R2 + R1min}$$

The derivative of the voltage ranges was taken with respect to R2 giving the following equation:

$$\partial_{R2}\left(\frac{R2}{R1_{Min}+R2} - \frac{R2}{R1_{Max}+R2}\right) == \frac{R2}{(R2+R1_{Max})^2} - \frac{1}{R2+R1_{Max}} - \frac{R2}{(R2+R1_{Min})^2} + \frac{1}{R2+R1_{Min}}$$

By solving for zero and R2 as a positive value, the final equation becomes:

$$R2 = \frac{\sqrt{-R1_{max}{}^2 * R1_{min} + R1_{min}{}^2 * R1_{Max}}}{\sqrt{-R1_{max} + R1_{min}}}$$

which for the chosen bend sensors produces a fixed resistance of 39 kΩ. The wiring diagram for the 4 voltage dividers in the flexion of the fingers is shown in Figure 28.

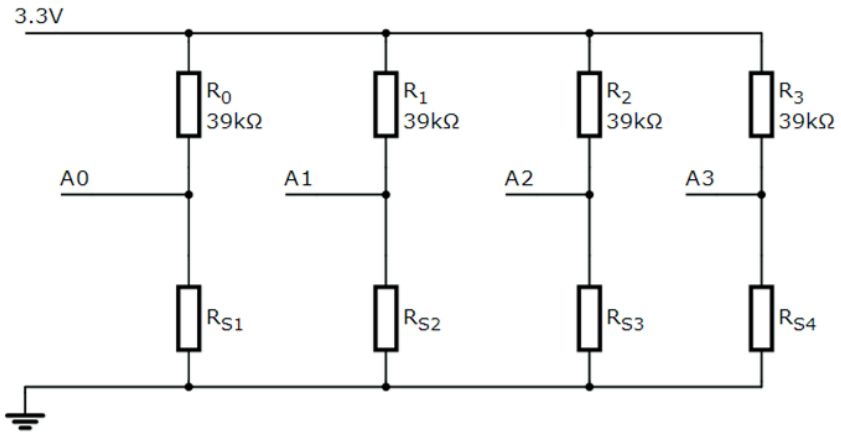

Figure 28. Simplified circuit diagram showing the first four flexion sensors with cascaded voltage dividers (Stevens, 2013). Reprinted with permission (see Appendix A).

3.4 Testing of the Initial Design

3.4.1. Grasping Tests

After producing the prototype of the initial design, grasping tests were conducted to evaluate the kinematics. Previously mentioned, the Cutkosky's Taxonomy (Cutkosky & Howe, 1990) of grasps was used. The taxonomy is comprised of grasps of varying levels of grasping power and precision, demonstrated on objects of varying size and geometry. The potential dexterity of many high profile robotic hands, such as the Robonaut hands, have been evaluated through the demonstration of the hands ability to achieve the grasps in Cutkosky's Taxonomy. The DASH hand was tested using a variety of different objects, such as spheres, discs, and cylinders of varying diameters, seen in Figure 29. The DASH Hand was capable of achieving 15 of the 16 grasps, demonstrating a respectable amount of potential dexterity.

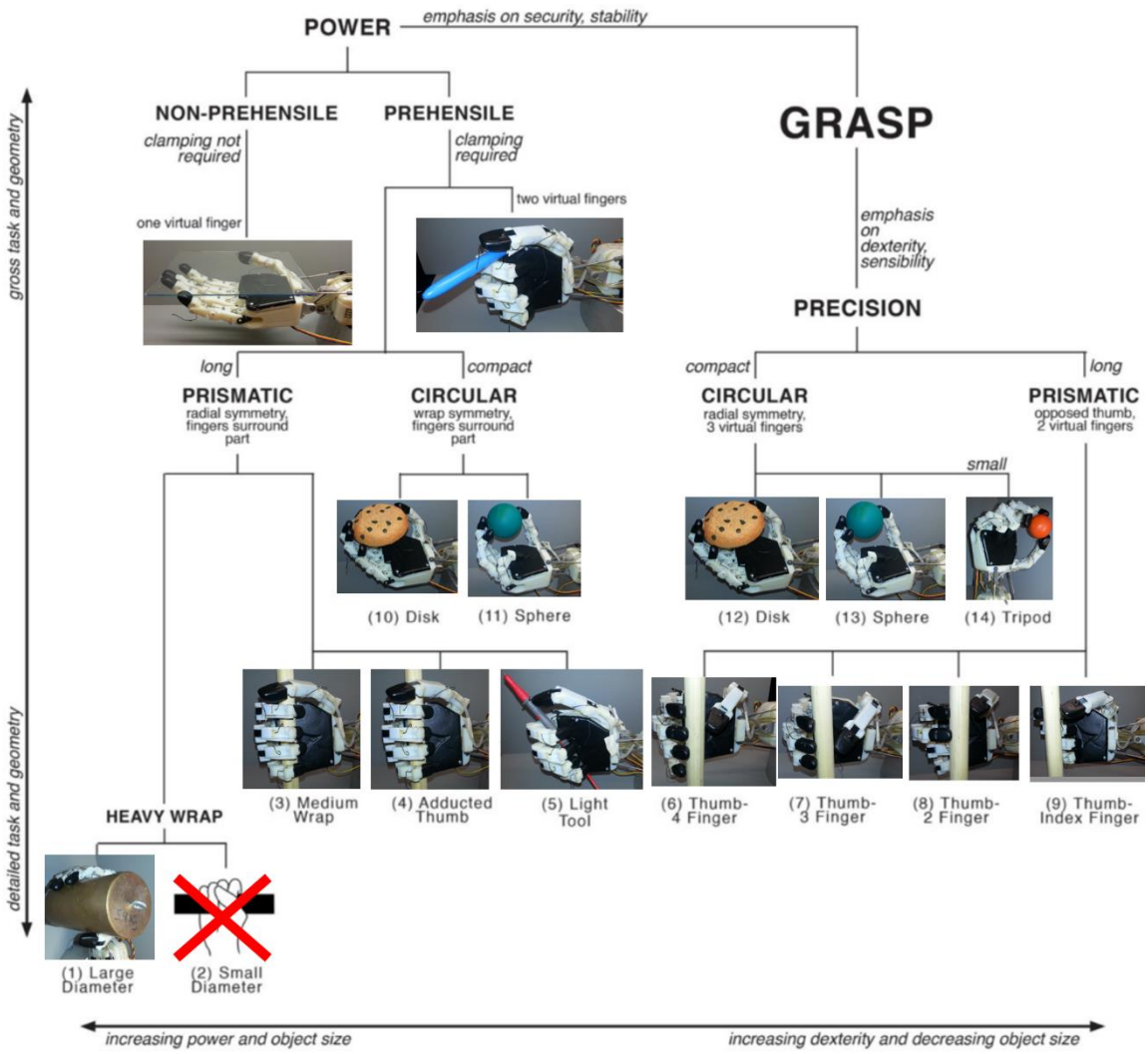

Figure 29. The DASH Hand demonstrating the grasps of Cutkosky's Taxonomy, accomplishing 15 of the 16 grasps.

3.4.2. Teleoperation via data glove

The preliminary DASH hand was interfaced with a low cost glove design, which is presented later in this paper. Because of the glove's lack of finger abduction/adduction and thumb rotation DoF, these were not controlled on the robotic hand. However, both systems worked as intended. From a teleoperation standpoint, the thumb rotation servo of the robotic hand can be adjusted by the user in the LabVIEW interface in order to meet the need of the desired application.

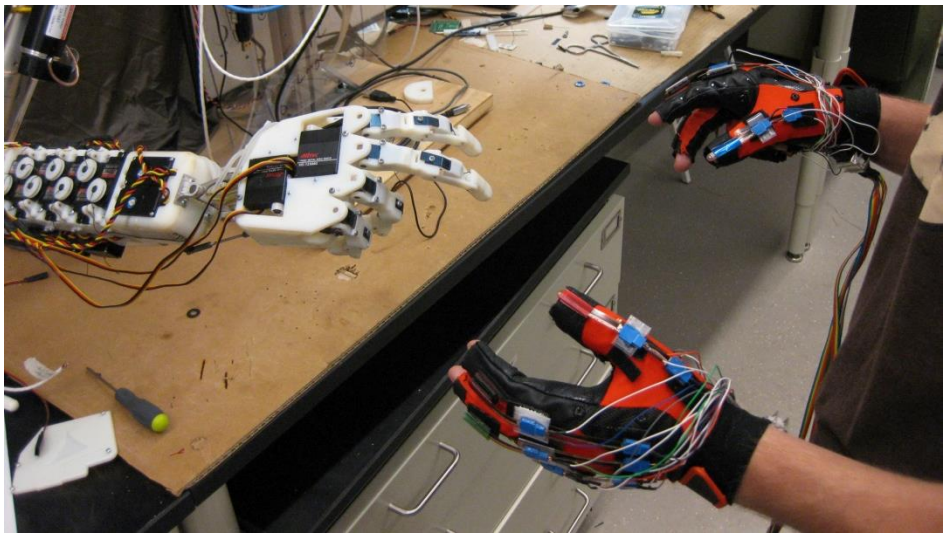

Figure 30. The DASH Hand teleoperated by data glove.

3.4.3. Conclusions of Testing

In the testing of the initial DASH hand, the kinematic design of the hand was found to be quite satisfactory and capable in manipulation. However, in the repeated use of the hand, some shortcomings were revealed that required correction in order for the system to function reliably as a platform.

The physical structure of the hand was found to be more fragile than initially expected, shown in Figure 31. Thin walled features printed in the VeroWhite material fractured after repeated use and in the occurrence of accidental collisions. The amount of force being transmitted through the finger caused damage at the locations of the thin 1.6mm stainless steel pin joints, cracking the bearing surfaces of these revolute joints. Additionally, the method of anchoring the tendons in the finger segments was susceptible to failure when experiencing high amounts of transmitted force, resulting in the fracture of the material surrounding the screw that secures the tendon.

Figure 31. Damage of the plastic structure of the DASH Hand. Damage prone areas included the locations of the revolute pin joints, as well as the screws that secure the tendons.

After repeated use, the spring steel used for providing the passive finger extension would plastically deform, preventing the finger from returning to the fully extended position, which can be seen in Figure 32. The small bend radius at the location of each joint, also contributed to the spring steel deforming. This resulted in a diminished range of motion for each finger, which consequently resulted in diminished performance in the tendon driven actuation as the tendons rely on the quick extension response to maintain tendon tension. The spring steel mechanism also provided a large amount of friction, as the strip slides within a sheath on the phalange, which impedes the flexion motion.

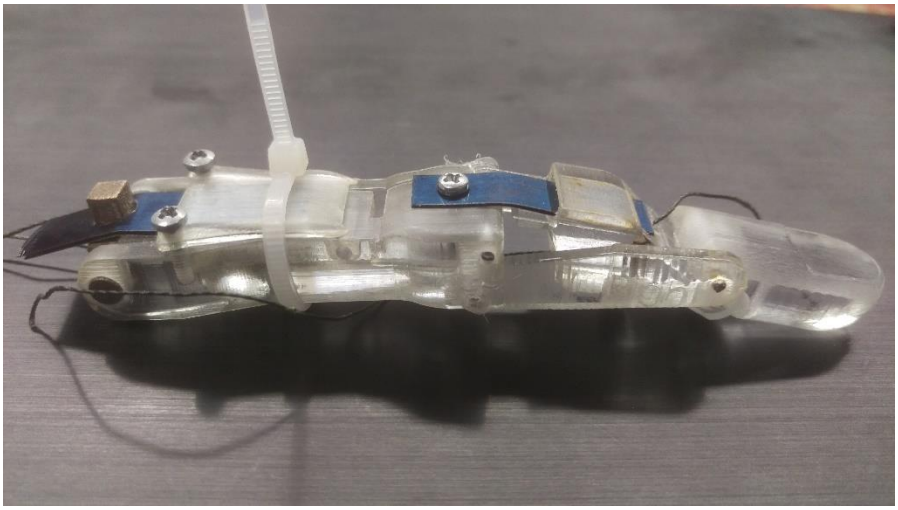

Figure 32. The deformed spring steel after repeated use.

The design of the internal tendon paths led to issues with coupled joint movement, as well as damage to the tendons due to friction. The tendon responsible for actuating the coupled medial-distal phalange was routed through the MP joint, however was not routed closely enough to the center of rotation of the joint. Because of this, when the proximal phalange would move in flexion, the tendon for the medial-distal phalanges, would be pulled as well, creating uncommanded movement. This coupled motion cannot be corrected with the control system with the $M=N$ actuation scheme. An $N + 1$ actuation scheme would mitigate this issue but would require an extra actuator in the system, increasing weight and complexity, thus a redesign is required for the fingers.

Finally, in most of the grasps found in Cutkosky's Taxonomy, the fingers were able to achieve the correct postures, however, security and stability of the grasps was precarious. The slender structures of the fingers lacked substantial contact area with the manipulated objects, making it impossible to envelope slender and small objects. Additionally the smooth surfaces on the palmar surface of the hand effected grasp security, as objects could slip out of grasp easily.

3.5 Updated Hand Design

In this section, several design changes are presented that were made to the DASH Hand design in order to address the shortcomings covered in section 3.4.3. The updated design, maintains most of the basic dimensions, ranges of motion, and DoF as the DASH Hand. In its current form, it lacks the abduction/adduction DoF for the index and pinky finger, as well as the position sensors. These missing features can be easily be reintegrated as a minor update.

3.5.1. Shaft-less Joints

The design of the revolute joints between the knuckles and phalanges was changed from a shaft based joint to a shaft-less joint. In this design, the preceding finger segment contains a radial bearing on each side and the succeeding segment features a cantilevered hub on the outside surface that fits into the radial bearing, as shown in Figure 33. The key advantage of this joint design over the previous one is that it allows for the tendons to pass through the center of rotation of the joint (see Figure 34), which will eliminate any coupling effect between the consecutive MP joint and the PIP- DIP joints. With no shaft passing through the center of the whole joint, space is available for components such as torsion springs to be integrated. Additionally, with the integration of bearings, friction in the joints will be greatly reduced, allowing the spring elements to perform the extension movement of each segment with less resistance.

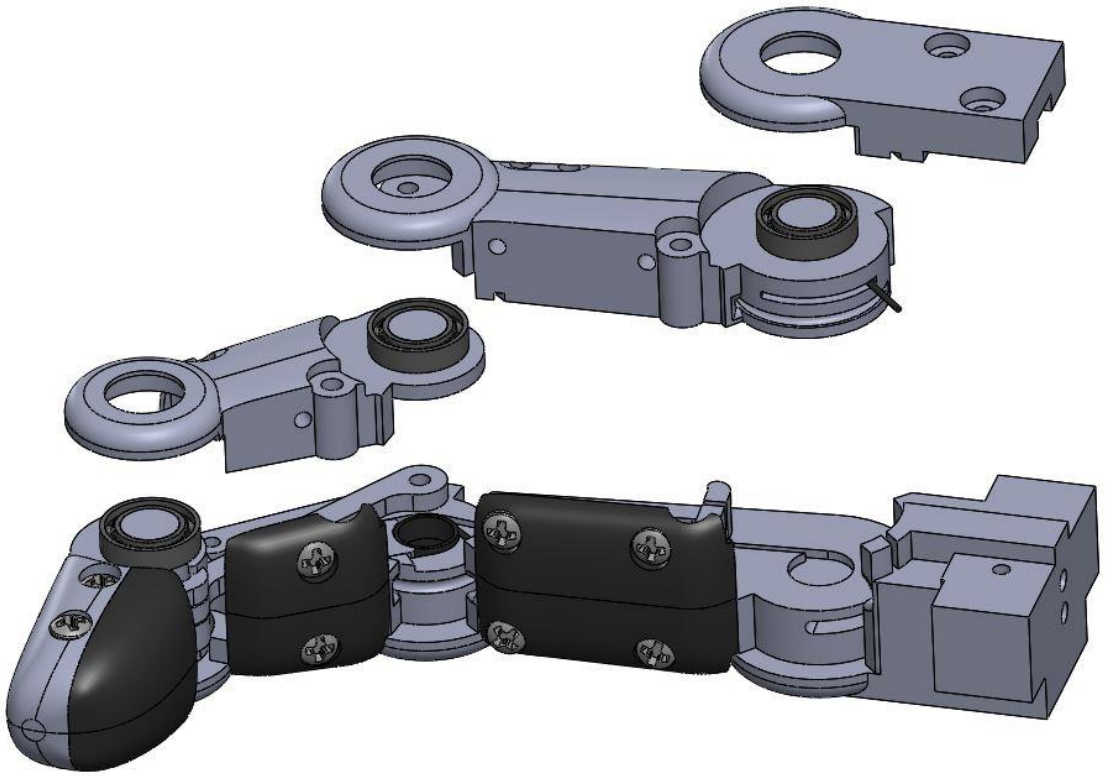

Figure 33. An exploded view of the finger, showing the shaft-less joint design, comprised of cantilevered hubs with radial bearings.

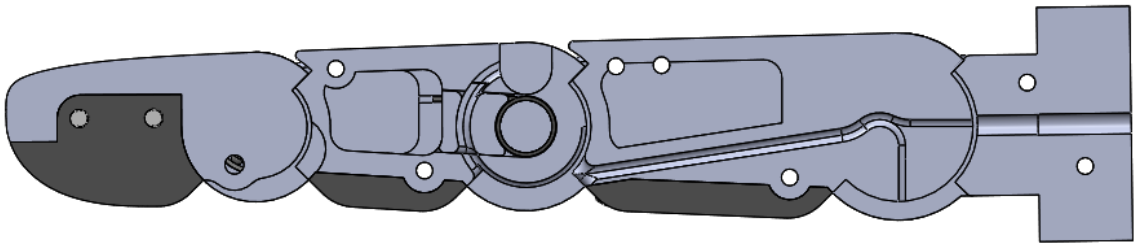

Figure 34. A cutaway view of the finger, showing the tendon channel of the proximal phalange.

3.5.2. Integrated Pulley

For each actuated finger segment, a pulley is integrated into the body of the phalange, as seen in Figure 35. The tendon wraps around the pulley and is routed through a channel that leads to a termination point. This design keeps the tendon constantly tangent to the pulley, providing a constant joint torque.

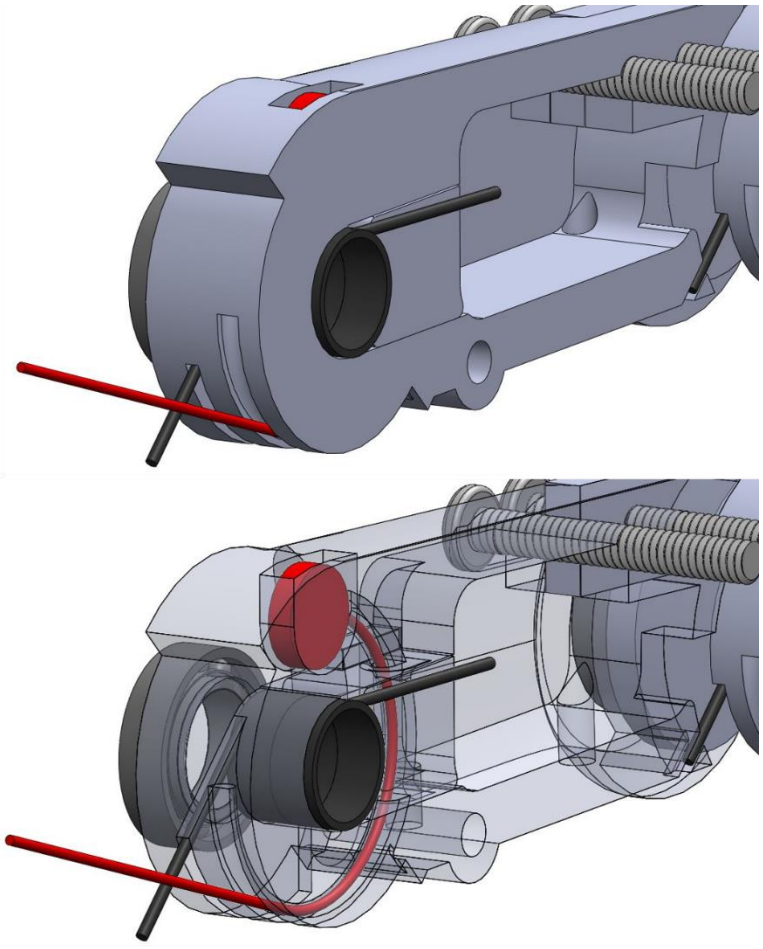

Figure 35. The integrated pulley of the MC joint of the proximal phalange.

The integrated pulley diameters, servo horn diameters, and the motor torque are the governing variables for the force output of the robotic hand. In the goal of maintaining an anthropomorphic form, space constraints play a large role in the determination of each of these, so pulleys in the MP joint and the PIP joints were designed to be 18 mm and 15 mm, respectively. In future iterations, the pulley sizes can be modified if so desired.

3.5.3. Tendon path routing

The internal tendon routing design was designed in order to reduce friction and wear in the tendons evident in the initial design. This was accomplished through providing the straightest and shortest path as well as minimizing the contact on the tendon. The tendon to actuate the MCP joint leaves the sheath cable in the palm and enters the knuckle component that is attached to the palm. This tendon is wrapped around the integrated pulley of the proximal segment (see Figure 36a and Figure 36c).

As previously mentioned, the shaft-less joint design allows the tendons to pass through the center of rotation of the joints of the proximal segments. To allow this, a 90 degree cutout is present in order to allow the finger segment to rotate without influencing the movement of the tendon for the entire 90 degree ROM. This contact point between the joint center and the tendon is a corner in reality, but is filleted in the design because a sharp corner would result in friction, as well as cause wear on the tendon. The path beyond the proximal joint center is a direct, straight path to the integrated pulley of PIP joint. Inside the bounds of the finger, there are only two points of contact if the tendon is taut: at the approximate joint center fillet and the groove of the integrated pulley of the PIP joint, shown in Figure 36(b) and (d).

The tendon terminates by being wrapped around the integrated pulley and exiting at a notch that is located at the 12 o’clock position at the top surface of the phalange. The end of the tendon has a small metal nut tied to the end and the nut sits in the notch. The motor horn position is adjusted to provide the correct tension on the tendon.

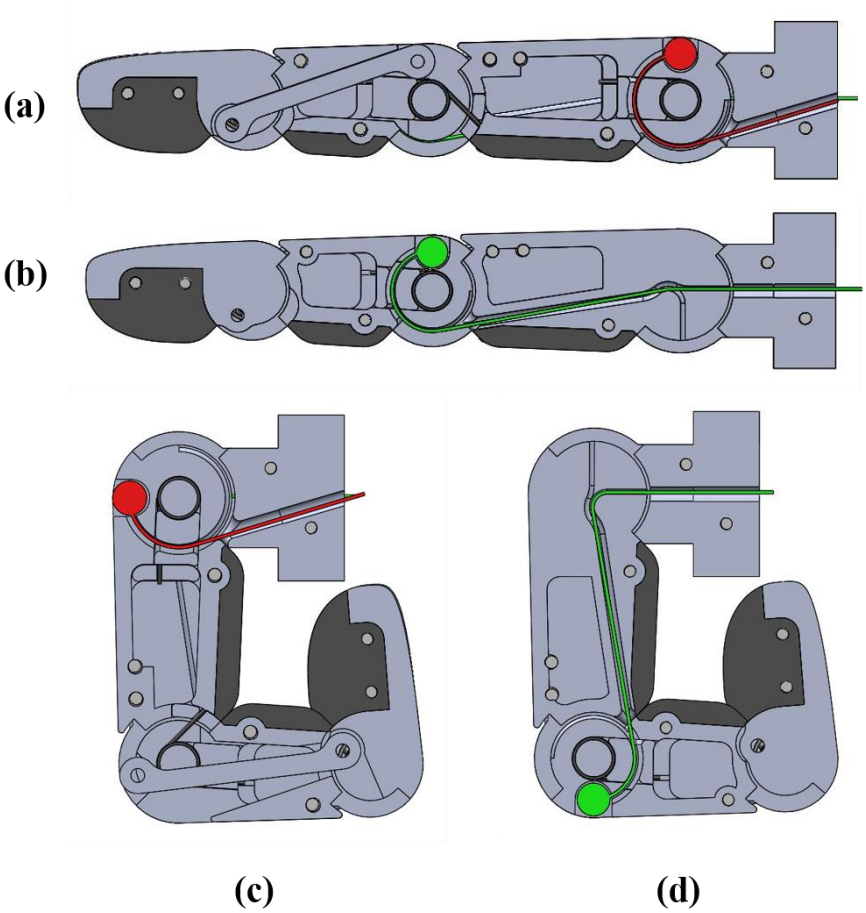

Figure 36. The tendon routing of both the (a) proximal and (b) medial phalange in the fully extended as well as in the (c) proximal and (d) medial phalanges in the fully flexed positions.

3.5.4. Torsion Springs

Due to the deformation and fatigue issues encountered in the use of strips of spring steel, COTS torsion springs were selected to provide a more reliable means of providing return force for the flexion movement of the fingers. A torsion spring is located at the center of both the MP and PIP joints. In an effort to efficiently allocate space in each finger phalange, the torsion spring is located in the center of the phalange's integrated pulley, as seen in Figure 35. In order to insert or remove the spring, a small portion of the integrated pulley, secured by press fit, can be slid in and out of the shell of the segment. This disassembly procedure is shown in Figure 37.

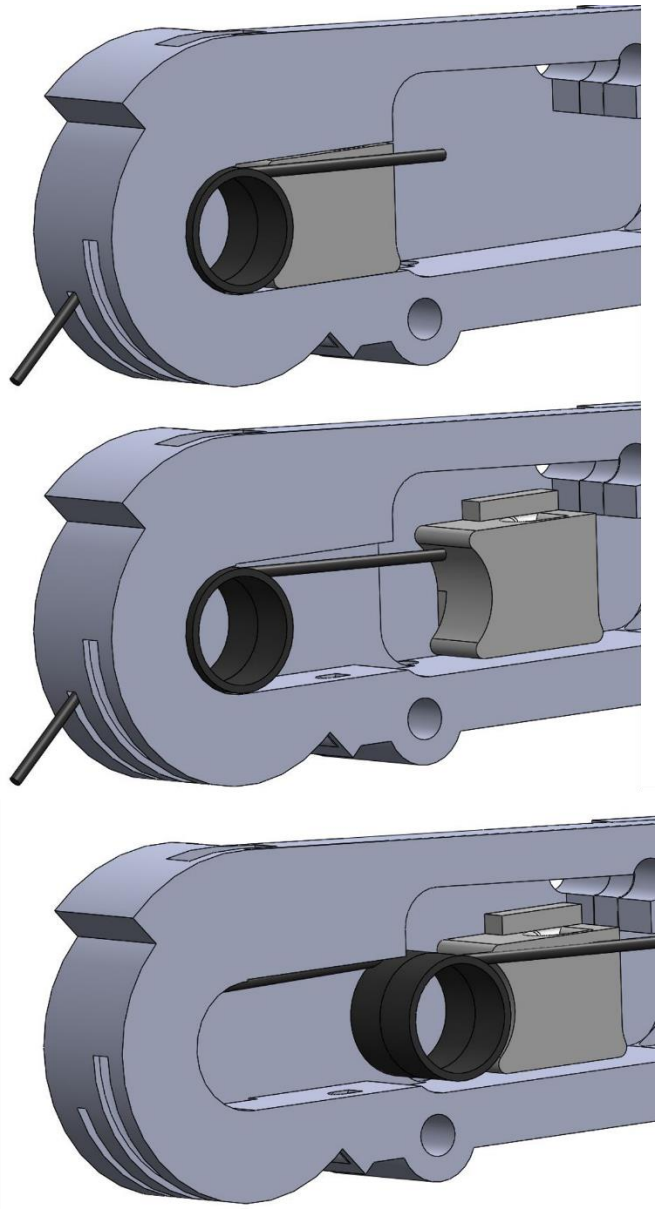

Figure 37. A press fit section of the integrated pulley is slid away to allow the torsion spring to be released.

3.5.5. Improved durability

In the updated design, efforts were made to increase the durability of the hand, as fragility of the initial DASH Hand design proved to be problematic. The shaft-less joint design, presented in Section 3.5.1, offers significant robustness over the simple pin design of the initial design. Wall thicknesses at critical locations such as the bearing surfaces of the segments have been increased. The addition of more robust mechanical limits at each joint restrict the movement of the segment to its prescribed range of motion, protecting the joint in the event of the motor continuing to actuate beyond desired (Figure 38).

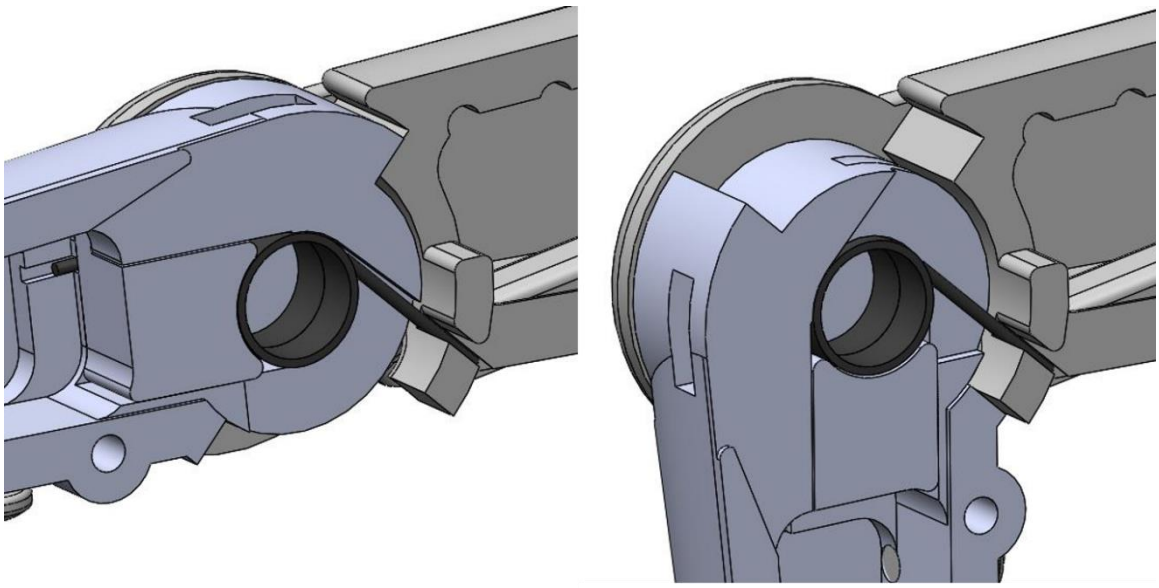

Figure 38. Mechanical limits restrict the flexion range of motion to 90°.

Because the coupler link of the initial design's four bar linkage mechanism was a key point of failure in the initial design, the mechanism has been integrated into the shell of the medial phalange. The mechanism was synthesized, using dimensional synthesis software, so that it would fit within the volume of the segment (Purwar, Toravi, and Ge, 2014). This feature protects the mechanism and eliminates moving parts on the outside of the finger that could be subjected to outside interferences, as well as helps convey a clean, anthropomorphic appearance.

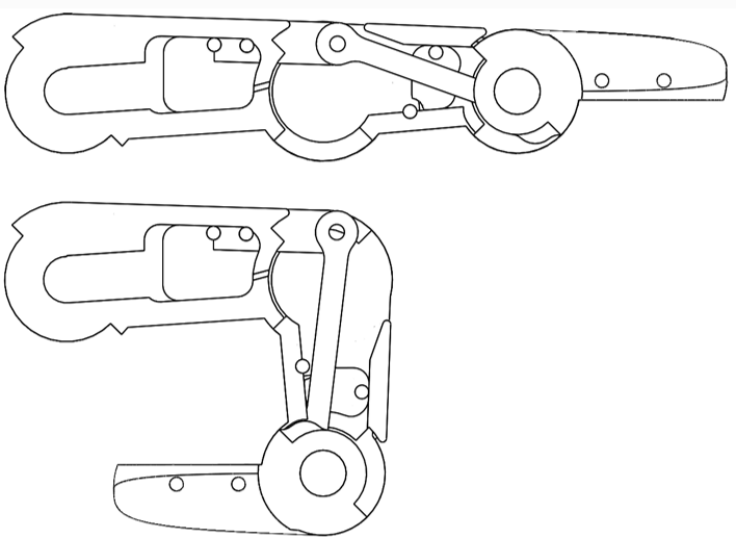

Figure 39. The encapsulated four bar linkage mechanism that is responsible for coupling the PIP and DIP movement.

3.5.6. Improved Anthropomorphism and Modularity

In order to approach more human-like hand function, efforts have been made to increase the anthropomorphism of the hand. In designing the fingers, the overall thickness and exterior contours were designed to be closer to the human finger form,

allowing it to perform more closely like a human hand (Figure 40). The new form of the fingers provides additional surface area to aid in the secure and stable grasping of objects. The fingers have been fitted with removable rubber pads that attach on the palmar side, where contact during grasping occurs. These pads are rapid prototyped on an Objet Eden 260V 3D printer using the flexible, soft Tango material. The rubber pads provide additional gripping friction during grasps, reducing the chances of an object slipping out of the grasp of the hand.

Secondly, the slightly larger thickness provides more space for sensors to be incorporated at the discretion of the user. Each segment contains a hollow cavity inside, which can serve as the location of future sensorization of the hand. The CAD file for the finger module was designed in a "top-down" work flow, meaning that a master part file can be changed using a few parameters in a spreadsheet, mainly the length and width of each segment and the diameter of the joint. New features that may be conceived later on can be applied easily to create an updated finger version.

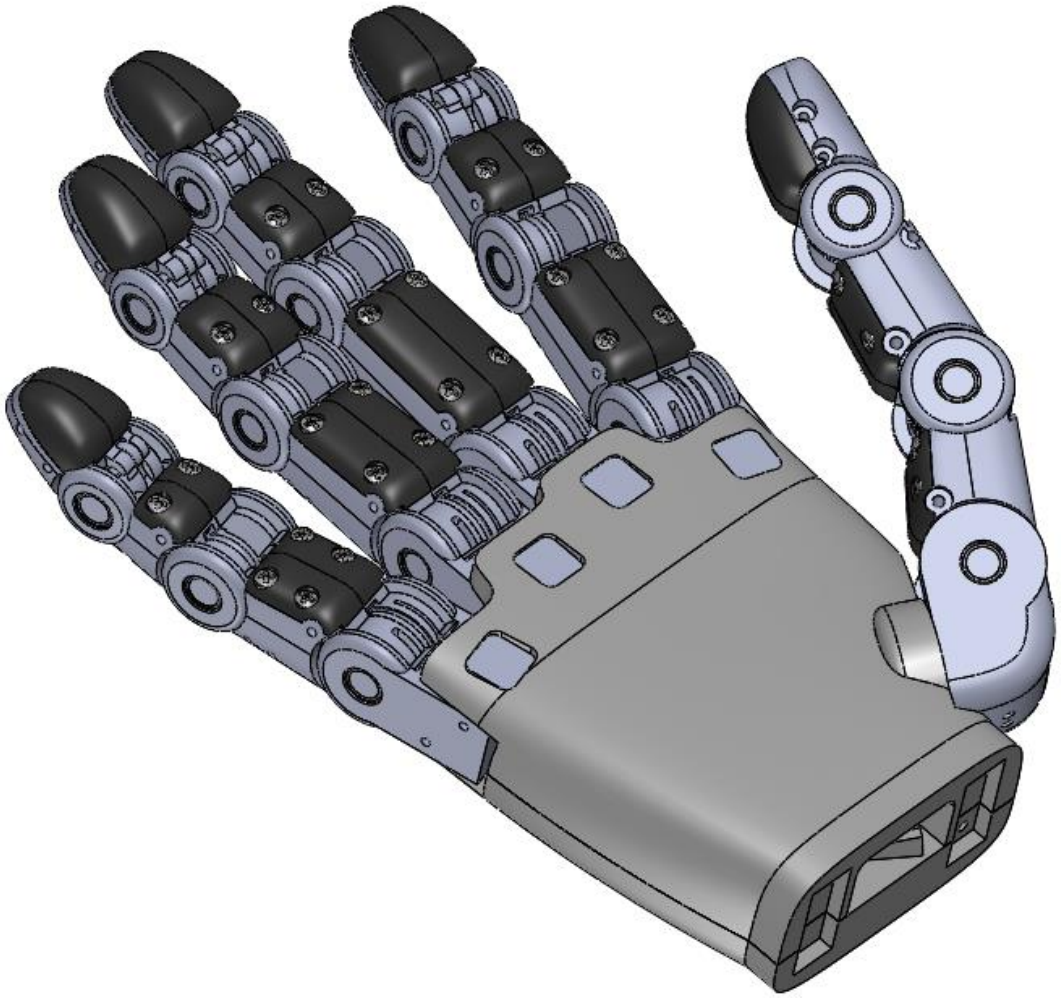

Figure 40. The updated hand design, featuring more a more anthropomorphic form which contributes to enhanced functionality and robustness.

3.5.7. Grasp testing

Virtual testing of the design's grasping ability was completed in SolidWorks where the hand demonstrated the grasps featured in Cutkosky's Taxonomy (shown in Figure 41. The updated hand design was capable of performing all of the grasps in the taxonomy, including the "small diameter" grasp that was unable to be performed by the initial design of the hand. Based on this virtual modelling of the grasps, it is believed that the increased thickness of the fingers, the more human-like form, and the rubber finger pads, will greatly improve the performance by providing more secure grasps.

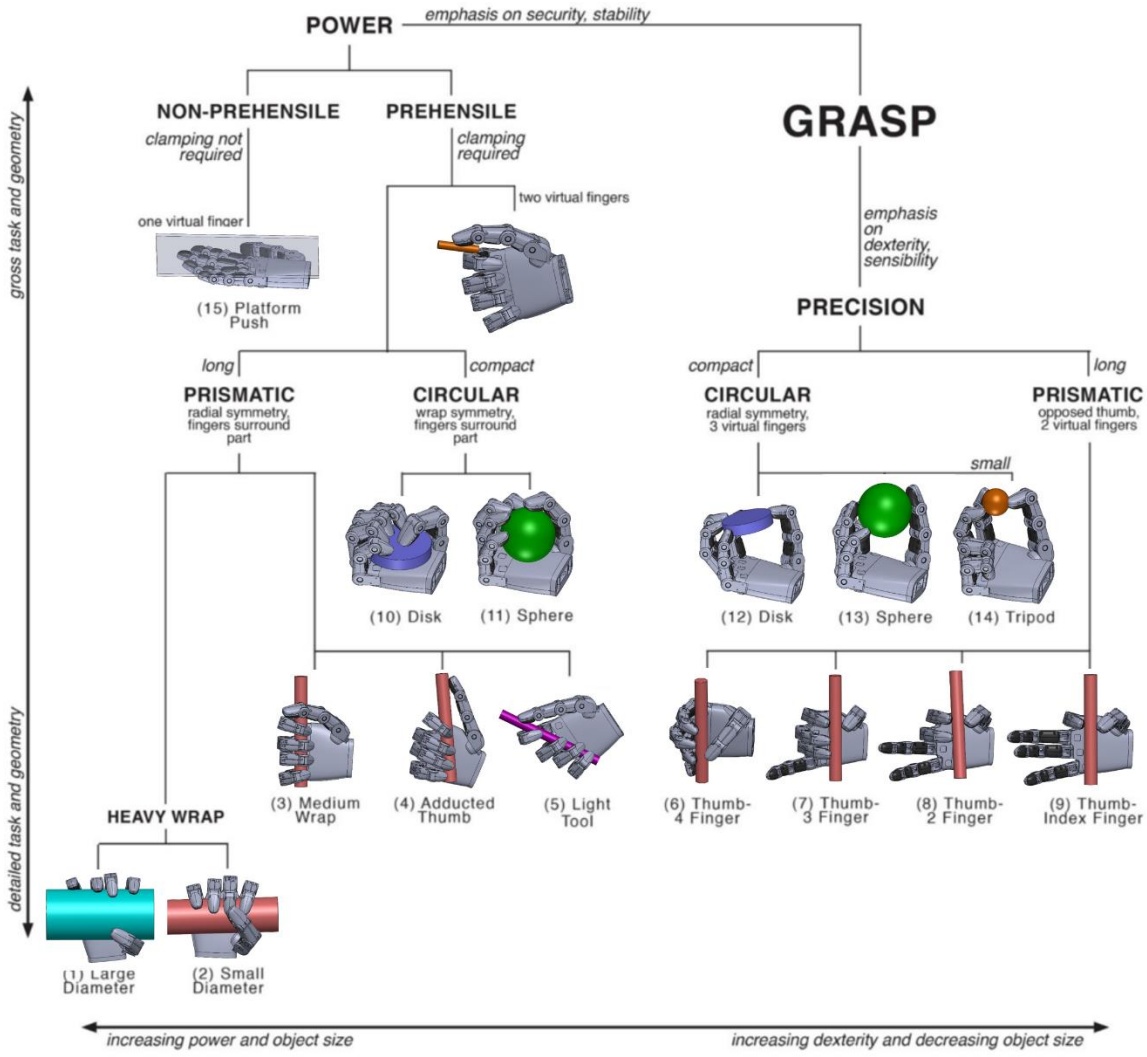

Figure 41. The updated hand performing the grasps of Cutkosky's Taxonomy.

3.5.8. Future work

Due to the design changes made between the initial design and the updated one, the bend sensors used for position feedback control were not integrated. Currently direct feedback at the joints is not available. In the next phase of the hand, the addition of analog Hall Effect sensors is desired, due to their low-profile, good reliability, and low cost. A low-profile diametric magnet can be mounted at the joint center and the sensor

placed very closely by on the preceding phalange as shown in Figure 42. These sensors provide contactless sensing. Alternatively, there is available interior space in each phalange, so locating the sensor internally is also a viable option.

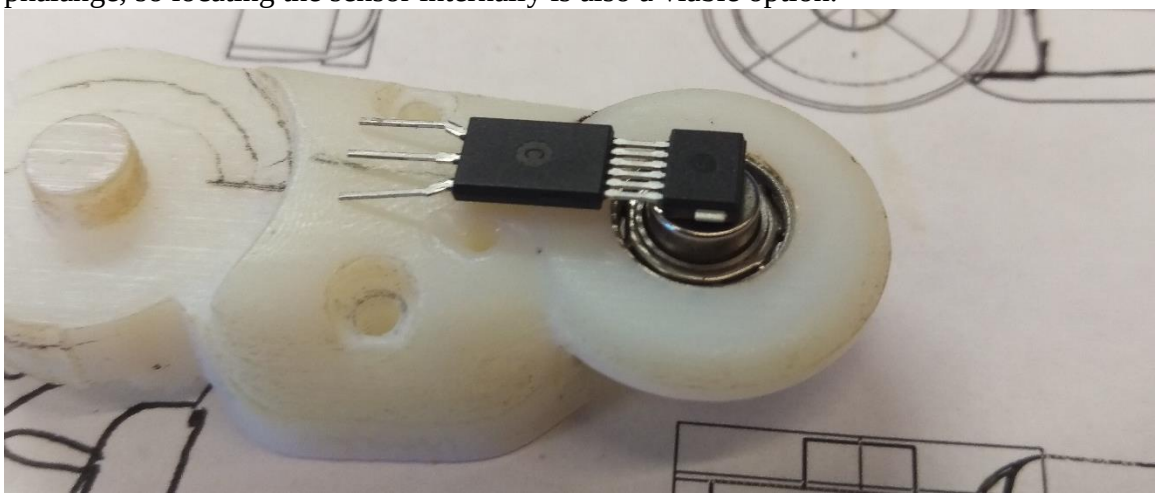

Figure 42. An analog Hall Effect sensor with magnet shown on a phalange prototype.

Additionally, the palm does not include the abduction/abduction motors, eliminating two active DoF. In an incremental update, slight modifications of the palm and the knuckles of the index and pinky fingers can be made to accommodate the mechanism featured in the initial design of the DASH Hand.

Lastly, as was intended by the nature of the design, additional experimentation with sensors and control systems is desired and anticipated. Users can augment the capability of the hand as they see fit for their applications. In the next two following sections, the creation of a tactile sensor is presented, as well as a method of impedance control that minimizes the need for extra sensors.

3.6 Impedance Control

3.6.1. Introduction

The primary use of a human hand is to grip and manipulate objects, and robotic hands seek to achieve the same goals. In order to achieve this, the later attempts to mimic the methodologies of the former. In addition to controlling the joints on the hand to the desired position, humans are able to control the amount of force applied to an object using both the proprioceptive and somatosensory systems. The proprioceptive system is the ability for the body to feel the relative position of the finger joints and the amount of effort being exerted by the hand muscles. The somatosensory system is responsible for the sense of touch, including the ability to feel pressure (both axial and sheer), texture, vibration, temperature. Robotics are limited in the ability to mimic the somatosensory systems because they are typically not completely covered in sensors, while the human hand is covered in skin. If a force is applied to a point on the hand without a touch sensor, the robot is unaware of the location or direction of the force. Additionally, many of the sensors used on the robotic hands cannot sense both sheer and axial forces, leaving the control system with an incomplete set of kinetic data. Therefore, many robotic systems seek to mimic the proprioceptive system using impedance control.

3.6.2. Overview of Impedance control

Impedance control seeks to control the force of resistance to external motions that are imposed by the environment. In other words, a joint will be commanded to a specific position and velocity. If an external force is applied that resists the joint achieving this goal, the impedance control attempts to alter force the joint applies against the external force. Impedance control is typically implemented using kinematic and force/torque data. Position sensors on the actuator and/or the joints of the finger are used to measure kinematic data, and some robots use torque or force sensors on the joints to directly measure the external forces.

3.6.3. Need for impedance control in the sensor

Impedance control provides two primary advantages for this system: the ability to control the force of the grasp or touch of an objects, and the ability to protect the hand itself from damage caused either by grasping/pushing with too much force or from an collisions with the hand. The former would provide the hand with greater dexterity. Both advantages would be extremely useful when using the data glove to control the hand. Since the user would primarily be controlling the hands using visual feedback, the impedance control would allow the robot to compensate for user error or the lack of user knowledge of the object being manipulated. Additionally, the force data could be provided to the user in an effort to improve user performance.

3.6.4. Proposed 'Sensorless' Impedance Control Methodology

With the goal of this robotic hand to be a low-cost system, hobby servomotors are implemented as the actuators. These motors are operated in an open loop control system, where the motor is provided a desired position which it then attempts to achieve using its internal electronics. The user is not provided the actual motor position. Additionally, the hand does not currently include any sensors to measure the position of the finger or wrist joints. This means that the kinematic data is not available without additional hardware. However, the current applied to the motor is proportional to the torque applied by the motor. Therefore, the proposed method employs a 'sensorless' methodology, analogous to sensorless FOC used in the control of permanent magnet synchronous motors using only current sensors to negate the need for a rotor speed or velocity sensor (Akin, Bhardwaj, and Warriner, 2013). This method uses only the current supplied to the servomotor to interpolate any external forces being applied to the finger. No position sensors would be added to the design. Although the servomotor has an internal potentiometer, it cannot be accessed without significantly modifying the motor. Not including position or velocity sensors provides several key advantages:

- Less complex mechanical design.
- Less expensive.
- Simpler assembly due to fewer parts and the lack of need to calibrate each position sensor.

The use of current sensors provides additional advantages. The chips used to measure the servomotor current are physically small. The current sensing can also be

placed away from the actuator with the control electronics. This keeps the sensing protected, both physically and electromagnetically. Finally printed circuit boards are inexpensive and relatively easy to produce.

3.6.5. Limitations of the Proposed Method

Despite the proposed method being simple and inexpensive, a number of challenges also exist:

- Lack of finger torque/force feedback.

  Without directly measuring the force at the joint, the impedance algorithm must interpolate the external forces applied to a finger from other information instead of the true force.
- Lack of finger position feedback.

Without measuring the position of the joint, the impedance algorithm cannot determine if the finger is moving due to external, uncommanded forces.

- Lack of servo position feedback.
  - Cannot determine if a change in current is due to a motor action or external forces.
  - Cannot tell the direction that the motor is being moved.
  - Attempting to perform a closed loop impedance control around a nested closed loop system that cannot be observed.
  - The only information on motor movement is the command to the servomotor, meaning the time when the commanded position has been achieved is unknown.
- Single direction of controlled actuation.

Because the hand is tendon-based and uses springs to passively return the joints to straight, the controller cannot impact the finger if the external force is applied in the retract direction.

- Current applied to the servomotor is only in one direction.

The servomotor's internal circuitry determines the direction in which the current is applied to the motor, but the current always flows in the same direction into the motor. Therefore, the impedance controller cannot determine which direction the current is attempting to make the motor move, only the amplitude.

- Servomotor analog position controller.

The servomotor includes analog electronics that drive the motor to the desired position. The dynamics of the analog controller are unknown, and without the motor position from the internal position sensor it wouldn't be useful.

3.6.6. Experimental Setup

To develop the sensorless impedance controller, the servomotor was initially tested independently of the hand. The Hitec HS-645MG, which is one of the servomotors used for many joints in the hand, was controlled by an Arduino Mega 2560. An Allegro ACS712 Hall Effect current sensor was used to measure the current into the servomotor. A schematic of the experimental setup is shown in Figure 43.

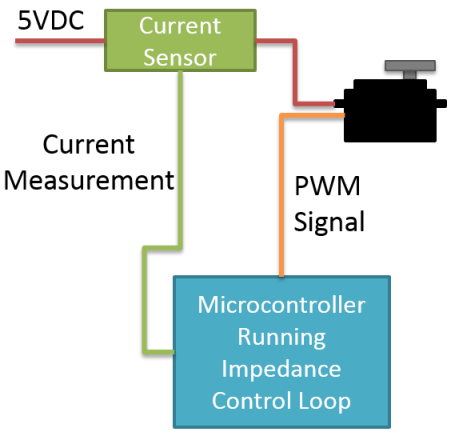

Figure 43. A schematic for the experimental setup of the 'sensorless' impedance controller.

3.6.7. Control Law

The impedance controller has two goals:

- Devise a simple, tunable algorithm with parameters that hold real-world meaning.
- Stable performance.

The impedance controller works by subtracting an offset from the commanded position in an effort to decrease the applied motor effort. This offset is initially zero until the measured current rises above the offset increase threshold. Then the offset begins to increase as long as the current remains above the increase threshold. This moves the finger away from its commanded position toward the fully retracted position. A second threshold, the offset decrease threshold which is lower than the increase threshold, is used to determine when the offset can begin to decrease. However, to reduce the joint limit cycling, the current must remain below the offset decrease threshold for a set period of time before the offset begins to decrease. This then moves the finger toward the commanded position. The rate in which the offset increases is separately tunable from the rate at which it decreases.

1. $\theta_{des} = \theta_{cmd} - \phi$

2. $$\phi = \begin{cases} \phi_{prev} + \alpha, \ \ if\ I > I_{\alpha} \\ \phi_{prev}, if\ \left(I < I_{\beta}\right)\ \&\ (T < T_{\beta}) \\ \phi_{prev} - \beta, if\ \left(I < I_{\beta}\right)\ \&\ (T < T_{\beta}) \end{cases}$$

3. $\phi_{min} < \phi < \phi_{max}$

Where θ_{des} is the desired position that is sent to the servo after the impedance control is applied, θ_{cmd} is the commanded servo position, ϕ is the offset from the commanded position generated by the impedance control. ϕ_{prev} is the pervious offset, α

is the offset increase per cycle, β is the offset decrease per cycle, I is the measured current into the servo, I_α is the current threshold to start increasing the offset, I_β is the current threshold to start decreasing the offset, T is the time since the current decreased below the decrease threshold, T_β is the time threshold for how long the current must remain below the decrease current threshold before the offset begins decreasing, ϕ_{min} is the minimum offset (which is always zero), and ϕ_{max} is the maximum allowable offset.

3.6.8. Control Results

At 7.3 seconds, an external torque was applied to the servomotor, as seen in Figure 44. The current then increased, and the impedance controller began decreasing the desired position (the position command sent to the servomotor). This continued until 9.3 seconds, when the external force was removed and the current decreased below the offset decrease threshold. The desired position then increased until it 10.6 seconds, when it again equaled the commanded position.

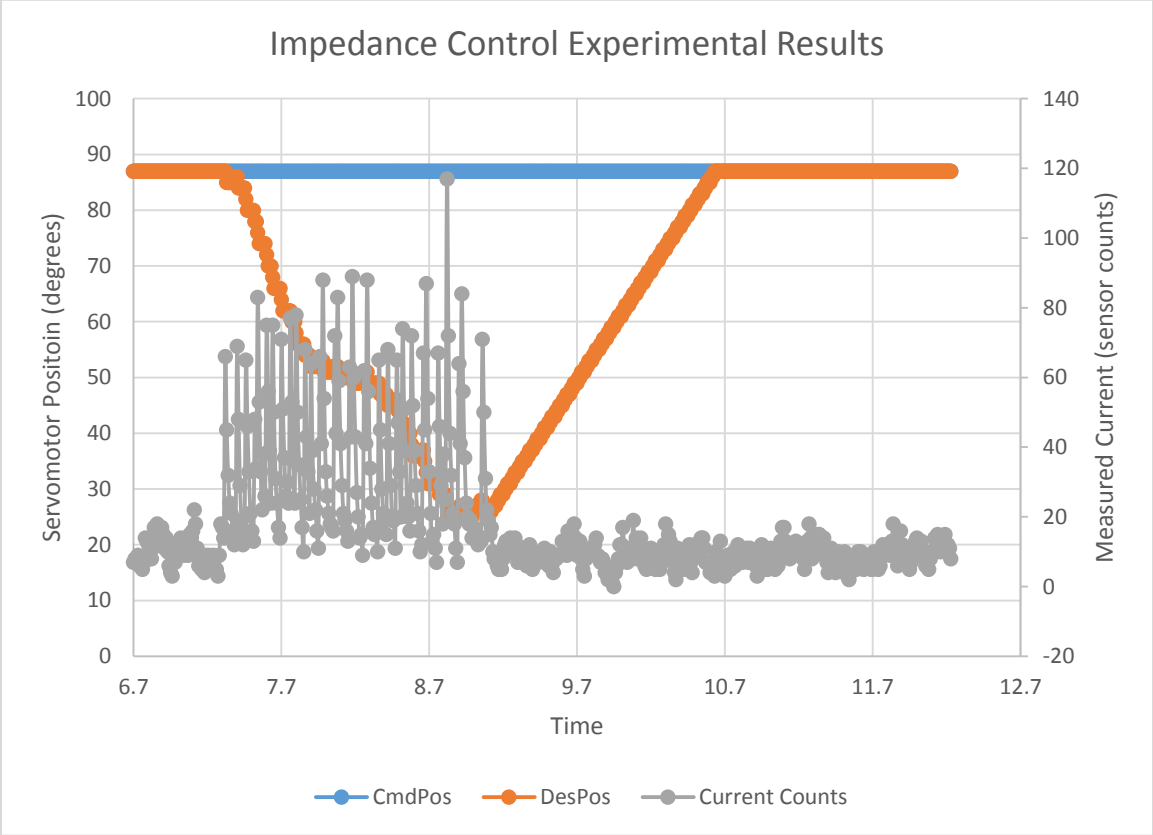

Figure 44. Experimental results of the impedance control of the servomotor.

4. Review of Data Glove Control

4.1 Need for Teleoperation

There are numerous application domains that require human operators to regularly expose themselves to dangerous situations and environments in the line of duty, such as

Explosive Ordinance Disposal (EOD) technicians, the agents tasked with containing the leakage during the Fukushima disaster, and even the astronauts. All of these tasks could ideally be performed by robots, and remove humans from harm's way. However, current control schemes for robotic automation have limitations as they cannot match a human's expertise, and thus humans must still risk life and limb to accomplish these dangerous tasks. In recent years, teleoperated robots have increasingly become available, but still lack full implementation into the wider world due to prohibitively high costs. If these robotics and their controllers could be made affordable, there would be an increased demand for human controlled robotics that function at the same level as a human technician. This scenario of humans remotely controlling the robot with the same degrees of freedom and range of motion as a human being will open many new possibilities.

4.2 Current Control Options

A human-like robotic manipulator provides an excellent compromise between strength and dexterity. However, the question that needs to be answered is "how to control the robotic manipulator?" In its ideal form, a human hand is comprised of 22 degrees of freedom, though this is often reduced using coupled motions to more simple versions such as the 16 degrees of freedom DASH hand, shown in Figure 45. However, more complex versions of robotic hands have been demonstrated, such as the Shadow Hand, which comprises of 22 fully actuated degrees of freedom.

Figure 45. The DASH Hand, shown in comparison with an adult male hand (Stevens, 2013). Reprinted with permission (see Appendix A).

When selecting a robotic controller the key concern is user familiarity. For example, a computer mouse is a simple two degree of freedom controller that is commonly utilized. Only, in some cases it requires specialized training for new users, particularly children who have not been trained on those specific motor skills (Joiner, Messer, Light, & Littleton, 1998). However, even with certain non-traditional mice that are used for gaming or other technical purposes, the maximum degrees of freedom that can be operated by one hand would be limited. Another controller option is a multi-axis mouse or joystick, which has become popular for Computer Assisted Drafting (CAD)

programs. These controllers allow for an object to be rotated, panned, zoomed, and tilted in 3-D space using a single hand. These tools require some training, as they are not as familiar to the average user as a simple mouse, though they allow for more complex control of a system.

While these tools have suitable features desired in a variety of applications, they fail to take advantage of one of the key features of a human-like manipulator and that is familiarity. Using a human-like hand for robotic teleoperation not only provides the capability of using many human tools that are essential but it also allows for a very clear association from the user to operate said manipulator as the user can use the manipulator to effectively mimic their own methods of using tools. As such, it would be ideal to give the user a controller that capitalizes on this inherent familiarity with a user's own hand to apply to the robotic manipulator.

4.3 Data Glove Technology

A human-like user control interface could be developed using a data glove. A data glove, which is also called a wired glove or sensor glove, is a fabric glove worn by a human user that utilizes sensors to detect the positions of the user's digits, and translate them to an external program to be further used to control or record hand positions. Using a data glove, it would be possible for a human user to effectively control a biomimetic robotic manipulator by directly mimicking their own motions, creating a seamless meshing of human teleoperative control.

One of the first data gloves invented was the "Sayre Glove," in 1977 as part of virtual reality simulations in an era where instrumentation and processing were in their infancy. The Sayre Glove used an early version of fiber-optic sensors consisted of small illuminated tubes whose light intensity varied based on the angle of bending in the finger (Sturman & Zeltzer, 1994). Since this initial foray into sensing hand positioning, there has been a keen interest in virtual reality applications in the 1990's (Carlson, 2003), which began to flow over into the commercial world, particularly with the Nintendo Power Glove (Sturman & Zeltzer, 1994). However, due to the difficulties in reading and processing analog signals, typical consumer applications remained limited due to prohibitive costs for accurately sensing and reading information. In the end, data glove technology ended as something of a gimmick.

Despite this initial setback into commercial realms, data glove technology continues to be explored, but in a limited scope. From a brief survey of the available data gloves, it becomes quickly apparent that typical data gloves are not affordable for the average consumer, as noted in Table 5.

Table 5. Commercially available and research data gloves, with their respective sensing methods, degrees of freedom, sensitivity, and cost.

Name	Degrees of Freedom(DOF)	Sensing Method	Sensitivity	Cost(USD)
5DT 5 Ultra [76]	5	Fiber Optic	< 1 degree	$1,000
5DT 14 Ultra [76]	14	Fiber Optic	< 1 degree	$5,500

[76] (Fifth Dimension Technologies, 2005)

Cyber Glove [77]	18, 22	Resistive	0.5 degree	$10000-15000
Cyber Glove 2 [78]	18, 22	Resistive	< 1 degree	$12000-$18000
Cyber Glove III [79]	18, 22	Resistive	0.5 degree	$15,000
VMG Lite [80]	11	Resistive	<1 degree	$600
DG5 VHand 2.0 [81]	10	Resistive	<1 degree	$400
P5 [82]	5	Resistive	0.5 degree	$79.00
Didjiglove [83]	10	Capacitive	<1 degree	$5000
Pinch Glove [84]	4	Contact Switch	Digital	$2000
Dextrous Hand Master [85]	20	Hall Effect	< 1 degree	$5000-$10000
DataGlove [85]	20	Fiber Optic	1 degree	$5000-$10000
Power Glove [86]	8	Resistive	3 steps	$75
Color Glove [87]	9	Color tracking	Unknown	$5 + optics
TCAS Glove [84]	8, 11, 16	Resistive	Unknown	$7000+

As is evident from the majority of the listed data gloves, obtaining an accurate data glove with more than 5 degrees of freedom is exceedingly expensive. In order to properly control most dexterous operations for anthropomorphic robotic hands, at least two degrees of freedom per finger must be independently measured and the thumb should have an additional degree of freedom for adduction and abduction. While 104 discrete data gloves have been developed for rehabilitation, entertainment, and virtual reality, only 34 have the proper number of measured degrees of freedom for grasping, reliability of not losing readings due to occlusion or other errors, and sensitivity for fine dexterous control (around 1 degree of sensitivity). A majority of camera-based methods were not included due to the risk of occlusion and loss of tracking, which would be catastrophic in medical or industrial applications where constant tracking is a safety issue. These final gloves have been detailed in Table 6, with details about their sensing technology and degrees of freedom measured. The feasible gloves for robotics applications, with considerations of cost, sensitivity and error, user friendliness, and implementation, are ranked and reported in best-first ordered. Thus one of the objectives of this study was to determine a methodology to create a data glove that (i) allows for at least 10 degrees of freedom, (ii) is user friendly, and (iii) can be used by numerous hand sizes. The goal was to achieve all of these features while keeping the costs of production below $250.

[77] (Cyber Glover Systems, LLC, 2011)
[78] (Tom's Hardware, 2005)
[79] (Cyber Glover Systems, LLC., 2011)
[80] (Virtual Realities, 2016)
[81] (DG5 VHand 2.0, 2008)
[82] (Cyberworld Inc., 2013)
[83] (Didjiglove, 2008)
[84] (Youngblut, Johnston, Nash, Wienclaw, Will, 1996)
[85] (Caldwell, Andersen, Bowler, Wardle, 1995)
[86] (Gardner, 1989)
[87] (Lamberti, Camastra, Tecnico, Enrico, 2011)

Table 6. Feasible data gloves for robot control, based on degrees of freedom, sensitivity, and reliability.

Glove Name	Institution	Sensing Technology	Degrees of Freedom Measured
VMG 30 [88]	Virtual Motion Labs	Bending (Ambiguous) Hand, Wrist 6DoF (IMU)	28
Tyndall/University of Ulster Glove [89]	University College Cork	Resistive bending (Flexpoint) 3DoF Accelerometers	23
SIGMA [90]	Sheffield University	Resistive bending (carbon ink)	30
CyberGlove 2 [91]	Cyberglove Systems, LLC	Resistive bending	18, 22
CyberGlove Data Glove [92]	Cyberglove Systems, LLC	Resistive bending (thin foil strain gauge)	18, 22
MoCap Glove [93]	Cyberglove Systems, LLC	Resistive bending	18, 22
SuperGlove [84]	Nissho Electronics	Resistive bending	10
5DT Data Glove 14 Ultra [94]	Fifth Dimension Technologies Inc.	Fiber Optics	14
Unnamed [95]	National Taipei University	IMU	16
TU-Berlin SensorGlove [96]	Technical University of Berlin	Inductive length encoder 3D Spatial tracking	15
Unnamed [97]	University of Dong-Eui	Resistive bending (Abrams Gentile Co)	11
HITEG-glove [98]	University of Rome "Tor Vergata"	Resistive bending (Flexpoint)	15

[88] (VMG 30)
[89] (O'Flynn et al., 2013)
[90] (Williams, 1997)
[91] (Cyberglove Systems, 2009)
[92] (Cyberglove Systems, 2007)
[93] (Cyberglove Systems, 2010)
[94] (Fifth Dimension Technologies)
[95] (Lin, Lee, Hsiao, Yang, & Chou, 2014)
[96] (Hofmann & Henz, 1995)
[97] (Park, Bae, & Moon, 2009)
[98] (Saggio, Bocchetti, Pinto, & Orengo, 2010)

Unnamed [99]	Saliwanchik Lloyd & Saliwanchik	Resistive bending (electrode resistance strain-related with separating conductive rubber)	24
TCAS Glove [84]	TCAS Effects Limited	Resistive bending	8, 11, 16
Unnamed [100]	Mahidol University	Conductive polymer strain gauges	10
PERCRO Data Glove [101]	Scuola Superiore Sant'Anna (PERCRO)	Magnetic (Goniometric)	11
3D Imaging Data Glove [102]	University of East Anglia University of Newcastle upon Tyne	Magnetic (inductive sensor in magnetic field)	11
Unnamed [103]	Arthur D. Little, Inc.	Hall effect	10
Humanglove [104]	Humanwave	Hall effect	20
SuperGlove Jr [105]	Nissho Electronics	Resistive bending	10
The Sensing Glove [106]	University of Pisa, Italy	Resistive bending (conductive elastomer, piezoresistive)	10
Unnamed [107]	Stanford	Resistive bending (strain gauge)	14
Unnamed [108]	Modern Cartoons, Ltd	Resistive bending	12
Unnamed [109]	The Waikato Polytechnic	Potentiometer IR Deflection	22
Rutgers Master II - New Design [110]	Rutgers University	Magnetic (Hall Effect) Infrared reflective distance	15
Dextrous Hand Master [84]	Exos	Hall effect	20
Unnamed [111]	Pioneer Electronic Corporation	Ultrasonic or Infrared distance sensors	21

[99] (Daum, Gunther, Husert, & Scherr, 2002)
[100] (Tongrod, Lokavee, Watthanawisuth, Tuantranont, & Kerdcharoen, 2013)
[101] (Portillo-Rodriguez et al., 2007)
[102] (Su et al., 2003)
[103] (Marcus, Lawrence, & Churchill, 1991)
[104] (Dipietro, Sabatini, & Dario, 2003)
[105] (Ishikawa & Matsumura, 1999)
[106] (Tognetti, Carbonaro, Zupone, & De Rossi, 2006)
[107] (Kramer, Lindener, & George, 1991)
[108] (Walker & Baheshti, 2000)
[109] (Iredale, Farrington, & Jaques, 1997)
[110] (Bouzit, Burdea, Popescu, & Boian, 2002)
[111] (Araki, 1996)

Rutgers Master II [112]	Rutgers University	Infrared reflective distance Magnetic (Hall Effect) Hand 6DoF (Polhemus)	21
Sensor Glove 2 [113]	University of Tokyo	Rotary encoders	20
Z-Glove [114]	Visual Programming Language Research	Ultrasonic positioning/orientation Optical flex sensors (Fiber optic)	20
DataGlove [114]	Visual Programming Language Research	Magnetic Position/orientation (Polhemus) Optical flex sensors (Fiber optic)	20
Stringlove [115]	Kyoto University Hospital	Magnetic (inductocoders)	22
Unnamed [116]	National Taiwan University of Science and Technology	Magnetic induction	10
Data Glove Input System [85]	University of Salford	Hall effect	9

4.4 Sensing Methods

One of the most important factors when designing a data glove is determining the method through which the finger positions will be sensed. In the past 30 years of research on data glove development multiple methods for sensing have been investigated. The most prevalent methods for finger joint tracking are visual, magnetic, and infrared spatial tracking; direct measurement using resistive bend sensors, fiber-optic bend sensors, and rotary encoders; and indirect tracking using magnetic inductance, Hall effect sensors, and accelerometers.

4.4.1. Spatial tracking

The bulk motion of the hand, as well as the motion of the fingers, can be tracked in the space of an operating environment. Once the coordinates and orientations of each joint or link location are determined, forward and inverse kinematics can be used to form the model of the hand in space or relative to the back of the hand.

[112] (Gomez, 1997)
[113] (Tsagarakis, Kenward, Rosander, Caldwell, & von Hofsten, 2006)
[114] (Zimmerman, Lanier, Blanchard, Bryson, & Harvill, 1987)
[115] (Kuroda, Tabata, Goto, Ikuta, & Murakami, 2004)
[116] (Fahn & Sun, 2005)

4.4.1.1. Visual

The motion of the hand can be tracked in the operating volume while using an external camera system and landmarks or discrete trackers on the hand. The cost effective solution for commercial applications, such as the P5 glove (Lam, Zou, & Komura, 2004), utilizes an infrared locating system for reflective markers on the data glove. However, the resolution and repeatability of this method is lower than desired for precision tasks. The simplest forms of visual tracking include using a single camera with markers along the user's hand to determine joint locations (Han, 2010) or using a combination of a traditional camera and depth-mapping camera to give a 3D image of the hand (Biswas, 2011). These markers can be discrete reflective trackers, such as with VICON systems, or simple painted patterns around the glove the can be tracked using an RGB camera (Wang & Popović, 2009; Lamberti, Camastra, Tecnico, & Enrico, 2011). This method is popular because it is very inexpensive, only requiring a camera and relatively simple software. Furthermore, the user is not tethered to any machinery, allowing for mostly uninhibited movement. However, there are some distinct flaws in this method. Namely, using markers along each joint of a human hand requires a significant amount of time to place each marker in their designated spot. Furthermore, if any marker falls off or becomes hidden from the viewing cameras, the software will not be able to recognize the position of the hand. As such, this method is typically limited to academic settings or entertainment due to the availability of large operating volumes, multiple cameras, and several sizes of tracking markers that circumvents the problems of occlusion and freedom of movement. However, usage of depth mapping and traditional cameras is quickly becoming a more popular method of tracking joint locations. This system has already been available on a larger scale for tracking human limbs in the Microsoft Kinect (Microsoft, 2013; Zhang, 2011), while a smaller system called the Leap Motion (Leap Motion, 2013) is available to consumers for the purpose of tracking hand movements and gestures for computer user interfaces. Still, like traditional cameras, the Kinect and Leap Motion are limited to what is visible in the camera's field of view, and as such, lacks portability for users and scale for industrial operations.

4.4.1.2. Magnetic

By attaching magnetic sensing coils to the hand, fingers, and arm, an external magnetic field source can be utilized to triangulate the position and orientation of landmarks in space. The most popular devices for magnetic tracking of objects in space are the Polhemus (Burdea, Zhuang, Roskos, Silver, and Langrana, 1992; Polhemus Navigation Sciences Division, 1987; Gomez, 1997; Hong and Tan, 1989) and Ascension Flock of Birds systems (Kallmann & Thalmann, 1999; Oz & Leu, 2005). As mentioned before, the spatial coordinates can be reduced to angular positions relative to the arm or hand (Su, Allen, Geng, Burn, Brechany, Bell, & Rowland, 2003). However, similar issues of portability and scale are limiting for widespread applications of magnetic tracking systems. In addition, magnetic field tracking, especially in close proximity of other tracking systems and the earth's magnetic field, has inherent interference that may need additional calibration and filtering.

4.4.1.3. Optical

For accurate and more sensitive photosensitive systems with affordable cost, several optical sensor based data glove techniques have been suggested in recent years. An optoelectronic joint angular sensor that consists of LED (light source) and photodiode (detector) couple mounted to two continuous phalanges of robotic hands have been considered to track the joint angles in data glove. When the finger joints are flexed, the angle between LED and photodiode is changed, leading to changing irradiated light intensity to the photodiodes. The angular displacement can be determined by the measured photocurrent of the photodiodes in this system (Cavallo, De Maria, Natale, & Pirozzi, 2009). This system was reported to have good repeatability and linearity, and low noise of data signal with low cost for system construction. In similar way for an alternative optical based data glove technique, a novel sensor based on optical linear encoder have been introduced (Li, Chen, & Yeo, 2010; Li, Chen, Yeo, & Lim, 2011; Lim et al., 2008). The optical linear encoder is a small size optical sensor that generates a pulse signal as it detects an interruption to its reflective path. It consists of an infrared emitter and a receiver couple in a single module. The infrared light from the emitter is reflected off a reflective linear code strip, which is fabricated using a photo-plotter engraved with parallel lines onto reflective linear code strips, and the reflected light is detected by the receiver. When the finger joints are flexed, the light is reflected and the receiver outputs two electrical pulses that are 90° out of phase. The out of phase electrical pulses indicate the direction of travel of the fingers as the encoder moves over the linear code strip. This technique enables capturing multi-finger motion in data glove device with compact size, light weight, and low power consumption. Furthermore, good linearity and accuracy of the digital output signal of optical linear encoder provide high repeatability and reliability in both the gripped and flat hand positions.

4.4.2. Indirect tracking

Although direct sensing of the position of the fingers and hand is desired for accuracy and limited processing, mechanical means for angular measurements typically increase resistance for the operator and rely on mechanical phenomena that may lose accuracy over time due to fatigue and wear. In addition, the housings for mechanical sensing methods add additional weight to the glove, which increases strain on the user with prolonged use. Therefore, indirect measurements allow lower strain on the user with minimal reduction in accuracy.

4.4.2.1. Magnetic sensing

Instead of spatially tracking the position of magnetic elements in space, magnetic inductance and Hall Effect sensors can be used for tracking local magnetic landmarks. Magnetic coils fixed on the hand can generate a local magnetic field at a prescribed frequency, and sensor coils at the tips of the fingers can generate a voltage proportional to the distance and angle from the generator (Fahn & Sun, 2010). In addition, by isolating the magnetic signal at different frequencies the position and orientation from other generators can provide feedback for adduction and abduction in the fingers. As with magnetic spatial tracking, magnetic interference can add additional noise or biasing that requires filtering and calibration.

As a compromise between low resistance on movement and the accuracy of direct sensing, Hall Effect sensors are integrated into multiple unique sensor packages for data gloves. The most popular application is the measurement of rotary joints in line with the finger joints or in parallel in a linkage structure. By using magnets that are coupled with the sensor but rotate in opposition during joint movement, the relative motion is sensed and relayed in a feedback signal from the Hall sensor (Bouzit, Burdea, Popescu, & Boian, 2002; Gomez, 1997; Marcus, Lawrence, & Churchill, 1991). Similar to the magnetic coils application, the relative motion of a Hall sensor on one link of a joint and a magnet on the opposite link of a joint causes relative translation and rotation during finger joint deflection, which in turn generates an electric signal (Caldwell, Andersen, Bowler, & Wardle, 1995). As a non-resistive alternative to bending sensors, a Hall Effect sensor can be placed at the base of a finger or a link with a proximal magnet attached to a flexible element or string. Instead of the flexion of the finger changing the direction and distance of a sensing element, the deflection causes displacement of the magnet due to the cable stretching or pulling and in turn initiate a signal due to relative displacement (Kuroda, Tabata, & Goto, 2004; Portillo-Rodriguez et al., 2007). The low cost and small size of these sensors, with discrete sensors and magnetic elements embedded in the gloves, enables low computation and setup time for sensing multiple degrees of freedom.

4.4.2.2. Inertial sensing

Due to the low cost, size, and weight of MEMS accelerometers and inertial measurement units, one of the most popular sensing methods for data gloves are gravitational and relative movement sensing. Static poses can be sensed by measuring the distribution of gravitational acceleration between the two or three axes of the accelerometer (Hernandez-Rebollar, Kyriakopoulos, & Lindeman, 2002; Lin, Lee, Hsiao, Yang, and Chou, 2014; Perng, Fisher, Hollar, & Pister, 1999). This can be resolved to the orientation of the sensor, and the relative orientation of the finger tips and links can be calculated to find joint angles. Since it is low cost and low interference to integrate 3 DoF accelerometers or full inertial measurement units, more sensors can be integrated on the glove. This also means that fewer sensors can determine multiple degrees of freedom in the hand due to physical constraints of link and joint positions. Many data gloves that utilize inertial sensing have too few degrees of sensing to function as robot control gloves, but they have enough readings to act as gesture identification data gloves. However, data gloves that use alternative sensing methods integrate accelerometers, gyroscopes, and IMUs in key locations such as the back of the hand to provide redundancy in the sensing of other sensors and establish a coordinate frame for the hand or forearm (O'Flynn et al., 2013).

4.4.3. Direct angle measurement

Directly measuring the angle of the finger joints based on physical deflection is the most reliable method for measuring finger position due to less computational requirements for decoupling and isolating joint angles, as well as physical constraints to the sensors. This enables onboard calculations and wireless data relaying to the home station of the robotic devices, which greatly improves usability as well as generalizability for different discrete applications in industry.

4.4.3.1. Rotary encoders and potentiometers

Rotary encoders or potentiometers in line with the joints or linked with joint movement through mechanical apparatus greatly reduce the error, cost, electrical setup, and computational power for correlation or acquisition. Rotary encoders directly measure the rotation of a joint by optically sensing openings in a slotted disk, which in turn sends a pulse from a series of photo diodes to a microcontroller that can be converted into a fraction of a full rotation or a discrete position. Non-directional rotary encoders require rotational reference calibration and a way to measure direction, while directional rotary encoders include a direction and zero reference when rotated. Potentiometers also directly measure the rotational location of a joint by rotating a wiper along a resistive path. Since angular deflection changes the resistance of the potentiometer, both position and direction can be determined with a single low-cost device. The response of potentiometers, especially if manufactured with higher quality control, are typically linear and can be easily correlated to rotary position. However, the physical wiper contact adds friction to the movement of the joint, and the wiper can wear out over time. While these parts are low cost and reliable, they still need mechanical fixtures to convert joint position into a rotation of the measuring input axis, and repair of worn potentiometers decreases the long-term usability of the sensors.

4.4.3.2. Fiber optic bend sensors

From the very onset of data glove technology, fiber optic bend sensors have been used in data gloves, highlighted in the Sayre Glove, which was noted to be the first of its kind (Sturman & Zeltzer, 1994). Fiber optic cables operate using thin glass or plastic tubes to project light along the length of the wire with little or no losses over long distances using total internal reflection along the interior of the cable. These cables have become popular in recent years due to their applications for transmitting data over long distances (Data Connect Enterprise, 2013). Fiber optics are also used for non-destructive evaluation as they can detect small deformations. As the change occurs in radius along the length of the cable there is modulation of the intensity at the end of the cable, which can be detected by a simple photosensitive cell. The change in light intensity can be further amplified using series of Fiber-Bragg gratings along the length of the wire located directly on the platform subjected to bending. As these gratings are rotated or shifted relative to the incoming light beam, the resultant change in light intensity is read by the photosensitive cell.

Despite this being one of the oldest technologies used by the data gloves, this method still remains popular for a number of reasons. Using specialized Fiber-Bragg gratings allows for very sensitive readings of joint locations, while minimizing the interference from outside sources, namely temperature dependence seen in some resistive sensors. It entirely eliminates the electromagnetic interference at the location of the sensor (Baek, Jeong, & Lee, 2002). As such, these sensors are the exclusive option for researchers intending to perform studies nearby large magnets, such as those of an fMRI used to assess a stroke patient's motor skills. However, these sensors are quite expensive, as producing a custom fiber optic sensor with the correct fiber-Bragg grating specifications makes the sensors themselves expensive, while also requiring a suitably sensitive photosensitive system to read varying light intensity from the sensors.

A third method that was selected for the design of the data glove in this study was resistive based strain sensors. Resistive sensors are common, inexpensive, and simple to use as they require a conventional circuit and small input voltage to return the relevant data. They have a large variety of uses, which range from detecting small deflections in structural elements of bridge (Kang, Schulz, Kim, Shanov, & Shi, 2006), to large deflection purposes such as observing changes in finger position (Gentner & Classen, 2009). Regardless of the application platform, the operation of resistive strain sensors remains the same. At their core, resistive sensors consist of conductive material that changes its resistance due to the volumetric changes under external strain. Since the sensor is placed above the finger joint, the deflection will be above the neutral axis and initiate tension in the sensor. Resistivity rules dictate that resistance $R = \rho L/A$, where ρ is the resistivity of a specific material, L is the length of the element, and A is the cross sectional area. Since resistivity is constant, resistance scales by L/A. As a material is put under tension the length will increase and the cross sectional area decrease, thus increasing resistance. The Poisson's ratio of the material will dictate whether length or cross sectional change will dominate in the behavior, and hence the strain characteristics of materials as a sensor. When the sensor is placed in a voltage divider, the voltage drop across the increasing resistance will increase and hence the output voltage between the divider elements will decrease. Resistance matching of the divider resistor to the operating range resistance of the sensor can tune the sensitivity and linearity of the sensor output voltage. The voltage change can then be correlated with the magnitude of strain observed by the sensor.

Figure 46. Flexpoint bend sensors, in 1", 2", and 3" lengths (Saggio, et al., 2014). Used under Open Access.

One of the most common resistive based strain sensors are simple wired strain gages that are used in various industrial applications. However, these sensors are typically limited to relatively small strains, such as bending and stretching of metal samples, which are very small (Kramer, Lindener, & George, 1991; Sturman & Zeltzer, 1994). These gauges can be adapted to larger strains by developing the shapes out of polymer materials (Tongrod, Lokavee, Watthanawisuth, Tuantranont, & Kerdcharoen, 2013), graphene nanopaper (Yan et al., 2014), Velostat carbon film (Jeong, Lee, & Kim,

2011), carbon nanotubes (Yamada et al., 2011), or other materials that can elongate under larger strain. In comparison to these samples, an ideal resistive sensor for the data glove would need to be able to absorb large magnitudes of bending to measure the position of a human finger as it bends. This has been accomplished by piezoresistive elastomers that are printed directly on the glove (Tognetti, Carbonaro, Zupone, & De Rossi, 2006), as well as widely used commercial resistive elements from Abrams Gentile Co. (Park, Bae, & Moon, 2009) and Flexpoint (O'Flynn et al., 2013; Saggio, Bocchetti, Pinto, & Orengo, 2010). As such, a commercial resistive sensor available from Flexpoint was selected for experimentation. Flexpoint bend sensors are designed specifically to detect various degrees of bending for a multitude of applications, including medical, robotics, and automotive uses, among others (Flexpoint Sensor Systems, 2005). The sensors work in a similar fashion as a wired resistive strain sensor, in that as the sensor is subjected to a bending mode strain, the resistance changes. However, unlike a conventional wired strain gage, Flexpoint bend sensors are comprised of proprietary conductive carbon ink, which undergoes mechanical deformation along its length as it bends. These mechanical deformations during increasing bending result in increasing structural failures that reduce the conductivity and flow of current through the sensor, resulting in an increase in resistance.

An additional benefit of using a Flexpoint bend sensor is that it exhibits a significant change in resistance and as such only requires a simple voltage divider and sensor as opposed to some strain gage circuits, which require up to 4 sensors to obtain accurate readings.

5. The Design of a Low Cost Data Glove

5.1 Sensor Analysis

Using the data glove to control a robotic hand is a complex situation when relying on an array of sensors. On one hand, the optimal sensors would precisely and accurately capture very fine motions of the user's hands so that the robot would mimic those motions as closely as possible. On the other hand, with a human in the loop, the control system can be simpler and less accurate with the expectation that the user will close the loop using visual feedback of the robot. Indeed, since the intent of the glove was to be used by various people, a high level of accuracy would be very difficult to achieve. While the goal remained to ascertain the best sensor option available for the data glove, the application permits a range of acceptable performance quality.

In initial experiments, Flexpoint bend sensors showed that the resistance range of the sensors lie between 18 kΩ to 90 kΩ with some variation between each individual sensor. Because most development boards for prototyping hardware use a 3.3 V output, the development board for the data glove uses a voltage divider with a 22 kΩ resistor.

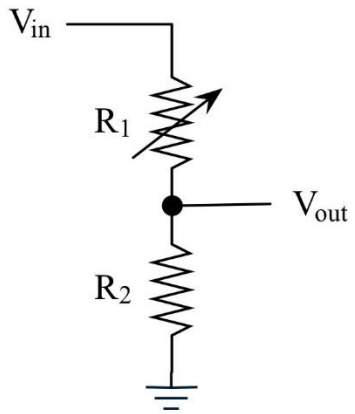

Figure 47. Voltage divider diagram. R_1 is the sensor, and R_2 is the static reference resistor.

$$V_{out} = \frac{R_2}{R_1 + R_2} * V_{in}$$

By applying the theoretical equation to the initially observed resistances, a change from 1.72 volts to .78 volts accounting for a change of roughly 1 volt difference was observed. This range could be further increased using an operational amplifier.

5.2 Sensor Placement

Having selected the sensor for the data glove, the next step was to consider how many sensors were necessary in order to control a human-like hand. For this data glove, 10 degrees of freedom were decided to be necessary to successfully control the DASH robotic hand and generate the desired grips in order to manipulate a number of tools. These degrees of freedom include finger proximal flexion, distal-medial flexion, thumb distal flexion, thumb medial flexion, and thumb proximal flexion. With sensors measuring these joints, the data glove was capable of differentiating between crucial grips, such as the power grip, precision pinch, and circular grip, which would encompass a majority of typical objects to be handled during teleoperation. Several other degrees of freedom were considered for the data glove but were not included due to difficulty in implementation. These degrees of freedom include finger abduction, wrist flexion/extension, and wrist ulnar and radial deviation.

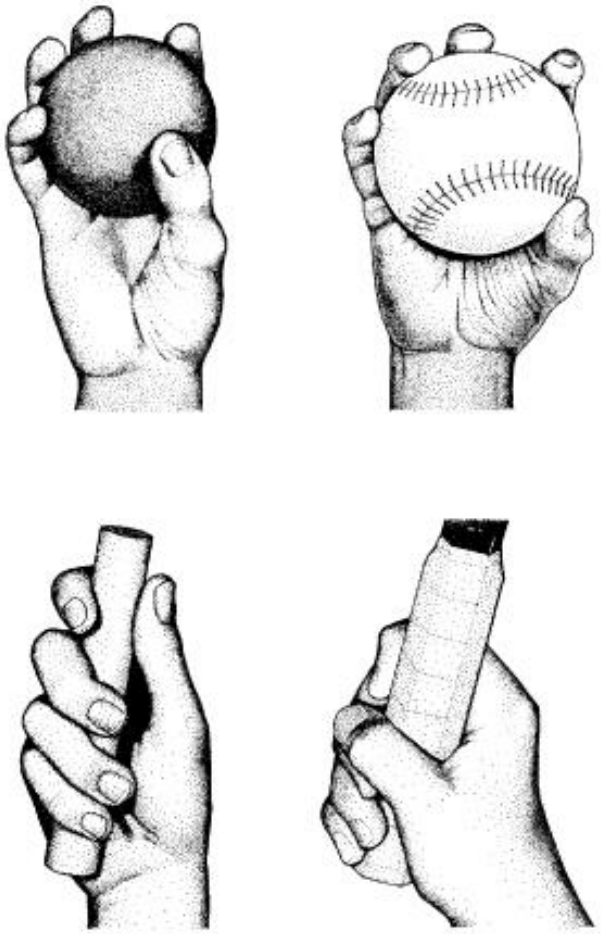

Figure 48. Circular grip (left) and power grip (right) are ideal grips for a number of teleoperative purposes. (Online Digital Education Connection, 2011). Used under fair use, 2016 (see Appendix A).

Placing the sensors required selecting two distinct contact points near the joint in question to track the desired degree of freedom. In typical data gloves, the sensors are sewn into the fabrics, allowing the sensor to bend naturally about the joint. However, one of the objectives of this data glove was to make it user friendly, and as such having sensors sewn into the fabric would be difficult to replace or troubleshoot components in the event of failure. Rather than try to fabricate a custom fabric glove, it was far more efficient to find a method to retrofit an existing glove.

5.3 Glove Selection

A variety of gloves were tested for both user comfort as well as adequacy for mounting sensors. Among several key factors is how well the glove fits multiple users, if the glove allowed full range of motion for the user, if the sensors would mount to the glove fabric, and if the glove was comfortable. Some gloves, such as thick rubber kitchen gloves, fit multiple users, allow for full range of motion, and support the sensors. However, the glove is exceedingly uncomfortable for a user, due to the lack of

breathability of the rubber. Other gloves, such as a thin cotton glove, fit multiple users comfortably, but the sensor was not suitably fixed to the glove, and would move from its fixed base, causing inconsistent readings from the bend sensors.

Considering several options, the best glove for retrofitting into a data glove was a battling glove from Under Armor. Consisting of a spandex and nylon weave with leather, the glove is both comfortable and flexible enough to fit a variety of hands. The fingertips were cut off from the glove to aid in comfort for the wearer as well as to allow for larger hand sizes to fit into the glove by not limiting the glove based on finger length alone. The sensors were attached using simple plastic dual lock connectors made by 3M (similar to hook and loop fasteners), which allowed for sensors to be moved with respect to the user's fingers to provide a more ideal fit and better bending angles for the sensors, while also providing the necessary stiffness to fix the sensors on the glove.

The other end of the sensor was slid into a small plastic slot. By folding the slot into quarters and then gluing the resultant slot, the binder unit becomes an excellent method to allow the sensor to bend, while also allowing the sensor to move axially along the finger. However, some problems arose with this method for the proximal sensors, as any slight abduction of the fingers would cause the sensor to buckle, creating unintentional bending and thus creating error in the readings. However, a solution was devised that involved using a wider slot, allowing the user to abduct their finger, while leaving the sensor free of buckling. Using the same hook and loop connectors, these slots were connected to the glove to allow for bending. Another potential issue is that the sensors for the proximal digits overlap with the sensors for the PIP-DIP joints while the user's fingers are fully extended. To solve this, the PIP-DIP sensor was attached directly to the slot to flex the proximal sensor, allowing the proximal sensor to pass beneath the medial-distal sensor without causing any issues. With that system laid out, dual lock tabs were attached directly to the glove fabric, eight two-inch sensors and three three-inch Flexpoint bend sensors were attached to the glove.

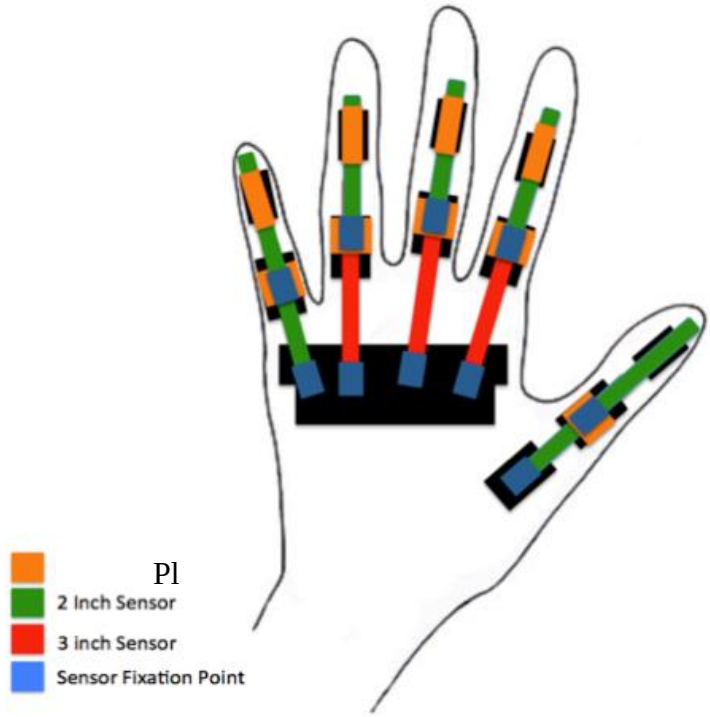

Figure 49. Data schematic (above) and the physical data glove prototype (below), with sensors attached to dual lock tabs, but without wires. Note that the proximal sensors are free to slide beneath the distal sensors to prevent sensor buckling (Paluszek, 2013). Reprinted with permission (see Appendix A).

Each sensor needs a voltage in and out to obtain a reading, requiring a total of 22 wires to run along the glove. To address concerns of wire clutter and tangles, it was determined necessary to use a 25-port D-Sub connector to act as an intermediary between the sensors and development board, which would allow the gloves to be independent of the board and enable the gloves to be interchangeable with different boards.

A Maple microcontroller board was chosen, which appears to be an ideal option for wiring a data glove. Powered by an STM32 processor, the Maple has 15 A/D ports with 12 bit conversion, allowing for a resolution of 0.8 mV. Since the observed change of

voltage from a bent sensor is about 1V, the microcontroller is able to resolve roughly 1175 individual values. Furthermore, the Maple board costs only $45, consistent with the goal of producing a cost-effective data glove.

5.4 Testing the Data Glove

Once the data glove prototype was built and wired, the next step was to determine the effectiveness of the data glove from a usability standpoint. With the developed glove and circuit the goal was to be able to observe a sensitivity of less than one flexion DoF in each digit. The testing was conducted using a National Instruments data acquisition system (DAQ) with a 16 bit A/D converter over a ±10 V range. This data acquisition system provides a minimum sensitivity of 0.3 mV, which is even more precise than the 0.8 mV resolution of the Maple. Ideally, it will be possible to compare the data glove sensor's change in resistance (by measuring the output of the voltage divider) to the actual current finger position. To accomplish this, a high-speed camera in tandem with the DAQ was used. To successfully use the camera to track the joint angles, several distinct marks were placed on the side of the data glove being filmed, seen in Figure 50. Because the objective was to track the joint, three points were placed along the side of the glove, near the finger. Using white acrylic paint, a dot is placed before the knuckle, at the knuckle, and after the knuckle, which allowed an angle to be processed from the finger positions. Then, using a high-speed camera filming at 60 FPS, simple flexing motion was performed with the distal and proximal index joints.

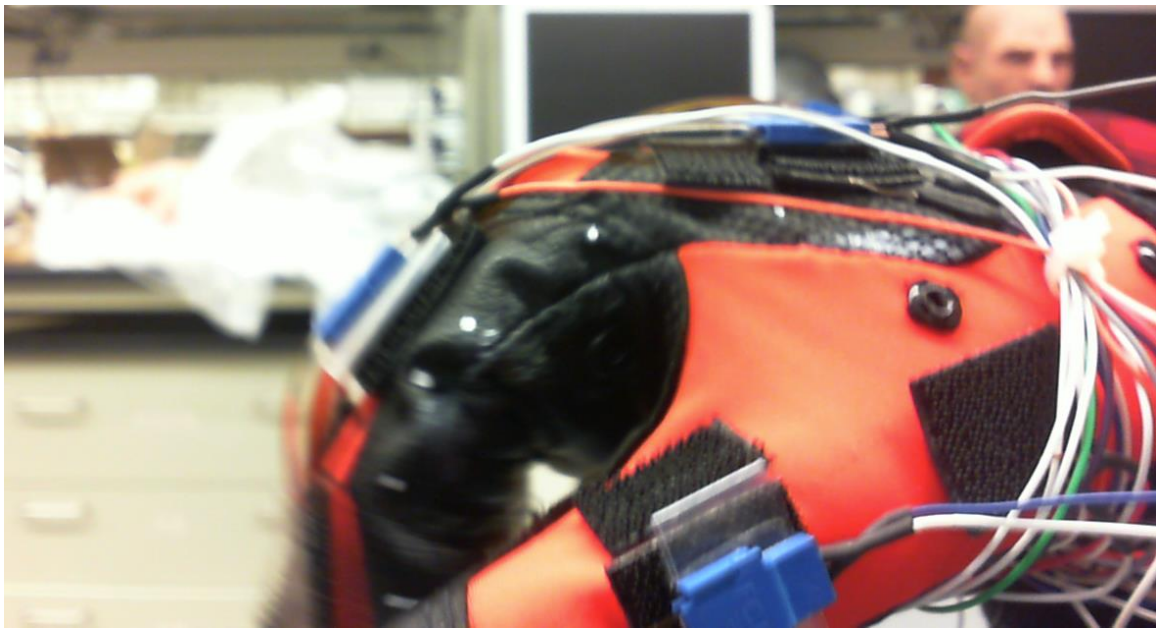

Figure 50. Tracking points on the data glove. A net total of five points were needed to accomplish tracking, having one dot along the palm of the hand, the proximal knuckle, the proximal digit, the medial knuckle, and the medial digit (Paluszek, 2013). Reprinted with permission (see Appendix A).

The next step was to find a method for synchronizing the camera frames to the recorded data. Because the camera and voltage data were recorded separately, a new

method must be used to synchronize the two sets of data. To accomplish this, the circuit had a small flip switch between the voltage divider and DAQ. By flipping the switch in front of the camera, the exact frame can be determined where the voltage jump corresponds to the switch being flipped.

Once the switch was flipped, the degree of freedom was gradually flexed from fully extended to fully flexed, held for half a second, and then returned to the starting position. Then, using a freeware image processing program ImageJ, each of the dots along the data glove were manually marked in each frame to produce a series of coordinates of the marked pixels. Then using these points to determine two lines and the respective angle between them gives the angle of flexion. Using these two data sets, correlation can be made between the angle of flexion and the voltage output from the voltage divider.

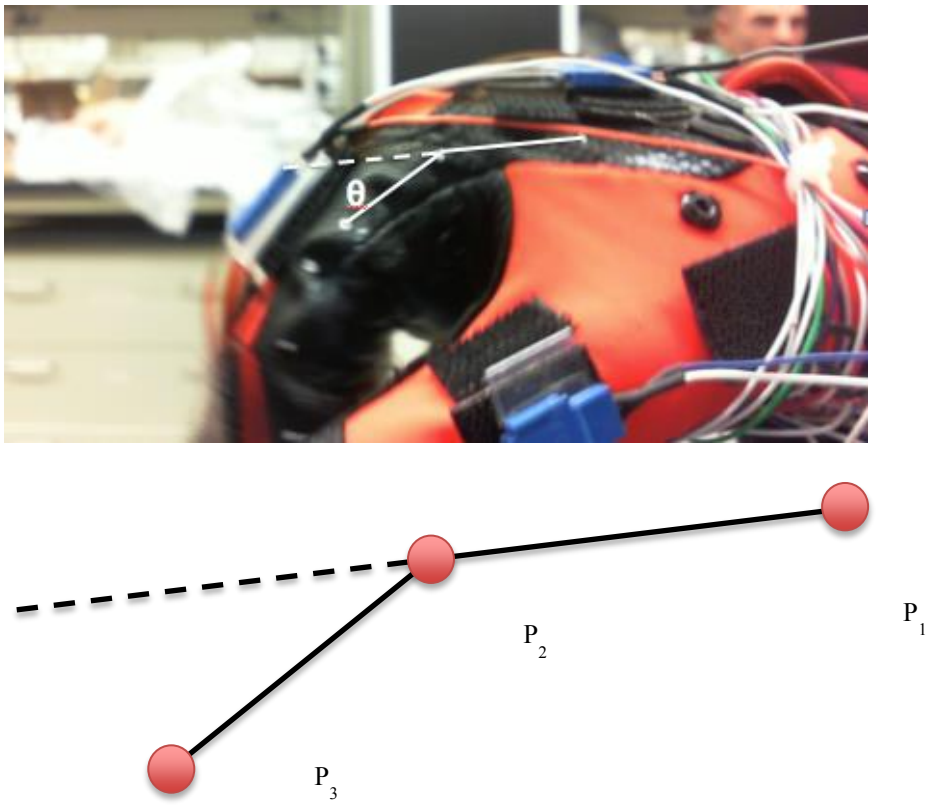

Figure 51. Data Glove with tracking points (above) and link segment model (below). Each dot is recorded as a series of x and y coordinate pixels, which were used to find the relative positions of each link (Paluszek, 2013). Reprinted with permission (see Appendix A).

$$h_1 = \sqrt{(P_{1x} - P_{2x)}{}^2 + (P_{1y} - P_{2y)}{}^2}$$

$$h_2 = \sqrt{(P_{2x} - P_{3x)}{}^2 + (P_{2y} - P_{3y)}{}^2}$$

$$d_1 = P_{1y} - P_{2y}$$
$$d_2 = P_{2y} - P_{3y}$$

$$\theta = \sin^{-1}\frac{d_2}{h_2} - \sin^{-1}\frac{d_1}{h_1}$$

5.5 Results

Using a linear fit to the data, a reasonably linear correlation between degree of flexion and voltage output was visible, with a residual norm for the distal joint at 0.21 and the proximal joint at 0.13. While ideally a residual norm of 0.05 or fewer would be preferable, there was little observed improvement in the fit by attempting higher polynomial fits. Even using a 4th order polynomial to fit to the data, the residual norm for the distal and proximal joints were 0.098 and 0.049, which did not account for enough of an improvement to justify the increased difficulty of future attempts at calibration for a user.

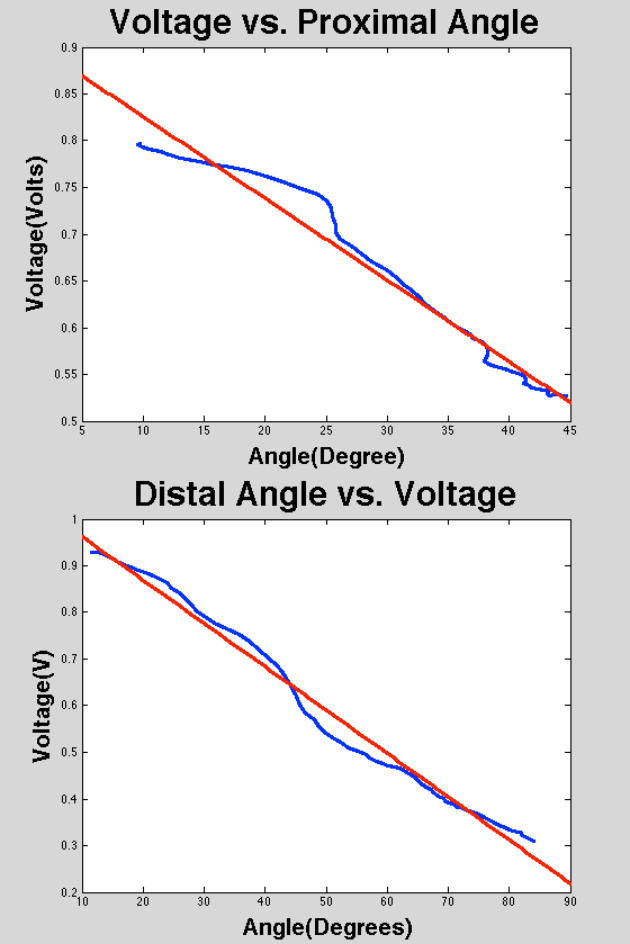

Figure 52. Proximal Angle vs. voltage with linear fit (above), Distal Angle vs. voltage with linear fit (below) (Paluszek, 2013). Reprinted with permission (see Appendix A).

Of particular interest is the behavior of the proximal bend sensor. Upon observing the data plot, there appear to be two different linear slopes, which transition after the 25-degree flexion mark, seen in Figure 52. Upon further investigation, there was a change in the bending of the sensor due to contact with the proximal knuckle. From 0-25 degrees of flexion, the sensor is not in contact with the proximal knuckle, 25 degrees on the sensor is in contact (Figure 53). This may explain the two distinctly different linear trends.

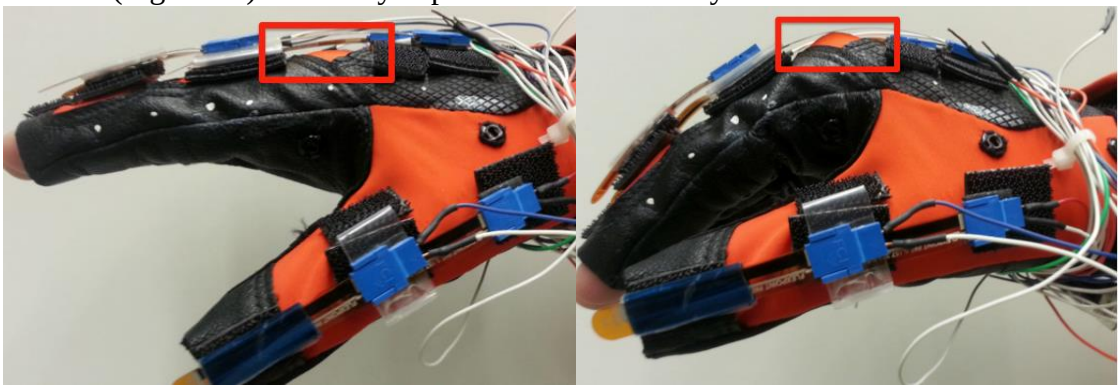

Figure 53. Data glove in the extended position (left) and at 25 degrees of flexion (right). Note the sensor is not in contact with the proximal knuckle in the extended position, but

is in contact in the flexed position (Paluszek, 2013). Reprinted with permission (see Appendix A).

However, this experimentation method was not without error. Due to the flexibility of the glove around the user's hand, the tracked points do not always accurately reflect the true position of the user's joint. Typically, marking points for tracking assumes a rigid and unmoving marker, which is not possible with this glove. Furthermore, because the points were tracked manually, some error is to be expected during the process, especially since relatively small errors, such as selecting the edge of a dot rather than the center, can significantly skew data. The tracking data presented here is the result of several attempts, and appears to be adequate.

5.6 Noted issues and Future Fixes

While the data glove appears to perform well for a low-cost solution, there are several issues which should be accounted for in future versions. First and foremost, while the design of fixing sensors to the outside of the glove made troubleshooting and attaching sensors user friendly, it produced other concerns, such as sensor buckling and external influences to the sensors. The proximal digit sensors would occasionally be obstructed by the dual lock pads, resulting in the sensors producing a high resistance, which would be interpreted as a high angle of flexion. Ideally, the next generation of this glove would follow the methods of other data glove groups and use an inlaid sensor design to mount the sensors directly onto to the hand, without the possibility for external interference.

Furthermore, additional degrees of freedom on the data glove would be necessary to track a user's hand for other hand positions. Most importantly would be to add a sensor to detect thumb rotation and abduction, which would allow for inclusion of a key or card grip. Finger abduction sensors would also be able to take advantage of additional degrees of freedom on the robotic hand described earlier. Also, it would be ideal to eventually track wrist position on the data glove. This could be performed with IMUs, but this would substantially increase the cost of the glove, which would conflict with the goal of making the glove as cost efficient as possible. Thus, alternative solutions for sensing should be explored.

5.7 Method to Control the Robot

Although the goal would be to teleoperate the system, the software development in this study focused around implementation of the communication between the microcontroller on the glove and the robotic hand via a shared computer. The Maple microcontroller communicates with a LabVIEW application running on a computer via a serial connection and the computer is also connected to the robotic hand via a second serial connection. There are several necessary steps in order to go from obtaining a voltage reading from the data glove's sensors to controlling the robotic hand. First, the computer must obtain and parse a string of values from the Maple board corresponding to readings from the bend sensors, and then take these values to relay an angular position interpreted from these values. These angular positions are then translated and relayed to the robotic hand, which will then mimic these positions to give control using the data glove. In Figure 54, the steps of the process to control the robotic hand is shown.

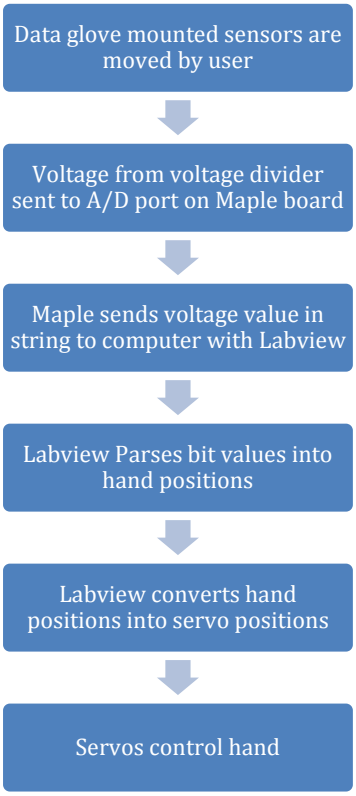

Figure 54. Simple flow chart explaining the process of obtaining, parsing and using signals to control the robotic hand (Paluszek, 2013). Reprinted with permission (see Appendix A).

5.8 Labview Code

Having obtained an array of 12-bit values from the Maple board, it is necessary to translate these values into angular position that is interpreted from the user's hand. The previous section established that while a linear fit is not a wholly accurate approximation of the response of the bend sensors with changes in finger position, but having a user closing the loop permits this linear fit to be acceptable. As such, two points are needed to create a linear fit, which can be most easily accomplished by using the start and end position corresponding to 0° and 90° of flexion. While a human's hand has variations in degrees of flexion, 0° and 90° act as an approximation. This convention breaks each degree of freedom into a fully flexed (90°) and fully extended position (0°). Because the data glove encompasses proximal and distal flexion of both the fingers and thumb for a total of 10 DoF, it would not be ideal to calibrate each individual position. Instead, there will be a series of hand poses, which will be used to determine the fully flexed and extended positions. The initial hand pose is the whole hand fully extended, also called "Neutral", which acts as the first value for both the proximal and distal sensors for the fingers and thumb. In determining the additional pose, it is important to select sensors whose motion will not impede or otherwise affect another sensor that is being recorded. With this in mind, the next pose is titled "Distal Flex", in which the index, middle, ring and pinky distal medial joints are flexed, and the values from the corresponding sensors are recorded. This is repeated for "Proximal flex", in which the four fingers are flexed

from the proximal joint. Because full range of motion in the thumb can impede the range of motion of other fingers, these portions were split into another set of poses, called "Thumb Distal" and "Thumb Proximal". In our test for each of these poses, a pose can be selected from a drop-down menu on the LabVIEW application. A button titled "Calibrate" commands Labview to save the calibration values for the corresponding sensors depending upon the drop down menu option that has been selected. This allows the calibration options to be performed in any order, and allows for easy re-calibration. This calibration process of the finger joints is shown in Figure 55, and the calibration process for the thumb joints is shown in Figure 56.

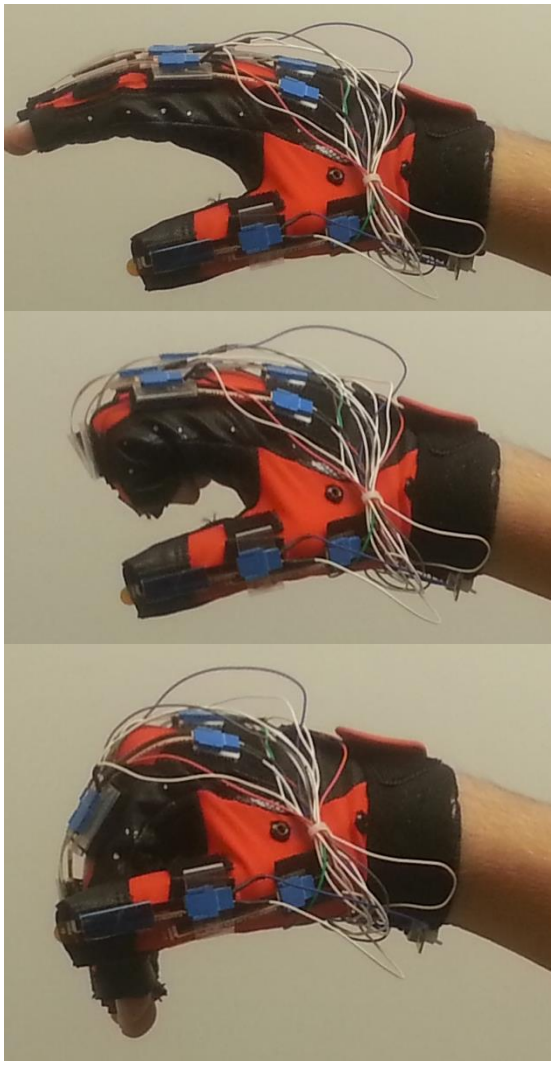

Figure 55. Neutral Hand Position (top), distal finger flexion (middle), proximal finger flexion (bottom) (Paluszek, 2013). Reprinted with permission (see Appendix A).

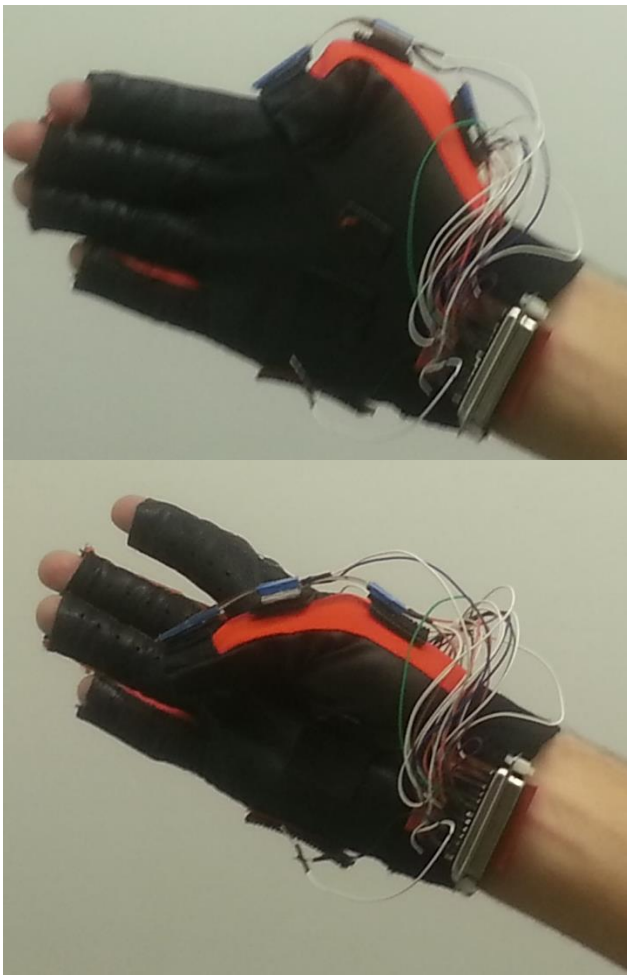

Figure 56. Thumb distal flexion (top) and thumb proximal flexion (bottom) (Paluszek, 2013). Reprinted with permission (see Appendix A).

Upon full calibration, Labview now has a 2x10 matrix of 12-bit integers, with one column being the "Neutral" values, and the other being the corresponding values from the flexed position calibrations. With these values, a linear calibration will translate the values from the maple board into a value between 0 and 90, which will correlate to a flexed and extended set of positions.

$$P = \frac{90}{V_f - V_e}(x - V_f)$$

where P is position, V_f is flexed bit value, V_e is extended bit value, and x is current sensor bit value.

However, noise and variation in the sensor resistances can result in values exceeding the calibration limits, so values were bound to a range of 0-90°. Once these calibrations were completed, a series of bars on the front panel allowed the user to visualize the output of the data glove following the prescribed conversion, while a constant readout of the bit values coming from the hand prior to conversion allows for

additional troubleshooting. Once the calibration is complete, the user can push a button labelled “Control” on the front panel, which will initialize the control of the robotic hand. With this control setup, the user is able to determine whether or not the data glove is sending the correct information to the robotic hand prior to actually controlling the hand, reducing risks of sending unexpected or incorrect values and causing potential damage to the motors or joints.

Table 7. Series of flexed and extended 12-bit values, observed bit values from the maple, translated values from governing equations, and values after stopper program (Paluszek, 2013). Reprinted with permission (see Appendix A).

Extended Bit Value	Flexed Bit Value	Bit Value In	Translated	With Stopper
2632	1687	2011	59.14	59.14
2985	1917	2556	36.15	36.15
2500	651	1232	61.72	61.72
1526	752	702	95.81	90
2125	887	2021	7.56	7.56
2118	917	2098	1.50	1.5
2226	1185	2326	-8.65	0
2359	821	2278	4.74	4.74
2265	966	1203	73.58	73.58
2011	455	1956	3.18	3.18

This full system allows usage of the data glove to control the robotic hand. However, there have been instances of failures in the data glove, namely when sensors become detached, or in cases where the motion of the sensor may be impeded. To deal with these issues, the front panel of the controller can enable the individual degrees of freedom of the robotic hand to be controlled through a series of LabVIEW slider controls. This also allows a user to produce hand poses that are typically difficult be generated or otherwise maintain. Furthermore, several degrees of freedom that are not tracked by the data glove can be controlled using this method, including thumb rotation, pinky abduction, and index abduction.

5.9 Future Work

While the current data glove controller appears to be effective, there are numerous improvements that could be implemented. Our studies in this paper focused around the development of data glove, thus the data glove and the robotic hand were connected to the same computer. Moving forward, in addition to glove development the focus would shift toward teleoperation control, in which the glove could be in a different location than the robot. This would provide a number of challenges, including latency and difficulty in receiving visual feedback of the environment. Additionally, it would be useful to have the ability to include readings from the fingertip sensors as part of the LabVIEW code to provide feedback to the user. As this code would develop, semi-autonomous control

could also be developed, such as setting in force limits on the fingertips or creating routines to maintain a grip on an object without input from a user.

5.10 Exploration of a PZL Based Data Glove

Many of the data gloves designs found in literature have inherent difficulty in user operation due to presence of wires, requirement of precisely placed markers and sensors, and need for expensive hardware such as IMUs. The optical sensing gloves have been shown to possess acceptable repeatability, linearity, accuracy, and resistance to disturbance yet they also suffer from some pitfalls. The optical sensing based data glove technique is based on light source and detector coupled system that is electrically wired with a power source. However, this complicated system tends to increase not only weight but also the cost of the data glove system. In order to overcome this complexity, we introduce a novel wireless optical sensing technique based on stretchable piezoluminescence (PZL) phenomena. The principle of PZL is described in the following section.

5.10.1. Piezoluminenscence

The PZL effect refers to light emission phenomena induced by mechanical stress enabling a high resolution dynamic strain sensing. The PZL phenomena has usually appeared in coupling of energy conversion between electroluminescence effect (light emission induced by electric field) and direct piezoelectric effect (electric field generation induced by stress). For example, doped ZnS, a well-known PZL material, has been used as an electroluminescent phosphor in displays and light sources and has piezoelectric properties since it has asymmetric crystal structure. Once a mechanical strain is applied to the doped ZnS, the electric potential is induced by the direct piezoelectric effect leading to light emission by electroluminescence effect. This phenomena is attractive for wireless control.

5.10.2. Fabrication of PZL rubber

PZL ceramic materials are brittle under stress. To mitigate this obstacle, a PZL rubber material can be fabricated where PZL micro-particles are simply mixed with the elastomer polydimethylsiloxane (PDMS) solution along with the curing agent in a weight ratio of 10:1. This is followed by stirring for 5 minutes to obtain a well-dispersed mixture. Next, vacuum evacuation is carried out for 20 min to remove air bubbles in the well dispersed PZL+PDMS solution in a vacuum desiccator. For solidification, the PZL+PDMS solution is cured at 80°C for 30 min in a conventional oven. The PZL rubber with high strain sensitivity and flexibility can be easily synthesized though this simple fabrication process flow (Jeong et al., 2014; Jeong, Song, Lee, and Choi, 2013). The PZL rubber generates light under strain without damaging (Figure 57(a) and (b)). Furthermore, the PZL rubber can be applied onto any surface of materials. Figure 57(c) and (d) shows PZL rubber applied on the cotton glove. As the wearer of the glove clenches their hand into a closed fist, the material is strained and emits light.

Some of the key merits of the flexible PZL rubber is that it is easy to manipulate color of a single light wavelength depending on the doping elements, and the intensity of PZL is determined by strain and acceleration of the motion. In ZnS based PZL materials,

the doping elements and concentration of the doping change the defect induced energy band structure in the materials. This defect engineering results in changing wavelength of the light emission (e.g. Mn doped ZnS: Orange and Cu doped ZnS: Green or Blue) and the PZL color can be simply manipulated by ionic substitutions. This is a very significant capability for design of a wireless optical emission based data glove.

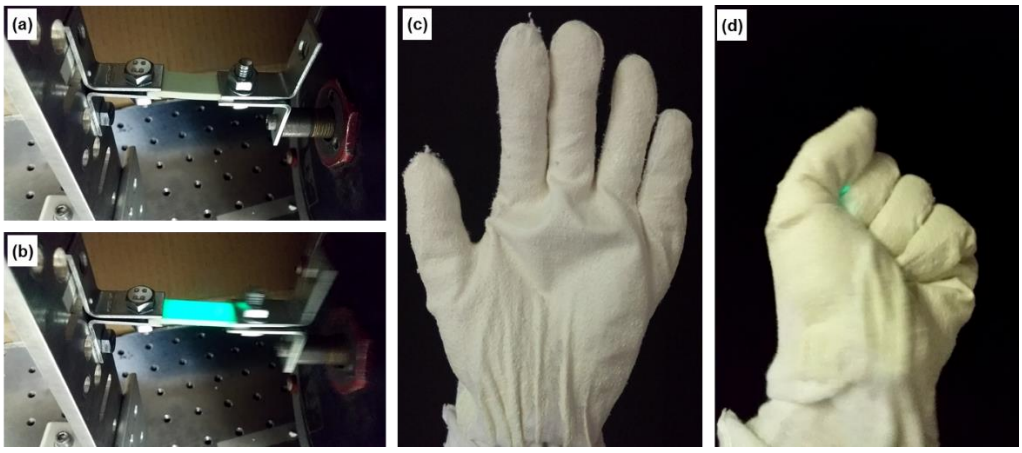

Figure 57. Piezoluminescent rubber (a) and (b) piezoluminescence under stretching-releasing motion, (c) and (d) piezoluminescence rubber applied on cotton glove.

5.10.3. A working basis of proposed system

The PZL rubber patches emitting different colors can be mounted on the joints of the data glove, then the degree of strain, motion speed, and coordinates of strained points can be detected using photo diode arrays placed around the glove.

In camera based sensing, additional cameras must be set up in the work space to expand the system's sight in order to minimize the occurrence of occlusion. This adds additional variables to the system and requires increased data processing. In methods such as Kinect and Leap Motion, the system's sight originates from a single device, also increasing the chances of occlusion. In literature, photodiode arrays have been used for image processing. In one of the prior studies, a camera was devised from a 30x40 array of photodiodes, like the one shown in Figure 58 (Nayar, Sims, & Fridberg, 2015). In a similar fashion, arrays of photodiodes can be fabricated and arranged in a three-dimensional space, encompassing the workspace of the PZL based gloves, such as in Figure 59. Such system is simple and the components to fabricate it are relatively inexpensive as photodiodes cost around few cents per unit. Resolving a kinematic model from the multiple arrays can be accomplished through transformation calculations by using the measurements from the active photo diodes like a coordinate system. Because the light emission center of PZL materials usually exhibits a single wavelength, the photo diode arrays can distinguish color signal at each joint with extremely low noise. This wireless data glove system can provide a simple structure of glove for better mobility, zero power consumption of light source, and low cost compared to other sensing method.

Figure 58. A photodiode array designed to function as a camera (Nayar, et al., 2015). Reprinted with permission, © 2015 IEEE (see Appendix A).

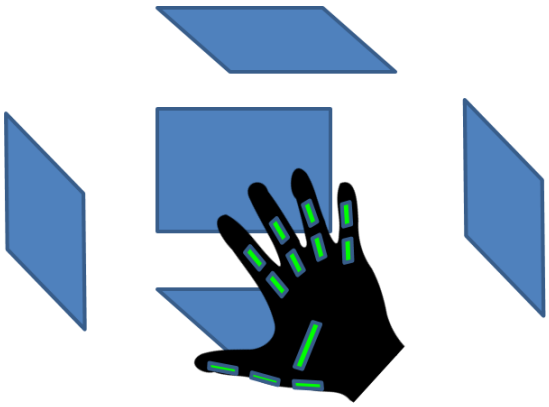

Figure 59. Photodiode arrays arranged to sense the PZL light emission.

In testing the PZL rubber for data glove, it will be necessary to create a patterned glove design on which the PZL rubber can be applied in a calculated geometry. A typical off-the-shelf glove such as the cotton glove shown in Figure 57(b) and (c) is much too loose fitting, where the entirety of the glove fabric can slide along the length of the hand. A design to isolate the discrete area of the measured joint is necessary. We propose three basic concepts of glove design a shown in Figure 60(a)-(c). The first PZL based glove concept is a glove that has segments of PZL rubber placed directly at the hand joints to be measured, shown in Figure 60a. This design concept leads to one of the simpler designs for the glove apparatus itself. However with the placement of PZL elements, the sensing procedure to detect the location, and intensity of the PZL's light emission may be more complicated. In the second glove concept, seen in Figure 60b, the majority of the PZL elements are consolidated to the dorsum of the hand. The PIP joint positions are measured indirectly in this concept. The PZL elements are remotely located on the dorsum and the PIP joint motion is transmitted to the PZL element via tension elements, such as a tendon-sheath transmission, which displaces the element linearly. The MP joint

positions can be measured either directly or indirectly like the PIP joint positions. The advantage of this arrangement is that the consolidation of the PZL elements to a general location may aid in easier visual tracking. However, there is a trade-off as the glove design does become more complex with the integration of the tension elements. The last glove concept introduces a method of color coding each joint. As mentioned previously, it is possible to create the PZL rubber with different color emission. Because of the vast amount of colors that can be created, each joint can be represented by its own color, simplifying the need to interpret which joint is being activated. Color coding can be applied to both of the other two concepts as well. This concept is shown in Figure 60c.

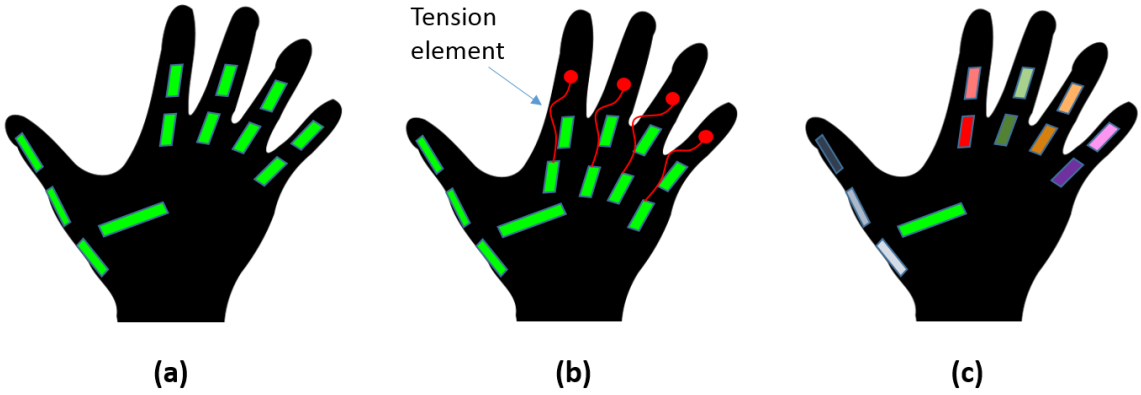

Figure 60. (a) A data glove design with PZL rubber element located at each joint, providing direct joint measurement. (b) A data glove design where the majority of the PZL rubber elements are located on the dorsum of the hand and the motion of the PIP joints are transmitted through tension elements. (c) A data glove concept featuring PZL elements of unique colors to easily distinguish the different joints of the fingers. Color coding can be used in the other concepts as well.

5.10.4. Additional PZL-based sensor concepts

The contactless, wireless sensing capabilities of PZL-based materials can also be utilized in the development of force and position sensors, as well as a hybrid sensor types where PZL capabilities can be combined with a conventional sensor.

We propose the concept of a hybrid sensor that combines the PZL rubber material with another more conventional sensor. In the context of data glove designs, a PZL rubber coating can be applied to the resistive bend sensors discussed earlier in this paper. A designer might find the versatility of a hybrid sensor type desirable because one function of the sensor may be more favorable in certain instances. For example, in a primarily PZL-based data glove design, there might be a DoF that is more difficult to sense using PZL, so the designer can utilize the resistive bend sensing functionality to mitigate the issue of occlusion. Conversely, in applications where wired sensors are predominantly used, the PZL functionality can be activated in order to reduce the number of wires on the system.

In literature, there have been low cost optical sensing technology based on source-sensor combinations, such as LEDs coupled with photodiodes. These sensors offer an inexpensive method of sensing. Similarly in principle, the luminescence of a PZL material can serve as the light source in an optoelectronic sensor type. This would

eliminate a wired source component, the LED, simplifying the sensor design. In literature, many of the sensor designs involved attaching an LED and photodiode onto a compliant structure. Forces applied to the compliant structure create a relative displacement, where the distance between the LED and photodetector is altered, resulting in a change in the photodiode's output. In the proposed method, a compliant structure can be coated with the PZL rubber or cast from it, and the photodiode will be able to detect the luminescence intensity to determine the force. Additionally, the PZL rubber can be suited for tactile sensing applications. A PZL based taxel can be fabricated comprising of a photodiode array on a flexible PCB which is covered in a layer of PZL based rubber. As pressure is applied to the sensor assembly, the PZL rubber layer will deflect and illuminate. The intensity and the location of the pressure can be sensed by the photodiode array.

5.10.5. Current challenges of PZL material in a data glove design

The PZL material is a promising choice towards demonstrating a novel wireless data glove technique with high sensitivity and low cost. However, many challenges still remain for practical deployment. In the current generation of materials, the PZL is invisible under a bright external light because of its low light emission intensity. To realize enhanced brightness, here we discuss the mechanisms of the PZL phenomena and suggest future design approaches. The PZL phenomena is the coupling between electroluminescence and piezoelectricity as mentioned above. For example, in Cu-doped ZnS (ZnS:Cu), ZnS wurtzite crystal has piezoelectricity which generates electric potential under strain. The ZnS:Cu particles includes a defect states with trapped electrons in the donor state and trapped holes in the acceptor state. Once a mechanical strain is applied to the ZnS:Cu, the conduction and valence band of the ZnS are tilted due to the piezoelectric potential. Owing to the internal electric field in ZnS:Cu, the trapped electrons are detrapped into conduction band and then recombination occurrs to Cu induced acceptor level with light emission (Figure 61).

The PZL intensity is mainly contributed to by the electron-hole recombination process. Based upon the operating mechanism of PZL, we can suggest two different ways to enhance the intensity. First, the enhancement of piezoelectricity of PZL materials increases detrapping and recombination rate of the electrons resulting from the increased internal electric field. Since, the PZL materials usually have low piezoelectric coefficients (e.g. longitudinal piezoelectric coefficient (d_{33}) of ZnS: ~3.3 pC/N), the strain induced internal electric field is not sufficient to excite all trapped electrons. Second, rising number of trapped electrons in the defect donor level can increase the electron-hole recombination pairs leading to high PZL brightness. The concentration of trapped electrons usually generated by anion defects in the PZL materials can be increased by doping and intrinsic vacancies. The doping elements and their concentration in the PZL determines not only number of trapped electrons but also color. Therefore, optimization of the defect structure of the PZL materials through defect engineering is one of the ways to obtain highly enhanced PZL light.

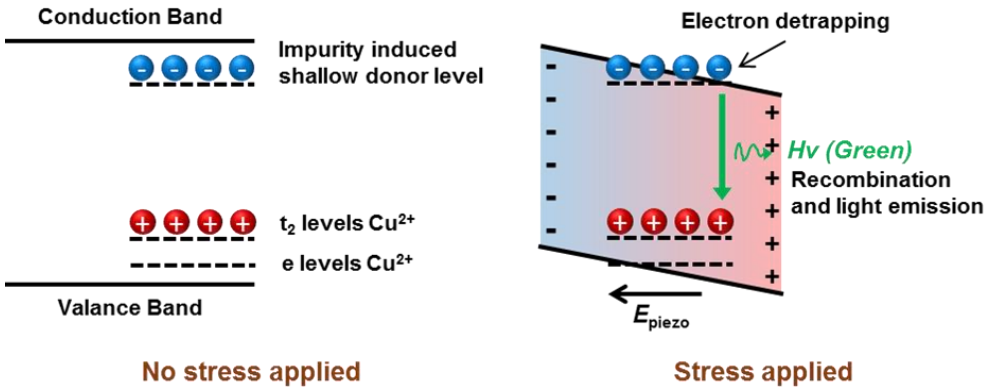

Figure 61. Schematics of energy band structure and driving mechanisms of PZL ZnS:Cu material.

The PZL phenomena is dependent on only change of strain which provides some obstacles in its application. In cases where the material is not experiencing a change of strain, such as if the joints of a finger are stationary while holding a grasp or if the hand is in a neutral position (all finger joints extended), then there will be no piezoluminescent response. The sensing will not be completely continuous and the finger will be assumed to be in the last recorded position from the previous measurement. It would be similar in principle to an incremental encoder. Another obstacle with the PZL for a data glove is the lack of directional information. The PZL emits light proportional to strain, but the response will be the same if that strain is in tension or contraction. With only amplitude of the change without directionality, methodologies or mechanisms would have be implemented to determine if the finger was bending or straightening. Incremental encoders overcome this by using a pair of offset sensors to interpret direction. Using multiple PZLs for each joint may provide a similar solution.

6. Summary and Conclusion

In this paper, a combined and comprehensive survey of anthropomorphic robotic hand design and data glove technology has been presented. Both technologies are often designed and implemented independent of each other. However, combining the two technologies in implementing practical teleoperated applications has great potential for assisting personnel's in medical, military, and domestic environments. Treatment of two technologies together will lead to platform specific metrics that will guide the further development of joint technology. Continuous advancement in the technology of actuators, sensing, and controls is necessary in order to improve the design, control, and precision of robotic hand and data gloves. A thorough review of the design of low-cost data glove and robotic hand hardware was presented, in order to accelerate the development of technology across multiple spectrum of application platforms.

In our efforts of exploring low-cost data glove based teleoperation of anthropomorphic robotic hands, a robotic hand-forearm platform, the DASH Hand, was developed at a cost of approximately $1500. The hand-forearm system possesses a total of 16 active DoF, maintains a human-like size and appearance, and can be integrated as the end effector for a humanoid robot platform. All the characterization was conducted on a 3D printed robotic hand. The robotic hand had low cost COTS bend-sensors for

position feedback control. Thorough testing led to few iterations of the hand with continued improvement in the functionality and reliability. A unique impedance based control method was introduced allowing the system to sense external resistance on the fingers. This provides the hand with feedback during grasping and senses external forces from the environment. This control technique requires minimal sensing hardware which results in low cost method of control.

In pursuit of a cost-effective and intuitive method of teleoperative robotic hand control, a low-cost data glove was designed and fabricated. The resulting design was a 10 DoF glove that cost around $300, making it a fraction of the cost of available data glove products. The design's sensing was accomplished through the use of COTS resistive bend sensors which are reconfigurable to accommodate a wide range of user hand sizes. Through careful analysis, the sensors of the glove were found to be adequately linear and sensitive for robotic hand control. Using the glove, teleoperation of the DASH robotic hand was successfully performed. With continued development, both devices have great potential for adoption by early stage researchers and graduate students in the robotics field.

7. **Future Work**

With much of the development of the low-cost data glove and robotic hand hardware complete, both systems can be improved to offer enhanced functionality and reliability to pursue exciting applications. Increasing the number of sensors on the data glove, such as adding an additional thumb DoF as well as abduction/adduction DoFs, can greatly enhance its ability to control high DoF robotic hand systems. Additional experimentation in teleoperation of the DASH robotic hand will be pursued, to explore new applications for robotic hands and control methods. In this paper, a new iteration of the DASH Hand was presented, where the design changes served to address issues with the initial prototype but to also expand its functionality as a research platform. Some features of the initial prototype must be reintegrated to the current version such as the index and little finger abduction/adduction DoF as well as absolute position sensing in the joints. Further sensorization of the robotic hand is anticipated to enable the system to more adeptly perform manipulation tasks. Additionally, further development of the novel PZL data glove concept will be pursued, to create a wireless, unpowered data glove. The PZL material also possesses great potential to be implemented in the creation of new hybrid technology sensors, and force and position sensing.

References

Atwell, C. (2012, Oct. 15). Are gesture-sensing interfaces set to replace your mouse and keyboard? ms digit and leap motion say yes. Retrieved from http://www.element14.com/community/community/news/blog/2012/10/15/are-gesture-sensing-interfaces-set-to-replace-your-mouse-and-keyboard-ms-digit-and-leap-motion-say-yes

Ahn, K., & Yokota, S. (2005). Intelligent switching control of pneumatic actuator using on/off solenoid valves. Mechatronics, 15(6), 683-702.

Akin, B., Bhardwaj, M., & Warriner, J. (2013). Sensorless Field Oriented Control of 3-Phase Permanent Magnet Synchronous Motors. Texas Instruments, Application Notes.

Akyürek, E., Kalganova, T., Mukhtar, M., Paramonov, L., Steele, L., Simko, M., Kavanagh, L., Nimmo, A., & Huynh, A. (2014). Design and development of Low cost 3D printed ambidextrous robotic hand driven by pneumatic muscles.

Aleotti, J., & Caselli, S. (2006, May). Grasp recognition in virtual reality for robot pregrasp planning by demonstration. In Proceedings 2006 IEEE International Conference on Robotics and Automation, 2006. ICRA 2006. (pp. 2801-2806). IEEE.

Araki, Y. (1996). Three Dimensional Coordinates Input Apparatus. US Patent 5512919.

Atzori, M., Gijsberts, A., Heynen, S., Hager, A. G. M., Deriaz, O., Van Der Smagt, P., ... & Müller, H. (2012, June). Building the Ninapro database: A resource for the biorobotics community. In 2012 4th IEEE RAS & EMBS International Conference on Biomedical Robotics and Biomechatronics (BioRob) (pp. 1258-1265). IEEE.

Bae, J. H., Park, S. W., Park, J. H., Baeg, M. H., Kim, D., & Oh, S. R. (2012, October). Development of a low cost anthropomorphic robot hand with high capability. In 2012 IEEE/RSJ International Conference on Intelligent Robots and Systems (pp. 4776-4782). IEEE.

Baek, S., Jeong, Y., & Lee, B. (2002). Characteristics of Short-Period Blazed Fiber Bragg Gratings for Use as Macro-Bending Sensors. Applied Optics, 41(4), 631-636.

Bekey, G. A., Tomovic, R., & Zeljkovic, I. (1990). Control architecture for the Belgrade/USC hand. In Dextrous robot hands (pp. 136-149). Springer New York.

Belter, J. T., & Segil, J. L. (2013). Mechanical design and performance specifications of anthropomorphic prosthetic hands: a review. Journal of rehabilitation research and development, 50(5), 599.

Bennett, D. A., Dalley, S. A., Truex, D., & Goldfarb, M. (2015). A multigrasp hand prosthesis for providing precision and conformal grasps.

Berka, R., & Goza, S. M. (2012). Telerobotics on Robonaut2. Journal of the Robotics Society of Japan, 30(6), 565-567.

Biswas, K. (2011). Gesture recognition using Microsoft Kinect. Automation, Robotics and Applications(ICARA) (pp. 100-103). Wellington: IEEE.

Bohren, J., Rusu, R. B., Jones, E. G., Marder-Eppstein, E., Pantofaru, C., Wise, M., Mosenlechner, L., Meeussen, W., & Holzer, S. (2011, May). Towards autonomous robotic butlers: Lessons learned with the pr2. In Robotics and Automation (ICRA), 2011 IEEE International Conference on (pp. 5568-5575). IEEE.

Bouzit, M., Burdea, G., Popescu, G., & Boian, R. (2002). The Rutgers Master II - New design force-feedback glove. IEEE/ASME Transactions on Mechatronics, 7(2), 256–263.

Bridgwater, L. B., Ihrke, C. A., Diftler, M. A., Abdallah, M. E., Radford, N. A., Rogers, J. M., Yayathi, S., Askew, R.S., & Linn, D. M. (2012, May). The robonaut 2 hand-designed to do work with tools. In Robotics and Automation (ICRA), 2012 IEEE International Conference on (pp. 3425-3430). IEEE.

Burdea, G., Zhuang, J., Roskos, E., Silver, D., & Langrana, N. (1992). A portable dextrous master with force feedback. Presence: Teleoper. Virtual Environ., 1(1), 18–28.

Butterfass, J., Grebenstein, M., Liu, H., & Hirzinger, G. (2001). DLR-Hand II: Next generation of a dextrous robot hand. In Robotics and Automation, 2001. Proceedings 2001 ICRA. IEEE International Conference on (Vol. 1, pp. 109-114). IEEE.

Butterfass, J., Hirzinger, G., Knoch, S., & Liu, H. (1998, May). DLR's multisensory articulated hand. I. Hard-and software architecture. In Robotics and Automation, 1998. Proceedings. 1998 IEEE International Conference on (Vol. 3, pp. 2081-2086). IEEE.

Caffaz, A., Casalino, G., Cannata, G., Panin, G., & Massucco, E. (2000). The DIST-hand, an anthropomorphic, fully sensorized dexterous gripper. IEEE Humanoids.

Caldwell, D. G., Andersen, U., Bowler, C. J., & Wardle, A. J. (1995). A high power / weight dexterous manipulator using ' Sensory Glove ' based motion control and tactile feedback. Trans Inst MC, 17(5).

Cannata, G., & Maggiali, M. (2005, December). An embedded tactile and force sensor for robotic manipulation and grasping. In 5th IEEE-RAS International Conference on Humanoid Robots, 2005. (pp. 80-85). IEEE.

Carlson, W. (2003). A Critical History of Computer Graphics and Animation. Retrieved April 10, 2013, from Ohio State Department of Design: http://design.osu.edu/carlson/history/lesson17.html

Carrozza, M. C., Suppo, C., Sebastiani, F., Massa, B., Vecchi, F., Lazzarini, R., ... & Dario, P. (2004). The SPRING hand: development of a self-adaptive prosthesis for restoring natural grasping. Autonomous Robots, 16(2), 125-141.

Casley, S., Choopojcharoen, T., Jardim, A., Ozgoren, D., Onal, C., & Padir, T. (2014). IRIS Hand Smart Robotic Prosthesis.

Cavallo, A., De Maria, G., Natale, C., & Pirozzi, S. (2009). Optoelectronic joint angular sensor for robotic fingers. Sensors and Actuators A: Physical, 152(2), 203-210.

Chalon, M., Wedler, A., Baumann, A., Bertleff, W., Beyer, A., Butterfaß, J., ... & Landzettel, K. (2011, May). Dexhand: a space qualified multi-fingered robotic

hand. In Robotics and Automation (ICRA), 2011 IEEE International Conference on (pp. 2204-2210). IEEE.
Challoo, R., Johnson, J. P., McLauchlan, R. A., & Omar, S. I. (1994, October). Intelligent control of a Stanford JPL hand attached to a 4 DOF robot arm. In Systems, Man, and Cybernetics, 1994. Humans, Information and Technology., 1994 IEEE International Conference on (Vol. 2, pp. 1274-1278). IEEE.
Che, D., & Zhang, W. (2010, November). A humanoid robot upper limb system with anthropomorphic robot hand: GCUA hand II. In International Conference on Social Robotics (pp. 182-191). Springer Berlin Heidelberg.
Cheng, G. (Ed.). (2014). Humanoid Robotics and Neuroscience: Science, Engineering and Society. CRC Press.
Choi, B., Lee, S., Choi, H. R., & Kang, S. (2006, October). Development of anthropomorphic robot hand with tactile sensor: SKKU Hand II. In 2006 IEEE/RSJ International Conference on Intelligent Robots and Systems (pp. 3779-3784). IEEE.
Cipriani, C., Controzzi, M., & Carrozza, M. C. (2011). The SmartHand transradial prosthesis. Journal of neuroengineering and rehabilitation, 8(1), 1.
Cohen, D., & Halgren, E. (2004). Magnetoencephalography. In B. S. G. Adelman, Encyclopedia of Neuroscience. Amsterdam: Elsevier.
Cutkosky, M. R., & Howe, R. D. (1990). Human grasp choice and robotic grasp analysis. Dextrous robot hands, 1, 5-31.
Cyber Glover Systems, LLC. (2011). Cyber Glove III. Retrieved Sept 2011, from Cyber Glove Systems web site: http://www.cyberglovesystems.com/products/cyberglove-III/overview
Cyberglove Systems (2007). CyberGlove Data Glove User Guide.
Cyberglove Systems (2010). MoCap Glove.
Cybergloves Systems. (2009). CyberGlove ® II. http://www.cyberglovesystems.com
Cyberworld Inc. (2013). P5 - Virtual Reality Data Glove. Retrieved Sept 2011, from Cyber World Store web site: http://www.cwonline.com/store/view_product.asp?Product=1179
Dalley, S. A., Bennett, D. A., & Goldfarb, M. (2012, August). Preliminary functional assessment of a multigrasp myoelectric prosthesis. In 2012 Annual International Conference of the IEEE Engineering in Medicine and Biology Society (pp. 4172-4175). IEEE.
Data Connect Enterprise. (2013). Fiber Optics: The Basics of Fiber Optic Cable. Retrieved Feb 18th, 2013, from Data-Connect Web Site: http://www.data-connect.com/Fiber_Tutorial.htm
Daum, W., Gunther, T., Husert, J., & Scherr, P. (2002). Data Glove. US 2002/0075232 A1.
Dautenhahn, K., Nehaniv, C. L., Walters, M. L., Robins, B., Kose-Bagci, H., Mirza, N. A., & Blow, M. (2009). KASPAR–a minimally expressive humanoid robot for human–robot interaction research. Applied Bionics and Biomechanics, 6(3-4), 369-397.
Davis, S., Tsagarakis, N. G., & Caldwell, D. G. (2008, December). The initial design and manufacturing process of a low cost hand for the robot icub. In Humanoid

Robots, 2008. Humanoids 2008. 8th IEEE-RAS International Conference on (pp. 40-45). IEEE.
Dillmann, R. (2004). Teaching and learning of robot tasks via observation of human performance. Robotics and Autonomous Systems, 47(2), 109-116.
Dipietro, L., Sabatini, A. M., & Dario, P. (2003). Evaluation of an instrumented glove for hand-movement acquisition. Journal of Rehabilitation Research and Development, 40(2), 179–189.
Dipietro, L., Sabatini, A. M., & Dario, P. (2008). A survey of glove-based systems and their applications. IEEE Transactions on Systems, Man, and Cybernetics, Part C (Applications and Reviews), 38(4), 461-482.
Dollar, A. M., & Howe, R. D. (2010). The highly adaptive SDM hand: Design and performance evaluation. The international journal of robotics research, 29(5), 585-597.
Englehart, K., & B., H. (2003). A Robust, Real-Time Control Scheme for Multifunction Myoelectric Control. IEEE TRANSACTIONS ON BIOMEDICAL ENGINEERING, 50(7), 848-854.
Fahn, C. S., & Sun, H. (2010). Development of a fingertip glove equipped with magnetic tracking sensors. Sensors, 10(2), 1119-1140.
Fahn, C., & Sun, H. (2005). Development of a data glove with reducing sensors based on magnetic induction. In Industrial Electronics, IEEE Transactions on (Vol. 52, pp. 585–594).
Ficuciello, F., Palli, G., Melchiorri, C., & Siciliano, B. (2011, September). Experimental evaluation of postural synergies during reach to grasp with the UB Hand IV. In 2011 IEEE/RSJ International Conference on Intelligent Robots and Systems (pp. 1775-1780). IEEE.
Fifth Dimension Technologies. (2005). 5DT Data Glove 5 Ultra. Retrieved Sept 2011, from Fifth Dimension Technologies web site: http://www.5dt.com/products/pdataglove5u.html
Fifth Dimension Technologies. 5DT Data Glove Ultra Series.
First steps: ISS's 'Robonaut' gets new legs for Easter. (2014, April 21). RT. Retrieved from https://www.rt.com/news/iss-robonaut-new-legs-760/
Fishel, J., Lin, G., & Loeb, G. (2013). BioTac® Product Manual. SynTouch LLC, February.
Flexpoint Sensor Systems, Inc. (2005). About the Bend Sensor. Retrieved Dec 2011, from Flexpoint flexible sensor systems: http://www.flexpoint.com/companyInfo/bendSensor.htm
Fukaya, N., Asfour, T., Dillmann, R., & Toyama, S. (2013, November). Development of a five-finger dexterous hand without feedback control: The TUAT/Karlsruhe humanoid hand. In 2013 IEEE/RSJ International Conference on Intelligent Robots and Systems (pp. 4533-4540). IEEE.
Fukaya, N., Toyama, S., Asfour, T., & Dillmann, R. (2000). Design of the TUAT/Karlsruhe humanoid hand. In Intelligent Robots and Systems, 2000.(IROS 2000). Proceedings. 2000 IEEE/RSJ International Conference on (Vol. 3, pp. 1754-1759). IEEE.
Gaiser, I., Schulz, S., Kargov, A., Klosek, H., Bierbaum, A., Pylatiuk, C., Oberle, R., Werner, T., Asfour, T., Bretthauer, G., & Dillmann, R. (2008, December). A

new anthropomorphic robotic hand. In Humanoids 2008-8th IEEE-RAS International Conference on Humanoid Robots (pp. 418-422). IEEE.
Gantz, B., Turner, C., Gfeller, K., & Lowder, M. (2005). Preservation of Hearing in Cochlear Implant Surgery: Advantages of Combined Electrical and Acoustical Speech Processing. Laryngoscope, 796-802.
Gardner, D. L. (1989). Inside story on: The power glove. Design News, 45(23), 63.
Gazeau, J. P., Zehloul, S., Arsicault, M., & Lallemand, J. P. (2001). The LMS hand: force and position controls in the aim of the fine manipulation of objects. In Robotics and Automation, 2001. Proceedings 2001 ICRA. IEEE International Conference on (Vol. 3, pp. 2642-2648). IEEE.
Geng, T., Lee, M., & Hülse, M. (2011). Transferring human grasping synergies to a robot. Mechatronics, 21(1), 272-284.
Gentner, R., & Classen, J. (2009). Development and evaluation of a low-cost sensor glove for assessment of human finger movements in neurophysiological settings. Journal of Neuroscience Methods, 178(1), 138-147.
Gomez, D. H. (1997). A dextrous hand master with force feedback for virtual reality. Rutgers University.
Graf, B., Reiser, U., Hägele, M., Mauz, K., & Klein, P. (2009, November). Robotic home assistant Care-O-bot® 3-product vision and innovation platform. In 2009 IEEE Workshop on Advanced Robotics and its Social Impacts (pp. 139-144). IEEE.
Grebenstein, M., Albu-Schäffer, A., Bahls, T., Chalon, M., Eiberger, O., Friedl, W., & Höppner, H. (2011, May). The DLR hand arm system. In Robotics and Automation (ICRA), 2011 IEEE International Conference on (pp. 3175-3182). IEEE.
Grebenstein, M., Chalon, M., Herzinger, G., & Siegwart, R. (2010, October). A method for hand kinematics designers. In 1st International conference on applied bionics and biomechanics.
Guizzo, E. (2011, January 25). Building a Super Robust Robot Hand. IEEE Spectrum. Retrieved from spectrum.ieee.org/automaton/robotics/humanoids/dlr-super-robust-robot-hand
Han, Y. (2010). A low-cost visual motion data glove as an input device to interprety human hand gestures. Consumer Electronics, 56(2), 501-509.
HDT Global. Adroit MK2 Systems Robotic Arm and Manipulator. Retrieved from http://www.hdtglobal.com/wp-content/uploads/2015/01/HDT_MK2robotics_16.pdf
Hernandez-Rebollar, J. L., Kyriakopoulos, N., & Lindeman, R. W. (2002). The AcceleGlove. Siggraph, 259.
Hofmann, F., & Henz, J. (1995). The TU Berlin SensorGlove. http://pdv.cs.tu-berlin.de/forschung/SensorGlove2_engl.html
Hong, J., & Tan, X. (1989). Calibrating a VPL DataGlove for Teleoperating the Utah/MIT Hand. In 1989 IEEE International Conference on Robotics and Automation (pp. 1752–1757).
Hopkins, J. (2014, December). Amputee Makes History with APL's Modular Prosthetic Limb. Retrived from www.jhuapl.edu/newscenter/pressreleases/2014/141216.asp

Iredale, F., Farrington, T., & Jaques, M. (1997). Global, Fine and Hidden Sports Data: Applications of 3-D Vision Analysis and a Specialized Data Glove for an Athlete Biomechanical Analysis System. In Mechatronics and Machine Vision in Practice (pp. 260–264).

Ishikawa, M., & Matsumura, H. (1999). Recognition of a hand-gesture based on self-organization using a dataglove recognition. In ICONIP99 ANZIIS99 ANNES99 ACNN99 6th International Conference on Neural Information Processing Proceedings Cat No99EX378 (Vol. 2, pp. 739–745).

Jacobsen, S. C., Iversen, E. K., Knutti, D. F., Johnson, R. T., & Biggers, K. B. (1986, April). Design of the Utah/MIT dextrous hand. In Robotics and Automation. Proceedings. 1986 IEEE International Conference on (Vol. 3, pp. 1520-1532). IEEE.

Jeong, E., Lee, J., & Kim, D. (2011). Finger-gesture Recognition Glove using Velostat (ICCAS 2011). 11th International Conference on Control, Automation and Systems, (Iccas), 206–210.

Jeong, S. M., Song, S., Joo, K. I., Kim, J., Hwang, S. H., Jeong, J., & Kim, H. (2014). Bright, wind-driven white mechanoluminescence from zinc sulphide microparticles embedded in a polydimethylsiloxane elastomer. Energy & Environmental Science, 7(10), 3338-3346.

Jeong, S. M., Song, S., Lee, S. K., & Choi, B. (2013). Mechanically driven light-generator with high durability. Applied Physics Letters, 102(5), 051110.

Jeong, S. M., Song, S., Lee, S. K., & Ha, N. Y. (2013). Color Manipulation of Mechanoluminescence from Stress-Activated Composite Films. Advanced Materials, 25(43), 6194-6200.

Johannes, M. S., Bigelow, J. D., Burck, J. M., Harshbarger, S. D., Kozlowski, M. V., & Van Doren, T. (2011). An overview of the developmental process for the modular prosthetic limb. Johns Hopkins APL Technical Digest, 30(3), 207-216.

Joiner, R., Messer, D., Light, P., & Littleton, K. (1998, September). It is best to point for young children: a comparison of children's pointing and dragging. Computers in Human Behavior, 14(3), 513-529.

Jones, L. A., & Lederman, S. J. (2006). Human hand function. Oxford University Press.

Kallmann, M., & Thalmann, D. (1999). Direct 3D interaction with smart objects. Proceedings of the ACM Symposium on Virtual Reality Software and Technology (VRST), 124–130.

Kaneko, K., Harada, K., & Kanehiro, F. (2007, April). Development of multi-fingered hand for life-size humanoid robots. In Proceedings 2007 IEEE International Conference on Robotics and Automation (pp. 913-920). IEEE.

Kaneko, M., Yamashita, T., & Tanie, K. (1991, June). Basic considerations on transmission characteristics for tendon drive robots. In Advanced Robotics, 1991.'Robots in Unstructured Environments', 91 ICAR., Fifth International Conference on (pp. 827-832). IEEE.

Kang, I., Schulz, M., Kim, J., Shanov, V., & Shi, D. (2006). A carbon nanotube strain sensor for structural health monitoring. Smart Materials and Structures, 737.

Kawasaki, H., Komatsu, T., & Uchiyama, K. (2002). Dexterous anthropomorphic robot hand with distributed tactile sensor: Gifu hand II. Mechatronics, IEEE/ASME Transactions On, 7(3), 296-303.

Kim, E. H., Lee, S. W., & Lee, Y. K. (2011). A dexterous robot hand with a bio-mimetic mechanism. International Journal of Precision Engineering and Manufacturing, 12(2), 227-235.

Kim, Y. J., Lee, Y., Kim, J., Lee, J. W., Park, K. M., Roh, K. S., & Choi, J. Y. (2014, May). RoboRay hand: A highly backdrivable robotic hand with sensorless contact force measurements. In Robotics and Automation (ICRA), 2014 IEEE International Conference on (pp. 6712-6718). IEEE.

Kochan, A. (2005). Shadow delivers first hand. Industrial robot: an international journal, 32(1), 15-16.

Konux. An Alternative to Sensors with Strain Gauge. Retrieved from (https://www.konux.com/sensors-with-strain-gauge/

Kramer, J., Lindener, P., & George, W. (1991). Communication system for deaf, deaf-blind, or non-vocal individuals using instrumented glove. US Patent 5,047,952.

Kurita, Y., Ono, Y., Ikeda, A., & Ogasawara, T. (2009, October). NAIST hand 2: Human-sized anthropomorphic robot hand with detachable mechanism at the wrist. In Intelligent Robots and Systems, 2009. IROS 2009. IEEE/RSJ International Conference on (pp. 2271-2276). IEEE.

Kuroda, T., Tabata, Y., Goto, A., Ikuta, H., & Murakami, M. (2004, September). Consumer price data-glove for sign language recognition. In Proc. of 5th Intl Conf. Disability, Virtual Reality Assoc. Tech., Oxford, UK (pp. 253-258).

Lam, W.C., Zou, F., & Komura, T. (2004). Motion editing with data glove. Proceedings of the 2004 ACM SIGCHI International Conference on Advances in Computer Entertainment Technology - ACE '04, 337–342.

Lamberti, L., Camastra, F., Tecnico, I., & Enrico, I. (2011). Real-Time Hand Gesture Recognition Using a Color Glove, 365–373.

Leap Motion, Inc. (2013). Leap Motion: Our Device. Retrieved Feb 16th, 2013, from Leap Motion Web site: https://www.leapmotion.com/product

Li, K., Chen, I. M., & Yeo, S. H. (2010, May). Design and validation of a multi-finger sensing device based on Optical linear encoder. In Robotics and Automation (ICRA), 2010 IEEE International Conference on (pp. 3629-3634). IEEE.

Li, K., Chen, I. M., Yeo, S. H., & Lim, C. K. (2011). Development of finger-motion capturing device based on optical linear encoder. Journal of Rehabilitation Research & Development, 48(1), 69-83.

Lim, K. Y., Goh, F. Y. K., Dong, W., Nguyen, K. D., Chen, I. M., Yeo, S. H., Duh, H.B.L., & Kim, C. G. (2008, May). A wearable, self-calibrating, wireless sensor network for body motion processing. In Robotics and Automation, 2008. ICRA 2008. IEEE International Conference on (pp. 1017-1022). IEEE.

Lin, B. S., Lee, I. J., Hsiao, P. C., Yang, S. Y., & Chou, W. (2014). Data glove embedded with 6-DOF inertial sensors for hand rehabilitation. Proceedings - 2014 10th International Conference on Intelligent Information Hiding and Multimedia Signal Processing, IIH-MSP 2014, 25–28.

Lin, L. R., & Huang, H. P. (1998). NTU hand: A new design of dexterous hands. Journal of Mechanical Design, 120(2), 282-292.

Liu, H., Meusel, P., Seitz, N., Willberg, B., Hirzinger, G., Jin, M. H., Liu, Y.W., Wei, R., & Xie, Z. W. (2007). The modular multisensory DLR-HIT-Hand. Mechanism and Machine Theory, 42(5), 612-625.

Liu, H., Wu, K., Meusel, P., Seitz, N., Hirzinger, G., Jin, M. H., Liu, Y.W., Fan, S.W., Lan, T. & Chen, Z. P. (2008, September). Multisensory five-finger dexterous hand: The DLR/HIT Hand II. In 2008 IEEE/RSJ international conference on intelligent robots and systems (pp. 3692-3697). IEEE

Lotti, F., Tiezzi, P., Vassura, G., Biagiotti, L., Palli, G., & Melchiorri, C. (2005, April). Development of UB hand 3: Early results. In Proceedings of the 2005 IEEE International Conference on Robotics and Automation (pp. 4488-4493). IEEE.

Lovchik, C. S., & Diftler, M. A. (1999). The robonaut hand: A dexterous robot hand for space. In Robotics and Automation, 1999. Proceedings. 1999 IEEE International Conference on (Vol. 2, pp. 907-912). IEEE.

Lucarotti, C., Oddo, C. M., Vitiello, N., & Carrozza, M. C. (2013). Synthetic and bio-artificial tactile sensing: A review. Sensors, 13(2), 1435-1466.

Maheu, V., Archambault, P. S., Frappier, J., & Routhier, F. (2011, June). Evaluation of the JACO robotic arm: Clinico-economic study for powered wheelchair users with upper-extremity disabilities. In 2011 IEEE International Conference on Rehabilitation Robotics (pp. 1-5). IEEE.

Mahmoud, R., Ueno, A., & Tatsumi, S. (2010, December). Dexterous mechanism design for an anthropomorphic artificial hand: Osaka City University Hand I. In 2010 10th IEEE-RAS International Conference on Humanoid Robots (pp. 180-185). IEEE.

Marcus, B., Lawrence, W. T., & Churchill, P. (1991). Hand position/measurement control system. US Patent 4,986,280.

Martin, J., & Grossard, M. (2014). Design of a fully modular and backdrivable dexterous hand. The International Journal of Robotics Research, 33(5), 783-798.

McGee, T. G., Para, M. P., Katyal, K. D., & Johannes, M. S. (2014, October). Demonstration of force feedback control on the Modular Prosthetic Limb. In 2014 IEEE International Conference on Systems, Man, and Cybernetics (SMC) (pp. 2833-2836). IEEE.

MekaBot. (2009). H2 Compliant Hand Datasheet. (2009).

Melchiorri, C., & Kaneko, M. (2008). Robot hands. In Springer Handbook of Robotics (pp. 345-360). Springer Berlin Heidelberg.

Melchiorri, C., Palli, G., Berselli, G., & Vassura, G. (2013). Development of the ub hand iv: Overview of design solutions and enabling technologies. IEEE Robotics & Automation Magazine, 20(3), 72-81. **[UB Hand IV]**

Microsoft. (2013). Kinect. Retrieved Feb 16th, 2013, from Xbox Website: http://www.xbox.com/en-US/kinect

Miller, S., van den Berg, J., Fritz, M., Darrell, T., Goldberg, K., & Abbeel, P. "A geometric approach to robotic laundry folding." The International Journal of Robotics Research 31.2 (2012): 249-267.

Mouri, T., Endo, T., & Kawasaki, H. (2011). Review of gifu hand and its application. Mechanics based design of structures and machines, 39(2), 210-228.

Mouri, T., Kawasaki, H., Yoshikawa, K., Takai, J., & Ito, S. (2002, October). Anthropomorphic robot hand: Gifu hand III. In Proc. Int. Conf. ICCAS (pp. 1288-1293).

Namiki, A., Imai, Y., Ishikawa, M., & Kaneko, M. (2003, October). Development of a high-speed multifingered hand system and its application to catching. In Intelligent Robots and Systems, 2003.(IROS 2003). Proceedings. 2003 IEEE/RSJ International Conference on (Vol. 3, pp. 2666-2671). IEEE.

NASA, J. (2000). ANTHROPOMETRY AND BIOMECHANICS. Retrieved from Man-System Integration Standards : http://msis.jsc.nasa.gov/sections/section03.htm

NASA, J. (2000). ANTHROPOMETRY AND BIOMECHANICS. Retrieved from Man-System Integration Standards : http://msis.jsc.nasa.gov/sections/section03.htm

NASA,. "Robonaut 2 (R2) Overview". 2010. Presentation.

Nayar, S. K., Sims, D. C., & Fridberg, M. (2015, April). Towards Self-Powered Cameras. In Computational Photography (ICCP), 2015 IEEE International Conference on (pp. 1-10). IEEE.

Nimbarte, A. D., Kaz, R., & Li, Z. M. (2008). Finger joint motion generated by individual extrinsic muscles: A cadaveric study. Journal of orthopaedic surgery and research, 3(1), 1.

O'Flynn, B., Sanchez, J. T., Angove, P., Connolly, J., Condell, J., Curran, K., & Gardiner, P. (2013). Novel smart sensor glove for arthritis rehabiliation. 2013 IEEE International Conference on Body Sensor Networks, BSN 2013.

Online Digitial Education Connection. (2011). The Human Story: The Hands. Retrieved from http://www.odec.ca/projects

Open Hand Project, Bristol (United Kingdom), Dextrus Hand, 2014.

Oz, C., & Leu, M. C. (2005). Recognition of Finger Spelling of American Sign Language with Artificial Neural Network Using Position / Orientation Sensors and Data Glove. In Second International Symposium on Neural Networks (pp. 157–164).

Palli, G., & Melchiorri, C. (2006, May). Model and control of tendon-sheath transmission systems. In Proceedings 2006 IEEE International Conference on Robotics and Automation, 2006. ICRA 2006. (pp. 988-993). IEEE.

Palli, G., Melchiorri, C., Vassura, G., Scarcia, U., Moriello, L., Berselli, G., Cavallo, A., De Maria, G., Natale, C., Pirozzi, S., May, C., May, C., Ficuciello, F., & Siciliano, B. (2014). The DEXMART hand: Mechatronic design and experimental evaluation of synergy-based control for human-like grasping. The International Journal of Robotics Research, 33(5), 799-824.

Paluszek, M. A. (2014). Methods and Applications of Controlling Biomimetic Robotic Hands (Master's Thesis, Virginia Tech). Retrieved from http://hdl.handle.net/10919/25335

Park, C. P. C., Bae, J. B. J., & Moon, I. M. I. (2009). Development of wireless data glove for unrestricted upper-extremity rehabilitation system. In 2009 Iccas-Sice (pp. 790–793).

Peerdeman, B., Valori, M., Brouwer, D., Hekman, E., Misra, S., & Stramigioli, S. (2014). UT hand I: A lock-based underactuated hand prosthesis. Mechanism and machine theory, 78, 307-323.

Pellerin, C. (1991). The salisbury hand. Industrial Robot: An International Journal, 18(4), 25-26.

Perng, J. K., Fisher, B., Hollar, S., & Pister, K. S. J. (1999). Acceleration sensing glove (ASG). Digest of Papers. Third International Symposium on Wearable Computers, (Figure 2), 2–4.

Perry, N. C., Evans, C. O., Van der Merwe, D. A., Coulter, S. M., Vlolette, K. D., & Doyon, T. A. (2012). U.S. Patent Application No. 13/566,736.

Polhemus Navigation Sciences Division (1987). SpaceIsotrak user's manual. Colchester, VT.

Pons, J. L., Ceres, R., & Pfeiffer, F. (1999). Multifingered dextrous robotics hand design and control: a review. Robotica, 17(06), 661-674.

Pons, J. L., Rocon, E., Ceres, R., Reynaerts, D., Saro, B., Levin, S., & Van Moorleghem, W. (2004). The MANUS-HAND dextrous robotics upper limb prosthesis: mechanical and manipulation aspects. Autonomous Robots, 16(2), 143-163.

Portillo-Rodriguez, O., Avizzano, C. A., Sotgiu, E., Pabon, S., Frisoli, A., Ortiz, J., & Bergamasco, M. (2007). A wireless Bluetooth Dataglove based on a novel goniometric sensors. Proceedings - IEEE International Workshop on Robot and Human Interactive Communication, 1185–1190.

Pratt, G. A., & Williamson, M. M. (1995, August). Series elastic actuators. In Intelligent Robots and Systems 95.'Human Robot Interaction and Cooperative Robots', Proceedings. 1995 IEEE/RSJ International Conference on (Vol. 1, pp. 399-406). IEEE.

Prudencio, A., Morales, E., García, M. A., & Lozano, A. (2014, December). Anthropometric and anthropomorphic features applied to a mechanical finger. In International Conference on Intelligent Robotics and Applications (pp. 254-265). Springer International Publishing.

Quigley, M., Salisbury, C., Ng, A. Y., & Salisbury, J. K. (2014). Mechatronic design of an integrated robotic hand. The International Journal of Robotics Research, 33(5), 706-720.**]**

Resnik, L., Klinger, S. L., & Etter, K. (2014). The DEKA Arm: Its features, functionality, and evolution during the Veterans Affairs Study to optimize the DEKA Arm. Prosthetics and orthotics international, 38(6), 492-504.

Rethink Robotics. (2015, October). Baxter Datasheet. Retrieved from http://www.rethinkrobotics.com/wp-content/uploads/2015/11/Baxter_Datasheet_Oct2015.pdf

Robotcub. (2005). Analysis and Pre-selection of the Sensor and Actuator Technologies. Retrieved from http://www.robotcub.org/index.php/robotcub/more_information/deliverables/deliverable_7_2_pdf

Robotiq. (2014, August). Robotiq Adaptive Gripper 3-Finger Specifications. Retrieved from http://robotiq.com/wp-content/uploads/2014/08/Robotiq-3-Finger-Adaptive-Gripper-Specifications-ES.pdf

Roccella, S., Carrozza, M., Cappiello, G., Dario, P., Cabibihan, J. J., Zecca, M., Miwa, H., Itoh, K., Matsumoto, M., & Takanishi, A. (2004, September). Design, fabrication and preliminary results of a novel anthropomorphic hand for humanoid robotics: RCH-1. In Intelligent Robots and Systems, 2004.(IROS 2004). Proceedings. 2004 IEEE/RSJ International Conference on (Vol. 1, pp. 266-271). IEEE.

Saggio, G., Bianchi, L., Castelli, S., Santucci, M. B., Fraziano, M., & Desideri, A. (2014). In vitro analysis of pyrogenicity and cytotoxicity profiles of flex sensors to be used to sense human joint postures. Sensors, 14(7), 11672-11681.

Saggio, G., Bocchetti, S., Pinto, C. A., & Orengo, G. (2010). Wireless data glove system developed for HMI. In 2010 3rd International Symposium on Applied Sciences in Biomedical and Communication Technologies, ISABEL 2010 (pp. 0–4).

Saliba, M. A., & Ellul, C. (2013). Dexterous actuation. Mechanism and Machine Theory, 70, 45-61.

Salisbury, J. K., & Craig, J. J. (1982). Articulated hands force control and kinematic issues. The International journal of Robotics research, 1(1), 4-17.

Sanchez, J., Revolutionizing Prosthetics. Retreived from http://www.darpa.mil/program/revolutionizing-prosthetics

Sandia National Laboratories. (2015). Lifelike, cost-effective robotic Sandia Hand can disable IEDs. Retrieved from https://share.sandia.gov/news/resources/news_releases/robotic_hand/#.V8NUcTVTWir

Saudabayev, A., & Varol, H. A. (2015). Sensors for Robotic Hands: A Survey of State of the Art. IEEE Access, 3, 1765-1782.

Schmeder, A. (2008, August 08). Optimizing the voltage divider pullup / pulldown circuit for resistive analog sensing. Retrieved from http://cnmat.berkeley.edu/: http://cnmat.berkeley.edu/user/andy_schmeder/blog/2008/08/08/optimizing_voltage_divider_circuit_resistive_analog_sensing

Schmitz, A., Pattacini, U., Nori, F., Natale, L., Metta, G., & Sandini, G. (2010, December). Design, realization and sensorization of the dexterous icub hand. In Humanoid Robots (Humanoids), 2010 10th IEEE-RAS International Conference on (pp. 186-191). IEEE.

Schunk. Servo-electric 5-Finger Gripping Hand Technical data. Retrieved from http://mobile.schunk-microsite.com/fileadmin/user_upload/broshures/SCHUNK_Technical_data_SVH.pdf

Scott, K. W. (2013). The Scott Hand: A Decoupled Solution to Robotic Prosthetics (Doctoral dissertation, Idaho State University).

Shadow Robot Company. (2013, 01 01). Shadow Dexterous Hand Technical Specification. Retrieved from shadowrobot.com: http://www.shadowrobot.com/wp-content/uploads/shadow_dexterous_hand_technical_specification_E1_20130101.pdf

Shadow Robot: Wave hello to my little friend. (2010, December 28). Independent. Retrieved from http://www.independent.co.uk/life-style/gadgets-and-tech/features/shadow-robot-wave-hello-to-my-little-friend-2170947.html

Slade, P., Akhtar, A., Nguyen, M., & Bretl, T. (2015, May). Tact: Design and performance of an open-source, affordable, myoelectric prosthetic hand. In Robotics and Automation (ICRA), 2015 IEEE International Conference on (pp. 6451-6456). IEEE.

Sousa, I. M., Couceiro, M. S., Barbosa, A. R., Figueiredo, C. M., & Ferreira, N. M. (2013, May). Exploiting the development of robotic hands. In SeGAH (pp. 1-7).

SOUVR. (2008). DG5 VHand 2.0. Retrieved from http://en.souvr.com/product/200808/1399.html

SOUVR. (2008). Didjiglove. Retrieved from http://en.souvr.com/product/200712/292.html

Stevens, M. A. (2013). Design and Teleoperative Control of Humanoid Robot Upper Body for Task-driven Assistance (Master's thesis, Virginia Tech). Retrieved from http://hdl.handle.net/10919/23108

Sturman, D. J., & Zeltzer, D. (1994). A survey of glove-based input. Computer Graphics and Applications, IEEE, 14(1), 30–39.

Su, Y., Allen, C. R., Geng, D., Burn, D., Brechany, U., Bell, G. D., & Rowland, R. (2003). 3-D motion system ("data-gloves"): Application for Parkinson's disease. IEEE Transactions on Instrumentation and Measurement, 52(3), 662–674.

Taylor, C. L., & Schwarz, R. J. (1955). The anatomy and mechanics of the human hand. Artificial limbs, 2(2), 22-35.

Thayer, N., & Priya, S. (2011). Design and implementation of a dexterous anthropomorphic robotic typing (DART) hand. Smart Materials and Structures, 20(3), 035010.

The Human Story: The Hands. (2011). Retrieved from Online Digital Education Connection

Tognetti, A., Carbonaro, N., Zupone, G., & De Rossi, D. (2006). Characterization of a novel data glove based on textile integrated sensors. In Annual International Conference of the IEEE Engineering in Medicine and Biology - Proceedings (pp. 2510–2513).

Tom's Hardware. (2005) 'CyberGlove key to more realistic movies and games?'. Retrieved from http://www.tomshardware.com/news/immersion-cyberglove,1739.html

Tongrod, N., Lokavee, S., Watthanawisuth, N., Tuantranont, A., & Kerdcharoen, T. (2013). Design and development of data glove based on printed polymeric sensors and Zigbee networks for Human-Computer Interface. Disability and Rehabilitation. Assistive Technology, 8(2), 115–20.

Treratanakulwong, T., Kaminaga, H., & Nakamura, Y. (2014, May). Low-friction tendon-driven robot hand with carpal tunnel mechanism in the palm by optimal 3D allocation of pulleys. In 2014 IEEE International Conference on Robotics and Automation (ICRA) (pp. 6739-6744). IEEE.

Tsagarakis, N. G., Kenward, B., Rosander, K., Caldwell, D. G., & Hofsten, C. von. (2006). " BabyGlove ": A Device to study Hand Motion Control Development in Infants. EuroHaptics.

Tuffield, P., & Elias, H. (2003). The shadow robot mimics human actions. Industrial Robot: An International Journal, 30(1), 56-60.

Ueda, J., Ishida, Y., Kondo, M., & Ogasawara, T. (2005, April). Development of the NAIST-Hand with vision-based tactile fingertip sensor. In Robotics and Automation, 2005. ICRA 2005. Proceedings of the 2005 IEEE International Conference on (pp. 2332-2337). IEEE.

Uluer, P., Akalın, N., & Köse, H. (2015). A New Robotic Platform for Sign Language Tutoring. International Journal of Social Robotics, 7(5), 571-585.

Venkataraman, S. T., Iberall, T., & SpringerLink (Online service). (1990). Dextrous robot hands. New York, NY: Springer New York. doi:10.1007/978-1-4613-8974-3

Virtual Motion Labs. VMG 30.

Virtual Realities, LLC. (2016). Data Gloves. Retrieved from www.vrealities.com/products/data-gloves

Walker, C., & Baheshti, B. (2000). U.S. Patent No. 6,049,327. Washington, DC: U.S. Patent and Trademark Office.

Wang, R. Y., & Popović, J. (2009). Real-time hand-tracking with a color glove. ACM Transactions on Graphics, 28(3), 1.

Wang, Z. H., Zhang, L. B., Bao, G. J., Qian, S. M., & Yang, Q. H. (2011). Design and control of integrated pneumatic dexterous robot finger. Journal of Central South University of Technology, 18, 1105-1114.

Wester, B. A., Para, M. P., Sivakumar, A., Kutzer, M. D., Katyal, K. D., Ravitz, A. D., Beaty, J.D., McLoughlin, M.P., & Johannes, M. S. (2013, November). Experimental validation of imposed safety regions for neural controlled human patient self-feeding using the modular prosthetic limb. In 2013 IEEE/RSJ International Conference on Intelligent Robots and Systems (pp. 877-884). IEEE.

Williams, N. W. (1997). The virtual hand: The pulvertaft prize essay for 1996. Journal of Hand Surgery: European Volume, 22(5), 560–567.

Willow Garage. (2010, June 15). The PR2 Plays Pool. Retrieved from http://www.willowgarage.com/blog/2010/06/15/pr2-plays-pool

Willow Garage. (n.d.). PR2. Retrieved from http://www.willowgarage.com/pages/pr2/overview

Wolpaw, J., & al., E. (2002). Brain-Computer Interfaces for Communication and Control. Clinical Neurophysiology, 113, 767-791.

Wright, A. K., & Stanisic, M. M. (1990, August). Kinematic mapping between the EXOS Handmaster exoskeleton and the Utah/MIT dextrous hand. In Systems Engineering, 1990., IEEE International Conference on (pp. 101-104). IEEE.

Xu, Z., Kumar, V., & Todorov, E. (2013, October). A low-cost and modular, 20-DOF anthropomorphic robotic hand: Design, actuation and modeling. In Humanoid Robots (Humanoids), 2013 13th IEEE-RAS International Conference on (pp. 368-375). IEEE.

Yamada, T., Hayamizu, Y., Yamamoto, Y., Yomogida, Y., Izadi-Najafabadi, A., Futaba, D. N., & Hata, K. (2011). A stretchable carbon nanotube strain sensor for human-motion detection. Nature Nanotechnology, 6(5), 296–301.

Yan, C., Wang, J., Kang, W., Cui, M., Wang, X., Foo, C. Y., Chee, K.J., & Lee, P. S. (2014). Highly stretchable piezoresistive graphene-nanocellulose nanopaper for strain sensors. Advanced Materials, 26(13), 2022–2027.

Youngblut, C., Johnston, R. E., Nash, S. H., Wienclaw, R. A., & Will, C. A. (1996). Review of Virtual Environment Interface Technology.

Yousef, H., Boukallel, M., & Althoefer, K. (2011). Tactile sensing for dexterous in-hand manipulation in robotics—A review. Sensors and Actuators A: physical, 167(2), 171-187.

Zecca, M., Cappiello, G., Sebastiani, F., Roccella, S., Vecchi, F., Carrozza, M. C., & Dario, A. P. (2004). 15 Experimental Analysis of the Proprioceptive and Exteroceptive Sensors of an Underactuated Prosthetic Hand. In Advances in Rehabilitation Robotics (pp. 233-242). Springer Berlin Heidelberg.

Zecca, M., Roccella, S., Cappiello, G., Ito, K., Imanishi, K., Miwa, H., Carrozza, M.C., Dario, P., & Takanishi, A. (2013). Biologically-Inspired Approach for the Development of RoboCasa Hand#1. ROMANSY 16: Robot Design, Dynamics and Control, 487, 287.

Zhang, Y. F., Liu, Y. W., Jin, M. H., & Liu, H. (2010, November). Design of a finger-tip flexible tactile sensor for an anthropomorphic robot hand. In International Conference on Intelligent Robotics and Applications (pp. 762-773). Springer Berlin Heidelberg.

Zhang, Z. (2011). Robust Hand Gesture Recognition Based on Finger- Earth Mover ' s Distance with a Commodity Depth Camera. Hand The, 1093–1096.

Zimmerman, T. G., Lanier, J., Blanchard, C., Bryson, S., & Harvill, Y. (1987). A hand gesture interface device. ACM SIGCHI Bulletin, 17(SI), 189–192.

Appendix A: Copyright Permissions

Permission to use material from (Paluszek, 2013) and (Stevens, 2013)

VirginiaTech
Invent the Future

Steve Powell <stevep7@vt.edu>

Thesis usage
1 message

Matt Paluszek <mattiep9@vt.edu> Fri, Aug 26, 2016 at 9:10 AM
To: Steve Powell <stevep7@vt.edu>

Steve,

You have my permission to use material from my thesis. Also, I am confirming that I am a coauthor on your manuscript.

-Matt Paluszek

Sent from my iPhone

VirginiaTech
Invent the Future

Steve Powell <stevep7@vt.edu>

Thesis submission
1 message

Mike Stevens <m.a.d.stevens@gmail.com> Fri, Aug 26, 2016 at 11:38 PM
To: Steve Powell <stevep7@vt.edu>

Steve,

You have my permission to use material from my thesis. Also, I am confirming that I am a coauthor on your thesis.
Regards,
Mike
--
Warm Regards,
Mike Stevens

Figure 3.

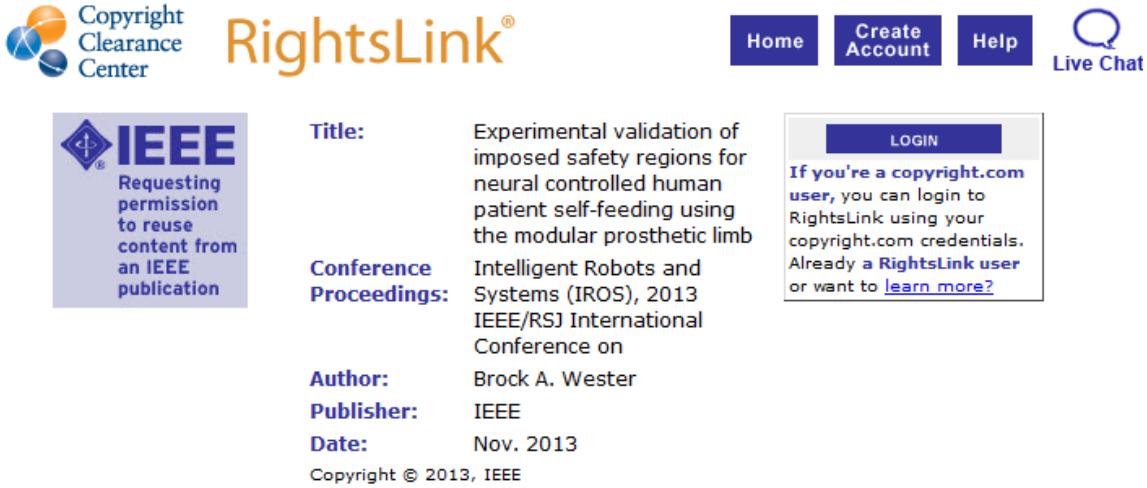

Thesis / Dissertation Reuse

The IEEE does not require individuals working on a thesis to obtain a formal reuse license, however, you may print out this statement to be used as a permission grant:

Requirements to be followed when using any portion (e.g., figure, graph, table, or textual material) of an IEEE copyrighted paper in a thesis:

1) In the case of textual material (e.g., using short quotes or referring to the work within these papers) users must give full credit to the original source (author, paper, publication) followed by the IEEE copyright line © 2011 IEEE.
2) In the case of illustrations or tabular material, we require that the copyright line © [Year of original publication] IEEE appear prominently with each reprinted figure and/or table.
3) If a substantial portion of the original paper is to be used, and if you are not the senior author, also obtain the senior author's approval.

Requirements to be followed when using an entire IEEE copyrighted paper in a thesis:

1) The following IEEE copyright/ credit notice should be placed prominently in the references: © [year of original publication] IEEE. Reprinted, with permission, from [author names, paper title, IEEE publication title, and month/year of publication]
2) Only the accepted version of an IEEE copyrighted paper can be used when posting the paper or your thesis on-line.
3) In placing the thesis on the author's university website, please display the following message in a prominent place on the website: In reference to IEEE copyrighted material which is used with permission in this thesis, the IEEE does not endorse any of [university/educational entity's name goes here]'s products or services. Internal or personal use of this material is permitted. If interested in reprinting/republishing IEEE copyrighted material for advertising or promotional purposes or for creating new collective works for resale or redistribution, please go to http://www.ieee.org/publications_standards/publications/rights/rights_link.html to learn how to obtain a License from RightsLink.

If applicable, University Microfilms and/or ProQuest Library, or the Archives of Canada may supply single copies of the dissertation.

Figure 4.

Thesis / Dissertation Reuse

The IEEE does not require individuals working on a thesis to obtain a formal reuse license, however, you may print out this statement to be used as a permission grant:

Requirements to be followed when using any portion (e.g., figure, graph, table, or textual material) of an IEEE copyrighted paper in a thesis:

1) In the case of textual material (e.g., using short quotes or referring to the work within these papers) users must give full credit to the original source (author, paper, publication) followed by the IEEE copyright line © 2011 IEEE.
2) In the case of illustrations or tabular material, we require that the copyright line © [Year of original publication] IEEE appear prominently with each reprinted figure and/or table.
3) If a substantial portion of the original paper is to be used, and if you are not the senior author, also obtain the senior author's approval.

Requirements to be followed when using an entire IEEE copyrighted paper in a thesis:

1) The following IEEE copyright/ credit notice should be placed prominently in the references: © [year of original publication] IEEE. Reprinted, with permission, from [author names, paper title, IEEE publication title, and month/year of publication]
2) Only the accepted version of an IEEE copyrighted paper can be used when posting the paper or your thesis on-line.
3) In placing the thesis on the author's university website, please display the following message in a prominent place on the website: In reference to IEEE copyrighted material which is used with permission in this thesis, the IEEE does not endorse any of [university/educational entity's name goes here]'s products or services. Internal or personal use of this material is permitted. If interested in reprinting/republishing IEEE copyrighted material for advertising or promotional purposes or for creating new collective works for resale or redistribution, please go to http://www.ieee.org/publications_standards/publications/rights/rights_link.html to learn how to obtain a License from RightsLink.

If applicable, University Microfilms and/or ProQuest Library, or the Archives of Canada may supply single copies of the dissertation.

Figure 5.

Media Usage Guidelines

NASA Logo

The NASA insignia logo (the blue "meatball" insignia), the retired NASA logotype (the red "worm" logo) and the NASA seal may not be used for any purpose without explicit permission. These images may not be used by persons who are not NASA employees or on products, publications or web pages that are not NASA-sponsored. These images may not be used to imply endorsement or support of any external organization, program, effort, or persons.

Still Images, Audio Recordings, Video, and Related Computer Files for Non-Commercial Use

NASA content - images, audio, video, and computer files used in the rendition of 3-dimensional models, such as texture maps and polygon data in any format - generally are not copyrighted. You may use this material for educational or informational purposes, including photo collections, textbooks, public exhibits, computer graphical simulations and Internet Web pages. This general permission extends to personal Web pages.

News outlets, schools, and text-book authors may use NASA content without needing explicit permission. NASA content used in a factual manner that does not imply endorsement may be used without needing explicit permission. NASA should be acknowledged as the source of the material. NASA occasionally uses copyrighted material by permission on its website. Those images will be marked copyright with the name of the copyright holder. NASA's use does not convey any rights to others to use the same material. Those wishing to use copyrighted material must contact the copyright holder directly.

NASA has extensive image and video galleries online, including historic images, current missions, astronomy pictures, and ways to search for NASA images. Generally, each mission and program has a video and image collection on the topic page. For example, space station videos can be found at https://www.nasa.gov/mission_pages/station/videos/index.html. Content can also be found on our extensive social media channels.

For questions about specific images, please call 202-358-1900. For questions about specific video, please call 202-358-0309.

Figure 6.

Copyright Clearance Center RightsLink®

Home | Create Account | Help | Live Chat

SAGE Publishing

Title: The DEXMART hand: Mechatronic design and experimental evaluation of synergy-based control for human-like grasping:

Author: G. Palli, C. Melchiorri, G. Vassura, U. Scarcia, L. Moriello, G. Berselli, A. Cavallo, G. De Maria, C. Natale, S. Pirozzi, C. May, F. Ficuciello, B. Siciliano

Publication: International Journal of Robotics Research

Publisher: SAGE Publications

Date: 04/30/2014

Copyright © 2014, © SAGE Publications

LOGIN

If you're a copyright.com user, you can login to RightsLink using your copyright.com credentials. Already **a RightsLink user** or want to learn more?

Gratis Reuse

Permission is granted at no cost for use of content in a Master's Thesis and/or Doctoral Dissertation. If you intend to distribute or sell your Master's Thesis/Doctoral Dissertation to the general public through print or website publication, please return to the previous page and select 'Republish in a Book/Journal' or 'Post on intranet/password-protected website' to complete your request.

BACK | CLOSE WINDOW

Copyright © 2016 Copyright Clearance Center, Inc. All Rights Reserved. Privacy statement. Terms and Conditions.
Comments? We would like to hear from you. E-mail us at customercare@copyright.com

Figure 7.


Copyright Clearance Center
RightsLink
Home
Create Account
Help
Live Chat
SAGE Publishing
Title: Mechatronic design of an integrated robotic hand:
Author: Morgan Quigley, Curt Salisbury, Andrew Y. Ng, J. Kenneth Salisbury
Publication: International Journal of Robotics Research
Publisher: SAGE Publications
Date: 04/01/2014
Copyright © 2014, © SAGE Publications
LOGIN
If you're a copyright.com user, you can login to RightsLink using your copyright.com credentials.
Already a RightsLink user or want to learn more?
Gratis Reuse
Permission is granted at no cost for use of content in a Master's Thesis and/or Doctoral Dissertation. If you intend to distribute or sell your Master's Thesis/Doctoral Dissertation to the general public through print or website publication, please return to the previous page and select 'Republish in a Book/Journal' or 'Post on intranet/password-protected website' to complete your request.
BACK
CLOSE WINDOW
Copyright © 2016 Copyright Clearance Center, Inc. All Rights Reserved. Privacy statement. Terms and Conditions.
Comments? We would like to hear from you. E-mail us at customercare@copyright.com

Figure 59.

Thesis / Dissertation Reuse

The IEEE does not require individuals working on a thesis to obtain a formal reuse license, however, you may print out this statement to be used as a permission grant:

Requirements to be followed when using any portion (e.g., figure, graph, table, or textual material) of an IEEE copyrighted paper in a thesis:

1) In the case of textual material (e.g., using short quotes or referring to the work within these papers) users must give full credit to the original source (author, paper, publication) followed by the IEEE copyright line © 2011 IEEE.
2) In the case of illustrations or tabular material, we require that the copyright line © [Year of original publication] IEEE appear prominently with each reprinted figure and/or table.
3) If a substantial portion of the original paper is to be used, and if you are not the senior author, also obtain the senior author's approval.

Requirements to be followed when using an entire IEEE copyrighted paper in a thesis:

1) The following IEEE copyright/ credit notice should be placed prominently in the references: © [year of original publication] IEEE. Reprinted, with permission, from [author names, paper title, IEEE publication title, and month/year of publication]
2) Only the accepted version of an IEEE copyrighted paper can be used when posting the paper or your thesis on-line.
3) In placing the thesis on the author's university website, please display the following message in a prominent place on the website: In reference to IEEE copyrighted material which is used with permission in this thesis, the IEEE does not endorse any of [university/educational entity's name goes here]'s products or services. Internal or personal use of this material is permitted. If interested in reprinting/republishing IEEE copyrighted material for advertising or promotional purposes or for creating new collective works for resale or redistribution, please go to http://www.ieee.org/publications_standards/publications/rights/rights_link.html to learn how to obtain a License from RightsLink.

If applicable, University Microfilms and/or ProQuest Library, or the Archives of Canada may supply single copies of the dissertation.

Draft 09/01/2009

(Questions? Concerns? Contact Gail McMillan, Director of the Digital Library and Archives at Virginia Tech's University Libraries: gailmac@vt.edu)

(Please ensure that Javascript is enabled on your browser before using this tool.)

Virginia Tech ETD Fair Use Analysis Results

This is not a replacement for professional legal advice but an effort to assist you in making a sound decision.

Name: Stephen Powell

Description of item under review for fair use: Figure 1. The Shadow Dexterous Hand (Shadow, 2013). Source: Shadow Robot Company. (2013, 01 01). Shadow Dexterous Hand Technical Specification. Retrieved from shadowrobot.com: http://www.shadowrobot.com/wp-content/uploads/shadow_dexterous_hand_technical_specification_E1_20130101.pdf Figure 2. The DART Hand (Thayer & Priya, 2011). Source: Thayer, N., & Priya, S. (2011). Design and implementation of a dexterous anthropomorphic robotic typing (DART) hand. Smart Materials and Structures, 20(3), 035010. Figure 7. The Sandia Hand. Source: Sandia National Laboratories. (2015). Lifelike, cost-effective robotic Sandia Hand can disable IEDs. Retrieved from https://share.sandia.gov/news/resources/news_releases/robotic_hand/#.V8NUcTVTWir Figure 8. The bones and joints of the human hand. Source: Wpclipart. (n.d.). Hand bones Grays. Retrieved from http://www.wpclipart.com /medical/bones/hand_bones/hand_bones_Grays.png.html Figure 9. Cutkosky's Taxonomy of human hand grasps. Source: Cutkosky, M. R., & Howe, R. D. (1990). Human grasp choice and robotic grasp analysis. Dextrous robot hands, 1, 5-31. Figure 49. Circular grip (left) and power grip (right) are ideal grips for a number of teleoperative purposes. Source: Online Digitial Education Connection. (2011). The Human Story: The Hands. Retrieved from http://www.odec.ca/projects /2011/yuyuya/page14.html

Report generated on: 08-28-2016 at : 17:58:42

Based on the information you provided:

Factor 1

Your consideration of the purpose and character of your use of the copyright work weighs: ***in favor of fair use***

Factor 2

Your consideration of the nature of the copyrighted work you used weighs: ***in favor of fair use***

Factor 3

Your consideration of the amount and substantiality of your use of the copyrighted work weighs: ***in favor of fair use***

Factor 4

Your consideration of the effect or potential effect on the market after your use of the copyrighted work weighs: ***in favor of fair use***

Based on the information you provided, your use of the copyrighted work weighs: *in favor of fair use*